

# Chemical Tracer Techniques for Assessing Mixing Performance in Non-Newtonian Slurries for WTP Pulsed Jet Mixer Systems

A. P. Poloski  
L. A. Snow  
S. T. Arm

August 2004

Prepared for Bechtel National, Inc.  
under Contract 24590-101-TSA-W000-0004

## LEGAL NOTICE

This report was prepared by Battelle Memorial Institute (Battelle) as an account of sponsored research activities. Neither Client nor Battelle nor any person acting on behalf of either:

**MAKES ANY WARRANTY OR REPRESENTATION, EXPRESS OR IMPLIED,** with respect to the accuracy, completeness, or usefulness of the information contained in this report, or that the use of any information, apparatus, process, or composition disclosed in this report may not infringe privately owned rights; or

Assumes any liabilities with respect to the use of, or for damages resulting from the use of, any information, apparatus, process, or composition disclosed in this report.

Reference herein to any specific commercial product, process, or service by trade name, trademark, manufacturer, or otherwise, does not necessarily constitute or imply its endorsement, recommendation, or favoring by Battelle. The views and opinions of authors expressed herein do not necessarily state or reflect those of Battelle.

## **Chemical Tracer Techniques for Assessing Mixing Performance in Non-Newtonian Slurries for WTP Pulsed Jet Mixer Systems**

A. P. Poloski  
L. A. Snow  
S. T. Arm

August 2004

Test specification: 24590-WTP-TSP-RT-03-008, Rev. 0

Test plan: TP-RPP-WTP-296, Rev. 0

Test exceptions: 24590-WTP-TEF-RT-03-060, 24590-WTP-TEF-RT-03-081,  
24590-WTP-TEF-RT-03-090, 24590-WTP-TEF-RT-04-002,  
24590-WTP-TEF-RT-04-00004

R&T focus area: Pretreatment & Vitrification

Test Scoping Statement(s): B-100

  
for U. Tanosaitic

8/30/04

Battelle—Pacific Northwest Division  
Richland, Washington 99352

**ACCEPTED FOR  
PROJECT USE**

## ***Completeness of Testing***

*This report describes the results of work and testing specified by Test Specification 24590-WTP-TSP-RT-03-008, Rev. 0 and Test Plan TP-RPP-WTP-296, Rev. 0. The work and any associated testing followed the quality assurance requirements outlined in the Test Specification/Plan. The descriptions provided in this test report are an accurate account of both the conduct of the work and the data collected. Test plan results are reported. Also reported are any unusual or anomalous occurrences that are different from expected results. The test results and this report have been reviewed and verified.*

Approved:



Gordon H. Beeman, Manager  
WTP R&T Support Project

8/24/04  
Date

## Summary

This document describes work performed under Battelle—Pacific Northwest Division (PNWD) Test Plan TP-RPP-WTP-296 Rev 0 “Test Plan for Determination of Scaled Performance Data for Pulse Jet Mixers in Prototypic Ultrafiltration Feed Process (UFP) and HLW Lag Storage (LS) Vessels.” Pulsed Jet Mixer (PJM) technology has been selected for use to mix non-Newtonian fluids in the Hanford Waste Treatment Plant. This report describes the development of chemical tracer methods used to evaluate the mixing performance of PJM systems, sparging tubes, recirculation pumps (steady state jets), and combinations of the three. Both transparent and opaque simulants were used in this testing.

Evaluation of mixing performance in the PJM test vessels was assessed with two tracer chemicals, primarily Brilliant Blue (BB) Food Dye Color No. 1 and sodium chloride (Cl). Mass-balance equations were developed to determine the volume fraction of the test vessel that is well-mixed by measuring the concentration of the tracer chemical in several scenarios. The tracer chemical was mixed with a sample of the test simulant and injected into the PJM test vessel mixing cavern. Samples were taken periodically throughout the mixing test, and tracer concentrations were measured to meet the requirements of the mass-balance equations. A normalized concentration ratio termed the “mixing ratio” was then calculated. To augment the interpretation of results, an error analysis of these techniques was also performed.

Chemical tracer development studies for PJM mixing vessels have led to the following conclusions:

- BB and Ethyl Orange optical tracers are recommended for use with the transparent laponite simulant because of the reproducibility of the optical-absorbance values as a function of dye concentration.
- BB optical tracer is recommended for use as a tracer with the kaolin:bentonite opaque simulant. Samples should be centrifuged, and absorbance on the liquid phase should be analyzed. Dye adsorption isotherm data indicated that at low concentrations in the linear Beer’s law region, the distribution coefficient can be considered a constant.
- NaCl is recommended as a tracer with the kaolin:bentonite opaque simulant. Samples should be centrifuged and the supernate liquid analyzed with ion chromatography techniques. The use of a chloride ion selective electrode with centrifuged supernate liquid is an option that should be further evaluated. Adsorption of the chloride ion on the solid phase did not appear significant.
- Although developed for use with the opaque simulant, the combination of NaCl and chloride ion selective electrode could be used with the laponite simulant. However, rheological changes may be produced when adding salts to laponite. These rheological changes should be evaluated before implementing a tracer.
- The equation  $MR_j = \frac{C_f - C_j}{C_f - C_0}$ , where  $MR_j$  is the fraction mixed in the PJM vessel, should be used to

evaluate mixing performance with all recommended tracer/simulant combinations. This equation requires concentration determination in the liquid phase of an initial low-tracer baseline sample,  $C_0$ , a sample from the mixing cavern,  $C_j$ , and a sample from the vessel after complete homogenization,  $C_f$ . This equation requires an experimental method of homogenizing the tank contents. However, this equation has the advantage over alternative equations of not using isotherm, mass of tracer injected,

or mass fraction of solids data. Such data are often difficult to obtain in an accurate manner and can lead to a high degree of uncertainty.

- From this equation, when the sample tracer concentration is equal to the initial test concentration, the mixing ratio is unity, and the tracer has not reached the sample's location. When the sample tracer concentration is equal to the final test concentration, the mixing ratio is zero, and the vessel is nearly homogenous. Lastly, when the sample tracer concentration is above the final test concentration, the mixing ratio is negative. This corresponds to a situation where the sample location is within the mixing cavern, and the fraction mixed calculation may be performed.
- This equation was used to establish criteria to determine "good" mixing. The first criterion is that all samples at a particular time are consistent with a well mixed vessel condition (i.e., mixing ratio is zero) to two standard deviations on measurement error. The second criterion is to calculate the probability score of a well mixed vessel by calculating the probability of the mixing ratio being zero using the average mixing-ratio values and measurement error. The higher the probability score, the more confidence that a homogenous condition can be achieved in a PJM test vessel.
- When the BB dye results are compared to the chloride results, the values of the dye mixing ratios are consistently biased towards greater values than the chloride results. In many instances, the final mixing ratio for the BB dye exceeds zero while the chloride tracer results rarely exceed zero. These data suggest that a systemic issue with the BB dye exists where the 2-phase model of a well mixed cavern and quiescent phase does not hold. However, this model appears to hold for the chloride tracer. This behavior may be explained by the dye sorbing onto the clay particles in the stock solution while the chloride remains in solution. The stock solution clay particles loaded with BB dye may adhere to the tank walls more readily than the low dye clay. This behavior is consistent with observations of streaking along the tank walls during some tests. Conversely, the chloride remains mobile within the mixing cavern. During the tests, samples are taken and dye concentrations are reduced compared to the chloride measurements. During the final homogenization step, sufficient energy is supplied to incorporate the adhered dye into the simulant, resulting in greater-than-zero mixing-ratio values for the BB dye.
- To eliminate the BB dye bias problem, an obvious solution is to only use the chloride data for evaluating the tests. Unfortunately, the chloride analytical techniques possess a higher degree of error compared to the dye techniques. Therefore, the corresponding probability scores for the chloride tracer are significantly lower than the BB dye tracer scores. The current evaluation strategy is to use both techniques and interpret the results with the knowledge that bias may be present in the BB dye results. If a configuration is tested that possesses sufficient mixing energy, the adhered dye is removed, and zero mixing-ratio values are obtained. This situation is seen in Figure 8.8 where the BB dye and chloride results are in good agreement. When a promising configuration is identified, multiple tests should be performed with the chloride tracer. These multiple tests should allow for the error bars to be computed experimentally. With high test repeatability, confidence in the mixing potential for a given test configuration can be increased.
- The amount of chloride tracer used in each test may be increased to reduce uncertainty. Currently, a final concentration increase of 30 ppm chloride is used. Increasing this value to 100 ppm should reduce the associated error significantly. However, tradeoffs such as wastewater limitations for chloride ions and simulant rheological properties changes with salt concentration should be considered.

## Objectives

This investigation was conducted according to the Test Plan TP-RPP-WTP-296 Rev 0 “Test Plan for Determination of Scaled Performance Data for Pulse Jet Mixers in Prototypic Ultrafiltration Feed Process (UFP) and HLW Lag Storage (LS) Vessels” in response to the Test Specification 24590-WTP-TSP-RT-03-008, Rev. 0 “Development of Scaled Performance Data for PJM Mixers in the Ultrafiltration Feed and LAG Storage/Blend Tanks.” The test objective was satisfied. A summary of the test objective and how it was satisfied is provided in Table S.1.

**Table S.1. Test Objective Evaluation**

<b>Test Objective</b>	<b>Objective Met (Y/N)</b>	<b>Discussion</b>
The objective of this task is to provide data on the mobilization of non-Newtonian simulants for the assessment of PJM mixing system designs for the UFP and LS vessels.	Yes	This report discusses the development of tracer techniques to determine the “goodness of mixing” in PJM test vessels with non-Newtonian simulants. Results from these tracer tests can be interpreted as volume fraction of the vessel that is well mixed while the remaining volume of the tanks is considered quiescent or immobilized. Tracer tests were conducted in various test vessels, including UFP and LS scaled prototypes.

## Test Exceptions

Table S.2 discusses the test exceptions applied to this test.

**Table S.2. Test Exceptions**

<b>List Test Exceptions</b>	<b>Describe Test Exceptions</b>
24590-WTP-TEF-RT-03-060	Data are needed to help make an early decision by Waste Treatment Plant/U.S. Department of Energy Office of River Protection (WTP/DOE ORP) as to whether an alternative mixing test program needs to be initiated for the WTP non-Newtonian vessels.
24590-WTP-TEF-RT-03-081	Test data are needed to demonstrate adequate mixing in the UFP and LS prototypic test configurations deemed to be the best mixing design for the WTP non-Newtonian vessels using a particulate clay simulant that more closely matches actual waste rheological properties.
24590-WTP-TEF-RT-03-090	Test data with the baseline number of pulse tubes using sparging tubes to demonstrate that a mixing solution exists using a particulate simulant that has rheological properties deemed to be closer to actual waste is needed.
24590-WTP-TEF-RT-04-002	Include recirculation pump and air sparger combination to reduce plant redesign impact.
24590-WTP-TEF-RT-04-00004	Test data are needed with the baseline number of pulse tubes or less combined with sparging tubes and recirculation pumps, i.e., hybrid mixing systems, to demonstrate that a mixing solution exists using a particulate simulant that has rheological properties deemed to be closer to actual waste.

## Results and Performance Against Success Criteria

Table S.3 discusses the success criterion provided in Test Specification 24590-WTP-TSP-RT-03-008, Rev. 0 “Development of Scaled Performance Data for PJM Mixers in the Ultrafiltration Feed and LAG Storage/Blend Tanks.”

**Table S.3. Discussion of Test Success Criterion**

<b>List Success Criteria</b>	<b>Explain How the Tests Did or Did Not Meet the Success Criteria</b>
Tests will be deemed successful if a combination of PJM operating conditions and physical arrangement are demonstrated to provide full mobilization of the contents of the UFP tank and the high-level waste (HLW) lag storage and blend tanks.	Not directly applicable. This report discusses the development of tracer techniques that were used to determine if full mobilization of a mixing vessel had occurred. Results from several tests are provided in the Appendix section of this report. Discussion of specific LS and UFP test results will occur in other test reports whose scope is to provide design recommendations to Bechtel National Inc. (BNI) Process Engineering. However, tracer results do indicate that several of the tested designs in the LS and UFP scaled prototype systems achieved full mobilization.

## Quality Requirements

PNWD implements the RPP-WTP quality requirements by performing work in accordance with the PNWD Waste Treatment Plant Support Project quality assurance project plan (QAPjP) approved by the RPP-WTP Quality Assurance (QA) organization. This work will be performed to the quality requirements of NQA-1-1989 Part I, Basic and Supplementary Requirements, and NQA-2a-1990, Part 2.7. These quality requirements are implemented through PNWD’s *Waste Treatment Plant Support Project (WTPSP) Quality Assurance Requirements and Description Manual*. The analytical requirements are implemented through WTPSP’s Statement of Work (WTPSP-SOW-005) with the Radiochemical Processing Laboratory (RPL) Analytical Service Operations (ASO).

Experiments that are not method-specific were performed in accordance with PNWD’s procedures QA-RPP-WTP-1101 “Scientific Investigations” and QA-RPP-WTP-1201 “Calibration Control System” verifying that sufficient data were taken with properly calibrated measuring and test equipment (M&TE) to obtain quality results.

As specified in Test Specification, 24590-LAW-TSP-RT-02-008 Rev 0, BNI’s QAPjP, PL-24590-QA00001 is not applicable since the work will not be performed in support of environmental/regulatory testing, and the data will not be used as such.

PNWD addresses internal verification and validation activities by conducting an independent technical review of the final data report in accordance with PNWD’s procedure QA-RPP-WTP-604. This review verifies that the reported results are traceable, that inferences and conclusions are soundly based, and that the reported work satisfies the Test Plan objectives. This review procedure is part of PNWD’s *WTPSP Quality Assurance Requirements and Description Manual*.

## R&T Test Conditions

Table S.4 discusses the R&T test condition provided in Test Exception 24590-WTP-TEF-RT-04-00004.

**Table S.4. Discussion of R&T Test Condition**

<b>List R&amp;T Test Conditions</b>	<b>Were Test Conditions Followed?</b>
Colorimetric dye method for determining mixing volume and uniformity.	Yes, this method was implemented to determine the extent of mixing and uniformity in these tests. The development of the method is described in the body of the report while test results are provided in the Appendices.

## Simulant Use

Two clay simulants, Laponite and Kaolin:Bentonite, were used in this test to duplicate the properties of the non-Newtonian fluids that will be processed in the Hanford Waste Treatment Plant. However, simulant development is outside the scope of this report and will be discussed in other PJM-related WTP reports.

## Discrepancies and Follow-on Tests

No discrepancies were identified nor remain unresolved. However repeated testing of PJM vessels with the tracer techniques described in this report is recommended to develop confidence in the tracer method as applied to BNI selected prototype PJM systems.

## Acronyms

ASO	Analytical Service Operations
BB	Brilliant Blue FCF
BNI	Bechtel National Inc.
CCD	charged coupled device
DOE	U.S. Department of Energy
HLW	High Level Waste
IC	ion chromatography
ISE	ion-specific electrode
LS	Lag Storage
M&TE	Measuring and Test Equipment
ORP	Office of River Protection
PJM	Pulse Jet Mixer
PNWD	Battelle—Pacific Northwest Division
QA	Quality Assurance
QAPjP	Quality Assurance Project Plan
RPL	Radiochemical Processing Laboratory
RPP	River Protection Project
R&T	Research and Technology
SOW	statement of work

UFP	Ultrafiltration Process
UV-vis	Ultraviolet Visible
WTP	Waste Treatment Plant
WTPSP	Waste Treatment Plant Support Project

# Contents

Summary .....	iii
Acronyms .....	ix
1.0 Introduction.....	1.1
2.0 Quality Requirements .....	2.1
3.0 Mass Balance Equations .....	3.1
3.1 Multiple Sample Equations.....	3.1
3.2 Mass of Tracer Equation.....	3.3
4.0 Application to Transparent Simulants .....	4.1
4.1 Tracer Development Conclusions.....	4.11
5.0 Application to Opaque Simulants .....	5.1
5.1 Optical Dye.....	5.1
5.2 NaCl Tracer .....	5.2
5.3 Dye Absorption Kinetics .....	5.2
5.4 Equilibrium Dye Absorption .....	5.4
6.0 Error Analysis .....	6.1
7.0 Data Analysis.....	7.1
8.0 Test Results and Method Evaluation .....	8.1
9.0 Conclusions.....	9.1
10.0 References.....	10.1
Appendix A: Laponite Simulant Test Results.....	A.1
Appendix B: Kaolin:Bentonite Simulant Test Results.....	B.1

# Figures

Figure 1.1. Summary of Tracer Dye Technique Steps.....	1.1
Figure 4.1. Beer’s Law Correlation of Optical Absorbance to BB Dye Concentration in Water .....	4.3
Figure 4.2. Beer’s Law Correlation of Optical Absorbance to Fluorescein Concentration in Water .....	4.6
Figure 4.3. Beer’s Law Correlation of Optical Absorbance to BB Dye Concentration in Water for both Sample Sets .....	4.6
Figure 4.4. Beer’s Law Correlation of Optical Absorbance to Ethyl Orange Dye Concentration in Water .....	4.8
Figure 4.5. Beer’s Law Correlation of Optical Absorbance to BB Dye Concentration in Laponite .....	4.9
Figure 4.6. Beer’s Law Correlation of Optical Absorbance to Fluorescein Concentration in Laponite.....	4.10
Figure 4.7. Beer’s Law correlation of optical absorbance to Ethyl Orange concentration in Laponite.....	4.10
Figure 5.1. Kinetics Plot for 3.2 ppm BB in Kaolin:Bentonite Clay .....	5.3
Figure 5.2. Kinetics Plot for 7.9 ppm BB in Kaolin:Bentonite Clay .....	5.3
Figure 5.3. Linear Fit of Isotherm Data over the Linear Beer’s Law Region.....	5.6
Figure 5.4. Comparison of Measured to Published Isotherms .....	5.7
Figure 8.1. Schematic of Lag Storage Vessel Tracer Sampling Locations During Phase II Scaled Test Platform Tests.....	8.1
Figure 8.2. Schematic of Ultrafiltration Process Vessel Tracer Sampling Locations During Phase II Scaled Test Platform Tests .....	8.5
Figure 8.3. Mixing-Ratio Results from LS Test Sequence 21 Using BB Tracer (top) and Chloride Tracer Using IC Technique (bottom) .....	8.13
Figure 8.4. Mixing-Ratio Results from LS Test Sequence 19 Using BB Tracer (top) and Chloride Tracer Using ISE Technique (bottom) .....	8.15
Figure 8.5. Mixing-Ratio Results from LS Test Sequence 13 Using BB Tracer (top) and Chloride Tracer Using IC Technique (bottom) .....	8.16
Figure 8.6. Mixing-Ratio Results from UFP Test Sequence 12 Using BB Tracer (top) and Chloride Tracer Using ISE Technique (bottom) .....	8.17

Figure 8.7. BB Dye Adherence to Vessel Wall .....	8.19
Figure 8.8. Mixing-Ratio Results from UFP Test Sequence 3B Using BB Tracer (top) and Chloride Tracer Using ISE Technique (bottom) .....	8.21
Figure 8.9. Mixing-Ratio Results from LS Test Sequence 20 Using BB Tracer (top) and Chloride Tracer Using IC Technique (bottom) .....	8.22
Figure 8.10. Mixing-Ratio Results from LS Test Sequence 26 Core Samples using Chloride Tracer (top) and Chloride Concentration as a Function of Depth (bottom).....	8.24
Figure 8.11. Mixing-Ratio Results from LS Test Sequence 27 Core Samples Using Chloride Tracer (top) and Mixing-Ratio Results from Sampling Tubes (bottom).....	8.26
Figure 8.12. Mixing-Ratio Results from LS Test Sequence 28 Core Samples Using Chloride Tracer .....	8.27
Figure 8.13. Mixing-Ratio Results from UFP Test Sequence 15 Core Samples using Chloride Tracer .....	8.27
Figure 8.14. Mixing-Ratio Results from UFP Test Sequence 16 Core Samples Using Chloride Tracer (top) and Chloride Concentration as a Function of Depth (bottom) .....	8.28

## Tables

Table S.1. Test Objective Evaluation.....	v
Table S.2. Test Exceptions.....	vi
Table S.3. Discussion of Test Success Criterion .....	vii
Table S.4. Discussion of R&T Test Condition .....	viii
Table 4.1. Dyes Used in Preliminary Trials.....	4.1
Table 4.2. Samples for Calibration Curve of BB in Water .....	4.3
Table 4.3. Samples for Calibration Curve of Fluorescein in Water—Using Old Bottle of Fluorescein .....	4.4
Table 4.4. Samples for Calibration Curve of Fluorescein in Water—Using New Bottle of Fluorescein .....	4.5
Table 4.5. Samples for Calibration Curve of BB in Water .....	4.5
Table 4.6. Samples for Calibration Curve of Ethyl Orange in Water .....	4.7
Table 4.7. Samples for Calibration Curve of BB in Laponite.....	4.8
Table 4.8. Samples for Calibration Curve of Fluorescein in Laponite .....	4.8
Table 4.9. Samples for Calibration Curve of Ethyl Orange in Laponite.....	4.9
Table 5.1. Contact Times and Absorbance Values for Kinetics Study .....	5.2
Table 7.1. Mixing-Ratio Data Interpretation .....	7.1
Table 8.1. Mixing-Ratio Consistency Test for Lag Storage Vessel During Phase II Scaled Test Platform Tests .....	8.8
Table 8.2. Mixing-Ratio Consistency Test for Ultrafiltration Process Vessel During Phase II Scaled Test Platform Tests.....	8.9
Table 8.3. Mixing-Ratio Probability Score for Lag Storage Vessel During Phase II Scaled Test Platform Tests .....	8.11
Table 8.4. Mixing-Ratio Probability Score for Ultrafiltration Process Vessel During Phase II Scaled Test Platform Tests.....	8.12
Table 8.5. Mixing-Ratio Values from Chloride IC Data for Core Samples Taken During Phase II Scaled Test Platform Tests.....	8.23

Table 8.6. Mixing-Ratio Probability Score from Chloride IC Data for Ultrafiltration Process Vessel During Phase II Scaled Test Platform Tests .....	8.23
Table 8.7. Mass Balance Estimation From Chloride IC Data After Final Homogenization Step for both the Lag Storage and Ultrafiltration Process Vessels During Phase II Scaled Test Platform Tests .....	8.29

# 1.0 Introduction

Pulsed Jet Mixer (PJM) technology has been selected for implementation in the Hanford Waste Treatment Plant (WTP). This system has been selected for use in so called “black cell” regions of the WTP. Within these regions of the plant, maintenance capability will not be available for the operating life of the WTP. PJM technology was selected for use in these regions because of the lack of moving mechanical parts that will require maintenance. However, PJM technology with non-Newtonian fluids that will be processed through these tanks is not mature. Consequently, an effort has been undertaken to investigate PJM performance in scaled versions of PJM vessels with non-Newtonian fluids that behave similarly to the actual waste. This report describes the development of chemical tracer methods used to evaluate the mixing performance of PJM systems, sparging tubes, recirculation pumps (steady jets), and combinations of the three.

The concept behind PJM technology involves a pulse tube coupled with a jet nozzle. The tube is immersed in the tank while vacuum, vent, and pressurized air are sequentially supplied to the opposite end of the pulse tube periodically. Application of the vacuum, vent, and pressurized air functions create various operating modes for the pulse tube. These operating modes include the drive cycle (pressure) where the contents of the PJM tube are discharged at high velocity through the nozzle, the refill mode (vacuum) where the tank contents refill the pulse tube, and an equilibration mode (vent) where the pulse tube and tank fill levels approach the same level. These operating modes produce an operating cycle where the PJM system is operated in drive, vent, and vacuum modes. The PJM system uses this sequence of operating modes to produce a sequence of drive cycles that form a turbulent mixing region at the bottom of the tank (see Figure 1.1). The volume of this mixing region as a function of jet velocity and rheological properties is significant in evaluating the performance of the mixing system.

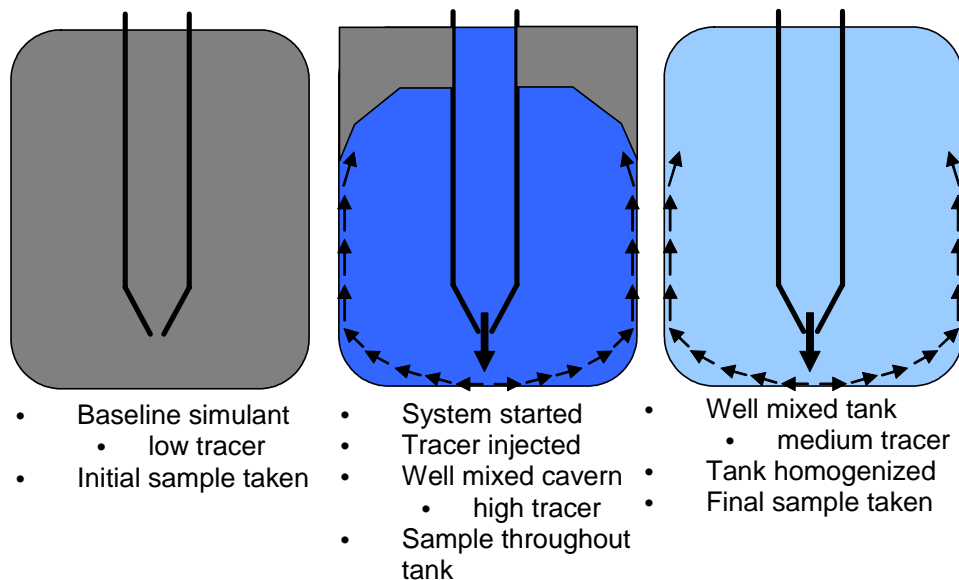


Figure 1.1. Summary of Tracer Dye Technique Steps

The size of the turbulent mixing cavern (i.e., mixing performance) in the PJM test vessels was assessed with tracer chemicals. The primary chemicals were sodium chloride (NaCl) and Food Dye Color No. 1, or Brilliant Blue FCF (BB). Initially, a sample of simulant was drawn from the test vessel to baseline the tracer levels. Next, a stock solution of the chemical being used was prepared by dissolution in water. This stock solution was then blended with a sample of the test simulant to raise the rheological properties (i.e., raise the viscosity) close to the actual test simulant. This solution was introduced into the center PJM tube during operation by opening a valve on a sample injection line during the PJM suction phase. During the drive phase, the valve was closed, and the injected dye was driven from the PJM tube. Using this procedure allowed for the gradual introduction of the tracer dye into the system over several drive/suction cycles and minimized the potential for a large amount of concentrated tracer to enter a stagnant region of the tank. This mechanism can occur if the concentrated tracer has significantly different physical properties from the bulk simulant. Such physical properties include density, entrained air due to surface tension, and rheological parameters. A schematic summary of the steps involved in using the tracer dye technique is shown in Figure 1.1.

The multiphase simulant used in the pulse jet mixing task was a suspension of kaolin and bentonite clays in water. This suspension was formulated such that certain rheological objectives were achieved. The basic formulation was a ratio of 3:1 dry kaolin:bentonite mixed to 27 wt% with water. The development of this simulant is discussed in detail in a separate report. This simulant is referred to as “kaolin:bentonite” throughout the report. The transparent simulant used was a dispersion of 2% Laponite in water. Laponite is a synthetic clay mineral produced by heat processing of a proprietary gel. Crystallizing the gel produces nanoscale crystals in the form of platelets that are approximately 1 nm thick and 25 nm across. When dispersed in water, Laponite forms transparent slurries. The transparency is a result of the small (colloidal) particle size. The slurries are thixotropic. They flow when subjected to shear stress and turn to stable gels at rest.

The objective of this work was to develop tracer methods for assessing the fraction mixed in mixing experiments. To accomplish this, several dyes were tested in preliminary trials to decide which was best suited for the purposes of these experiments. Calibration curves of the dyes that were chosen as the best candidates were made in water and Laponite. Based on the results of these tests, BB and Ethyl Orange were chosen as the primary tracer dyes for the percent mixing tests. A study of dye absorption kinetics was made with BB on the Kaolin:Bentonite simulant to determine the contact time needed to allow the BB to reach an equilibrium with the simulant. Dye adsorption isotherms were made to determine the distribution coefficients ( $K_d$ ) needed to calculate the extent of mixing.

## 2.0 Quality Requirements

Battelle—Pacific Northwest Division (PNWD) implements the River Protection Project (RPP)-WTP quality requirements by performing work in accordance with the PNWD Waste Treatment Plant Support Project quality assurance project plan (QAPjP) approved by the RPP-WTP Quality Assurance (QA) organization. This work will be performed to the quality requirements of NQA-1-1989 Part I, Basic and Supplementary Requirements, and NQA-2a-1990, Part 2.7. These quality requirements are implemented through PNWD's *Waste Treatment Plant Support Project (WTPSP) Quality Assurance Requirements and Description Manual*. The analytical requirements are implemented through WTPSP's Statement of Work (WTPSP-SOW-005) with the Radiochemical Processing Laboratory (RPL) Analytical Service Operations (ASO).

Experiments that are not method-specific were performed in accordance with PNWD's procedures QA-RPP-WTP-1101 "Scientific Investigations" and QA-RPP-WTP-1201 "Calibration Control System" verifying that sufficient data were taken with properly calibrated measuring and test equipment (M&TE) to obtain quality results.

PNWD addresses internal verification and validation activities by conducting an independent technical review of the final data report in accordance with PNWD's procedure QA-RPP-WTP-604. This review verifies that the reported results are traceable, that inferences and conclusions are soundly based, and that the reported work satisfies the Test Plan objectives. This review procedure is part of PNWD's *WTPSP Quality Assurance*

### 3.0 Mass Balance Equations

Two sets of equations have been developed to determine the extent of mixing in a vessel. The first equation discussed involves taking multiple samples at the beginning, middle, and end of the tests as discussed in Section 1.0. As will be shown in this section, this equation has the advantage of not relying on information specific to the simulant and test. For example, knowledge of the quantity of tracer used, the density of the simulant, the mass of the bulk simulant tested, the mass fraction of solids in the simulant, and the adsorption characteristics is not required. However, this equation requires that the bulk simulant be thoroughly mixed at the beginning and end of testing.

A second set of equations can also be derived that only uses a single measurement of tracer concentration from the mixing cavern. This equation requires knowledge of the quantity of tracer used, the density of the simulant, the mass fraction of solids in the simulant, and the adsorption characteristics. Consequently, the choice of equation produces a tradeoff between test knowledge and experimental techniques. It was discovered that the multiple sample technique produced the most reliable results and will be the focus of this report.

#### 3.1 Multiple Sample Equations

An equation used to calculate the fraction mixed is shown below:

$$X = \frac{V_{cavern}}{V_{tank}} \quad (3.1)$$

where  $V_{cavern}$  is the volume of the mixing cavern, and  $V_{tank}$  is the volume of the tank contents.

Using the definition of concentration, the equation can be rewritten as follows:

$$X = \frac{\left( \frac{m_{tracer}}{\rho_{sim} C_{cavern}} \right)}{\left( \frac{m_{tracer}}{\rho_{sim} C_{tank}} \right)} = \frac{C_{tank}}{C_{cavern}} \quad (3.2)$$

where  $m_{tracer}$  = mass of tracer added to the mixing cavern

$C_{cavern}$  = mixing cavern concentration of the tracer on a mass tracer to mass of simulant basis

$C_{tank}$  = tracer concentration after the entire tank contents have been homogenized on a mass tracer to mass of simulant basis

$\rho_{sim}$  = bulk density of the simulant.

If an initial amount of tracer is present at the beginning of the test, this concentration must be subtracted from the measured concentrations. Consequently, the equation can be written as follows:

$$X_j = \frac{C_f - C_0}{C_j - C_0} \quad (3.3)$$

where  $X_j$  = fraction mixed of the j-th tank sample  
 $C_f$  = tracer concentration of the final homogenized simulant  
 $C_0$  = tracer concentration of the initial baseline simulant  
 $C_j$  = tracer concentration of the j-th tank sample.

In a two-phase system (e.g., a slurry simulant), tracer absorption onto the solid phase must be considered. When the aqueous-phase tracer does not absorb onto the solid phase, the liquid-phase concentration can be measured with analytical measurement techniques, and Equation 3.3 can be used to directly calculate the fraction of the tank mixed. Unfortunately, often the tracer absorbs onto the clay particles in significant quantity. In this situation, Equation 3.3 still applies, but the concentrations used in the equation must account for both the liquid and solid phases. This is accomplished with the following equation:

$$C = Y_l C_l + Y_s C_s \quad (3.4)$$

where  $C$  = tracer concentration  
 $C_l$  = tracer concentration of the liquid phase  
 $C_s$  = tracer concentration of the solid phase  
 $Y_l$  = liquid phase mass fraction  
 $Y_s$  = solid phase mass fraction.

The distribution of tracer between the liquid and solid phases is typically described with a distribution coefficient as follows:

$$C_s = K_d C_l \quad (3.5)$$

where  $K_d$  is the distribution coefficient.

To complicate matters further, the distribution coefficient is also a function of liquid-phase dye concentration. When Equations 3.4 and 3.5 are substituted in Equation 3.3, the following equation results:

$$X_j = \frac{Y_l (C_f - C_0) + Y_s (K_{df} C_f - K_{do} C_0)}{Y_l (C_j - C_0) + Y_s (K_{dj} C_j - K_{do} C_0)} \quad (3.6)$$

where  $K_{df}$  is the distribution coefficient at the homogenized tank tracer concentration,  $K_{do}$  is the distribution coefficient at the initial baseline tracer concentration, and  $K_{dj}$  is the distribution coefficient at the j-th tank sample tracer concentration.

When  $K_d$  is null or constant, Equation 3.6 reduces to Equation 3.3. Note that as  $C_j$  approaches  $C_f$ , then  $K_{dj}$  approaches  $K_{df}$ , and the error associated in using Equation 3.3 approaches zero. This is

equivalent to stating that over a small tracer concentration range, the assumption of a constant distribution coefficient may be considered valid, and Equation 3.3 can be used. In addition, the distribution coefficient function will vary from batch to batch of simulant, and other factors, such as temperature and contact time, will also have an effect on the distribution coefficient function. These issues are considered later in this report. Lastly, the solid loading of the simulant was often varied for rheological purposes. For these reasons, Equation 3.3 is used as the primary equation to estimate the fraction mixed using tracer techniques.

### 3.2 Mass of Tracer Equation

Using the definition of concentration, the equation to calculate the fraction mixed, Equation 3.1, can be rewritten as follows:

$$X = \frac{\left( \frac{m_{tracer}}{\rho_{sim} C_{cavern}} \right)}{V_{tank}} = \frac{m_{tracer}}{\rho_{sim} V_{tank} C_{cavern}} \quad (3.7)$$

where  $m_{tracer}$  is the mass of tracer added to the mixing cavern,  $C_{cavern}$  is the mixing cavern concentration of the tracer on a mass of tracer to mass of simulant basis, and  $\rho_{sim}$  is the bulk density of the simulant.

If an initial amount of tracer is present at the beginning of the test, this concentration must be subtracted from the measured concentrations. Consequently, the equation can be written as follows:

$$X_j = \frac{m_{tracer}}{\rho_{sim} V_{tank} (C_j - C_0)} \quad (3.8)$$

where  $X_j$  = fraction mixed of the j-th tank sample  
 $m_{tracer}$  = mass of tracer added to the mixing cavern  
 $C_0$  = tracer concentration of the initial baseline simulant  
 $C_j$  = tracer concentration of the j-th tank sample  
 $V_{tank}$  = volume of the tank contents  
 $\rho_{sim}$  = bulk density of the simulant.

For multiphase simulants (i.e., slurries), tracer adsorption must again be considered. Substituting Equations 3.4 and 3.5 results in the following:

$$X_j = \frac{m_{tracer}}{\rho_{sim} V_{tank} [Y_l (C_j - C_0) + Y_s (K_{dj} C_j - K_{do} C_0)]} \quad (3.9)$$

where  $X_j$  = fraction mixed of the j-th tank sample  
 $m_{tracer}$  = mass of tracer added to the mixing cavern  
 $C_0$  = tracer concentration of the initial baseline simulant  
 $C_j$  = tracer concentration of the j-th tank sample  
 $V_{tank}$  = volume of the tank contents  
 $K_{do}$  = distribution coefficient at the initial baseline tracer concentration  
 $K_{dj}$  = distribution coefficient at the j-th tank sample tracer concentration  
 $\rho_{sim}$  = bulk density of the simulant  
 $Y_s$  = solid phase mass fraction.

In this case, the adsorption properties and mass fraction of solids and liquids do not cancel. These simulant properties must be well defined for the equation to hold. Adsorption properties vary with time, temperature, and simulant batch. During testing, the mass fraction of solids was often varied to achieve various rheological conditions. For these reasons, the equation presented above is much more difficult to implement and was not used as the primary method for determining mixing performance.

## 4.0 Application to Transparent Simulants

Optical dye samples were analyzed with an ultraviolet-visible (UV-vis) spectrometer (model USB2000; Ocean Optics Inc. Dunedin, FL, USA). This spectrometer consists of a 2048-element linear charged coupled device (CCD)-array detector. Light is transmitted through a single-strand optical fiber and through the sample cell. The light then disperses via a fixed grating across the linear CCD array detector, which is responsive in a wavelength range of 200 to 1100 nm. This signal is then converted to an absorbance value, and an absorption peak is obtained for each of the analytes of interest. According to Beer's law (Skoog et al. 1988), the magnitude of this absorbance peak is directly proportional to the concentration of dye in the system. Beer's Law states:

$$A = abc \quad (4.1)$$

where  $A$  = Absorbance (dimensionless)—measured  
 $a$  = absorbtivity ( $\text{kg mg}^{-1} \text{cm}^{-1}$ )—determined from calibration curve  
 $b$  = path length of the cell (cm)  
 $c$  = concentration of the solute ( $\text{mg kg}^{-1}$ )—known for calibration curve measurement; solved for mixing volume estimate.

The concentration of dye in an aqueous sample can be determined by applying Beer's Law. The first step in obtaining this correlation is to make a calibration curve of each dye in the solvents of interest (i.e., water, laponite, and Kaolin:Bentonite simulant). By measuring the absorbance of several known dye concentrations and plotting the resultant absorbance vs. concentration data, a calibration curve is obtained that can be used to determine the concentration of an unknown sample.

Several dyes (Green 1990) were used in preliminary trials to determine which would be best suited for the purposes of these experiments. The dyes and their wavelength of maximum absorption ( $\lambda_{\text{max}}$ ) are shown in Table 4.1.

**Table 4.1. Dyes Used in Preliminary Trials**

Dye	$\lambda_{\text{max}}$ (nm)	Solvent
Bromocresol Purple	585	NaOH
Congo Red	497	Water
Ethyl Orange	474	Water
Methyl Orange	507	Water + 0.5 mL 0.1 M HCl
Malachite Green	614	Water
Fluorescein	489	Water

Bromocresol Purple was eliminated because it is colorless in water. Methyl Orange was eliminated because it has a broad peak that is not well defined in water. Malachite Green was not used because it is colorless in basic solutions. The three remaining dyes all have maximum absorbance in the same region (474 to 497 nm) and have overlapping spectra. We wanted to be able to run tests with more than one dye; we therefore needed a dye with an absorbance outside of this region. The dye that was decided upon was

BB ( $\lambda_{\max} = 631$  nm in water). Of the remaining three dyes, Fluorescein was chosen because of its narrow, well-defined peak.

The absorbance value obtained from the spectrometer is proportional to concentration (see Equation 4.1), and Equation 3.3 can be rewritten for the BB tracer as follows:

$$X_j = \frac{A_f - A_0}{A_j - A_0} \quad (4.2)$$

where  $X_j$  = fraction mixed of the j-th tank sample  
 $A_f$  = optical absorbance of the final homogenized simulant  
 $A_0$  = optical absorbance of the initial baseline simulant  
 $A_j$  = optical absorbance of the j-th tank sample.

A calibration curve of BB in water was made by preparing several solutions of varying concentrations of BB. The absorbance of these samples was then measured and plotted against concentration. The data in this Beer's Law plot was fit with a linear regression. The concentrations and absorbance values of the samples are shown in Table 4.2. The Beer's Law plot is shown in Figure 4.1. The correlation shown in Figure 4.1 can be used to determine the concentration of dye in an aqueous sample. The results are only valid over a certain region of dye concentration. From visual inspection of Figure 4.1, the linear region is present up to an absorbance value of 1.5 (~9 ppm BB). When the dye concentration is above this level, the sample must be diluted with water and re-measured. The original dye concentration can be calculated by knowing the quantity of water used for the dilution.

**Table 4.2. Samples for Calibration Curve of BB in Water**

Sample ID	Conc. (mg/kg)	Absorbance
31A	7.69	1.209
31B	6.92	1.090
31C	6.14	0.960
31D	5.40	0.850
31E	4.61	0.721
31F	3.86	0.600
31G	3.08	0.485
31H	2.31	0.364
31I	1.55	0.238
31J	0.77	0.115
31M	15.70	2.276
31N	7.91	1.236
31O	11.65	1.770
31V	13.16	1.943
31W	14.27	2.093
31X	19.74	2.619
31Y	23.86	2.779
31Z	27.75	2.822

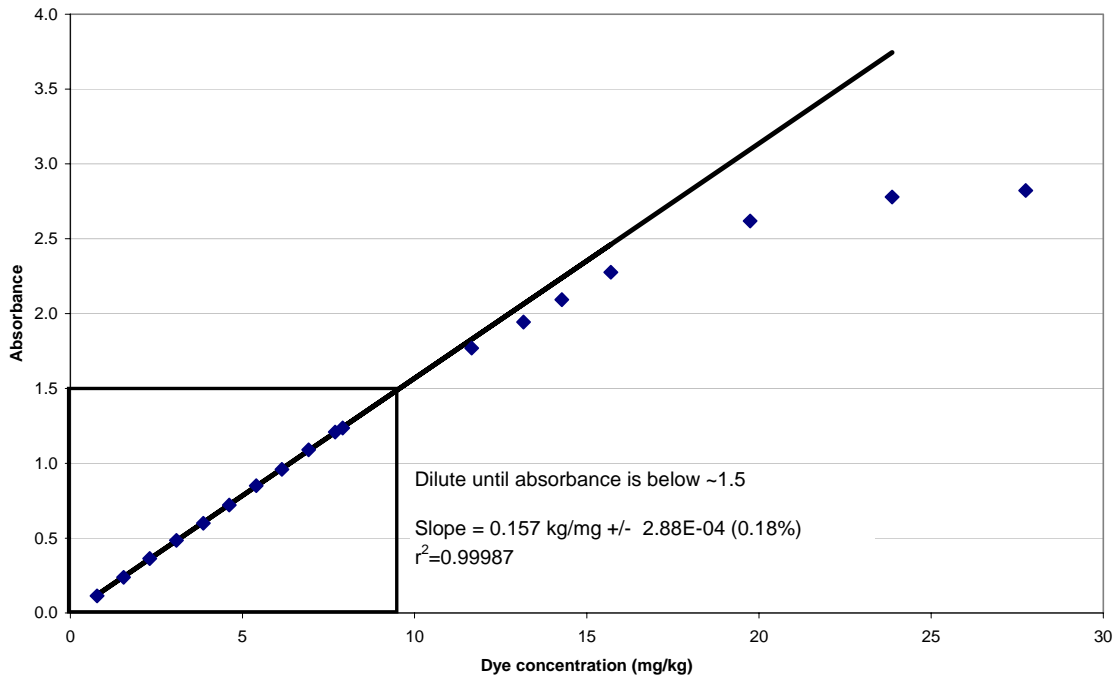


**Figure 4.1. Beer's Law Correlation of Optical Absorbance to BB Dye Concentration in Water**

The same experiment was carried out for Fluorescein in water. However, for Fluorescein, there was a great deal of scatter in the data, and a poor linear fit was obtained. A second series of Fluorescein samples was made to see if a better fit could be obtained. This set of data also had a great deal of scatter and differed greatly from the first set of samples. Data for these two sample sets are shown in Table 4.3. A new bottle of Fluorescein was purchased to determine if the scatter was caused by degraded Fluorescein. Two more sets of samples were made with the new Fluorescein, and it was concluded that Fluorescein did not have the good reproducibility that BB does. Data for all four sets of Fluorescein are plotted in Figure 4.2. Data for the sample sets with the new Fluorescein are shown in Table 4.4. In the meantime, another set of samples was made with the BB to determine the reproducibility. Data for this second set of samples are shown in Table 4.5 and are plotted together with the first set of data in Figure 4.2.

As can be seen in Figure 4.2, the absorbance values for the first two sets of data, made from the older bottle of Fluorescein, differ greatly, with the difference getting much larger at higher concentrations. While the two sets of samples made with the newer bottle of Fluorescein are much closer to one another, there is still more scatter in these sets of data than with the BB, as witnessed by the lower  $R^2$  values.

However, as can be seen in Figure 4.3, the sample sets made with BB overlap almost exactly, with more separation again being seen at higher values of absorbance. However, these differences are far above the linear Beer's Law region of the plot.

**Table 4.3. Samples for Calibration Curve of Fluorescein in Water—  
Using Old Bottle of Fluorescein**

Sample ID	Conc. (mg/kg)	Absorbance	Sample ID	Conc. mg/kg)	Absorbance
32C	36.80	2.214	41B	37.14	2.406
32D	18.40	1.428	41C	33.45	2.400
32E	11.10	0.633	41D	27.84	2.360
32F	3.66	0.200	41E	22.28	2.312
32G	3.28	0.169	41F	16.29	1.932
32H	2.56	0.120	41G	11.40	1.489
32I	1.82	0.081	41H	5.53	0.533
32J	0.73	0.039	41I	3.32	0.306
32K	21.67	0.988	41J	2.73	0.196
32L	25.36	1.185	41K	1.85	0.129
32M	28.79	1.564	41L	0.92	0.061
32N	32.89	1.628			
32O	12.98	0.788			
32P	14.86	0.806			
32Q	16.74	0.790			
32R	5.57	0.231			
32S	7.41	0.253			
32T	9.26	0.430			

**Table 4.4. Samples for Calibration Curve of Fluorescein in Water—  
Using New Bottle of Fluorescein**

Sample ID	Conc. (mg/kg)	Absorbance	Sample ID	Conc. (mg/kg)	Absorbance
45A	455.30	2.080	49A	444.01	2.452
45B	45.15	2.061	49B	42.52	2.351
45C	22.58	1.867	49C	22.05	2.126
45D	14.75	1.321	49D	13.96	1.527
45E	11.18	1.112	49E	10.61	1.208
45F	10.16	0.907	49F	8.50	0.701
45G	8.99	0.843	49G	6.36	0.543
45H	7.86	0.704	49H	5.31	0.493
45I	6.74	0.627	49I	4.21	0.299
45J	5.61	0.436	49J	2.66	0.158
45K	4.48	0.349	49K	1.66	0.095
45L	3.38	0.262	49L	1.11	0.068
45M	2.81	0.245			
45N	2.24	0.175			
45O	1.69	0.126			
45P	1.12	0.101			

**Table 4.5. Samples for Calibration Curve of BB in Water**

Sample ID	Conc. (mg/kg)	Absorbance
43B	312.38	2.908
43C	27.35	2.732
43D	23.39	2.677
43E	19.50	2.521
43F	15.62	2.213
43G	14.19	2.052
43H	12.53	1.849
43I	11.65	1.742
43J	10.62	1.602
43K	8.88	1.355
43L	7.60	1.160
43M	6.82	1.045
43N	6.03	0.927
43O	5.29	0.814
43P	4.51	0.696
43Q	3.73	0.573
43R	3.03	0.467
43S	2.27	0.346
43T	1.51	0.229
43U	0.75	0.113

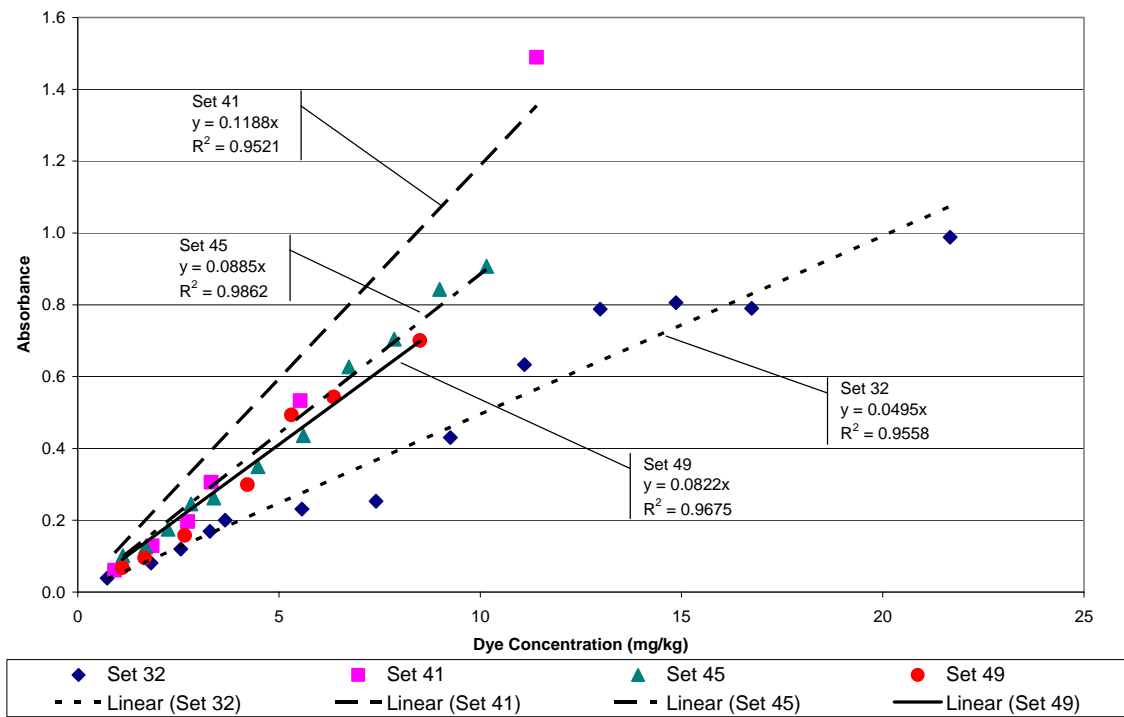


Figure 4.2. Beer's Law Correlation of Optical Absorbance to Fluorescein Concentration in Water

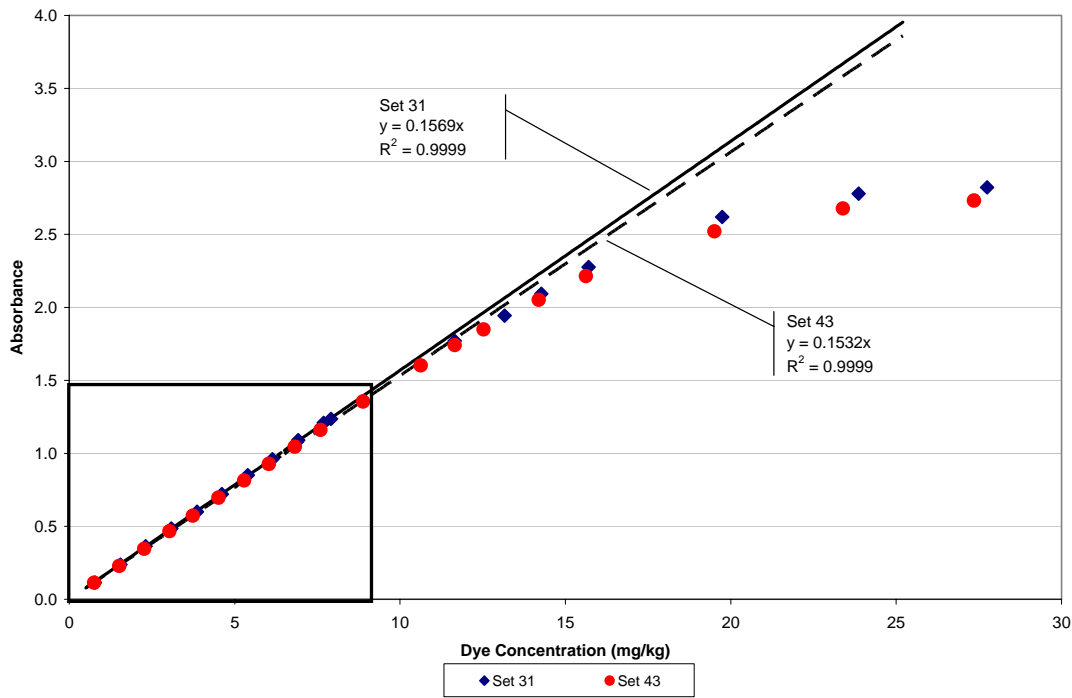
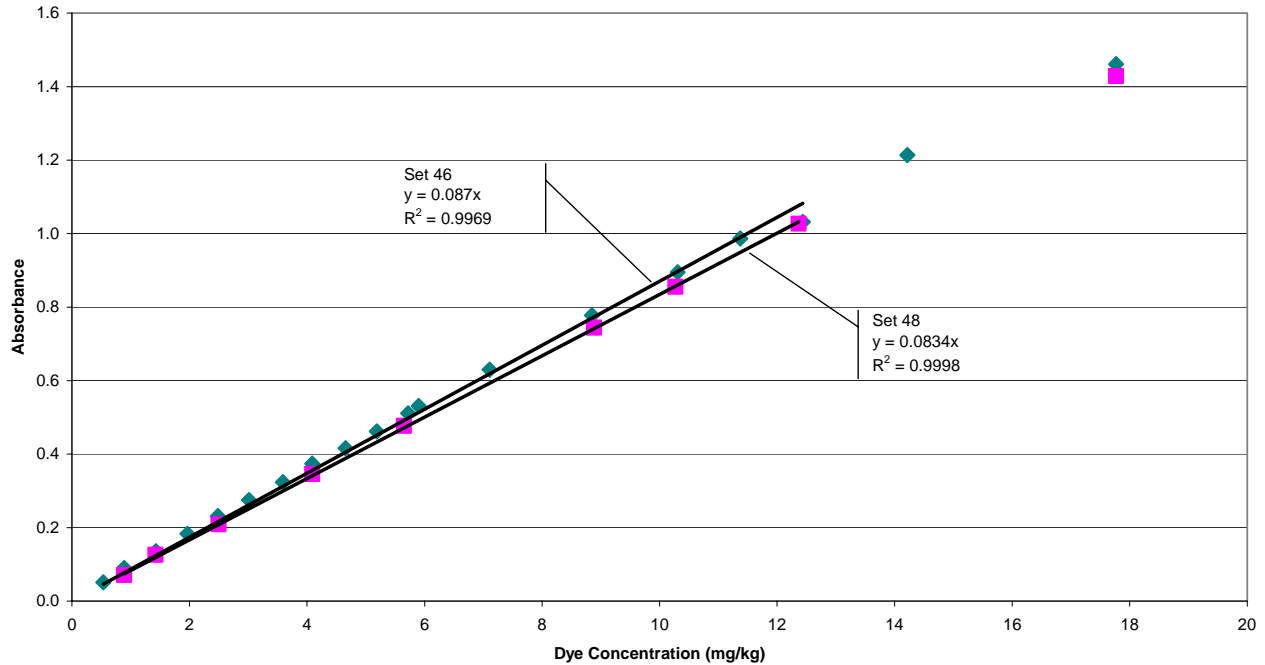


Figure 4.3. Beer's Law Correlation of Optical Absorbance to BB Dye Concentration in Water for both Sample Sets

A calibration curve for Ethyl Orange in water was also made. Two sets of samples were made to determine the reproducibility. Data for the two sample sets are shown in Table 4.6, and the results are plotted together in Figure 4.4. As with BB, data from the two sample sets overlap almost exactly, with more separation at higher values of absorbance.

**Table 4.6. Samples for Calibration Curve of Ethyl Orange in Water**

Sample ID	Conc. (mg/kg)	Absorbance	Sample ID	Conc. (mg/kg)	Absorbance
46C	25.02	1.851	48A	497.55	2.383
46D	8.85	0.778	48B	49.75	2.302
46E	7.11	0.63	48C	24.95	1.869
46F	5.90	0.531	48D	17.77	1.429
46G	5.72	0.511	48E	12.37	1.027
46H	5.19	0.462	48F	10.27	0.855
46I	4.66	0.416	48G	8.88	0.744
46J	4.09	0.374	48H	5.65	0.477
46K	3.59	0.324	48I	4.09	0.346
46L	3.01	0.275	48J	2.49	0.209
46M	2.48	0.231	48K	1.42	0.126
46N	1.97	0.183	48L	0.89	0.071
46O	1.43	0.136			
46P	0.89	0.09			
46Q	0.53	0.051			
46R	17.77	1.461			
46S	14.22	1.214			
46T	12.44	1.032			
46U	11.37	0.987			
46V	10.31	0.895			



**Figure 4.4. Beer's Law Correlation of Optical Absorbance to Ethyl Orange Dye Concentration in Water**

Beer's Law plots were also made for BB, Fluorescein, and Ethyl Orange in Laponite. The concentrations and absorbance values of the samples are shown in Table 4.7 through Table 4.9; and the Beer's Law plots are shown in Figure 4.5 through Figure 4.7. From the  $R^2$  values, we see that of the three dyes, BB has the least scatter and Fluorescein has the most.

**Table 4.7. Samples for Calibration Curve of BB in Laponite**

Sample ID	Conc. (mg/kg)	Absorbance
28C	11.40	1.734
28D	6.90	1.072
28F	4.15	0.682
28E	2.84	0.446
28G	1.47	0.233

**Table 4.8. Samples for Calibration Curve of Fluorescein in Laponite**

Sample ID	Conc. (mg/kg)	Absorbance
17E	14.76	1.716
17F	9.84	1.329
17G	4.92	0.699
17H	1.64	0.238

**Table 4.9. Samples for Calibration Curve of Ethyl Orange in Laponite**

Sample ID	Conc. (mg/kg)	Absorbance
14D	20.40	1.543
14E	15.30	1.202
14F	10.20	0.852
14G	5.10	0.431
14H	1.70	0.145

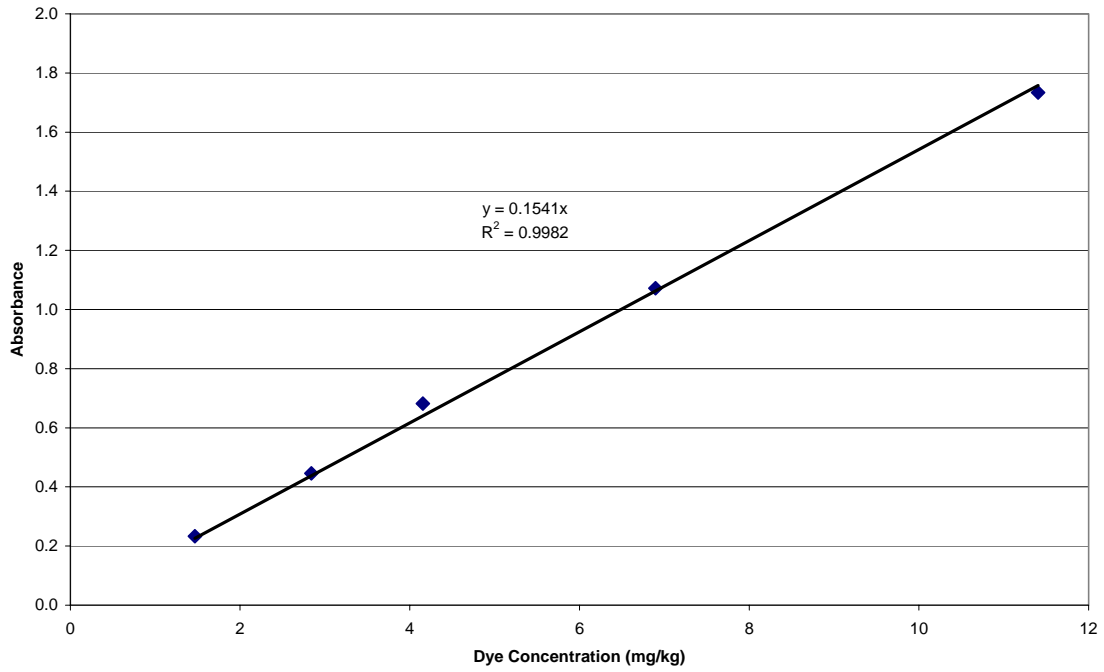


**Figure 4.5. Beer's Law Correlation of Optical Absorbance to BB Dye Concentration in Laponite**

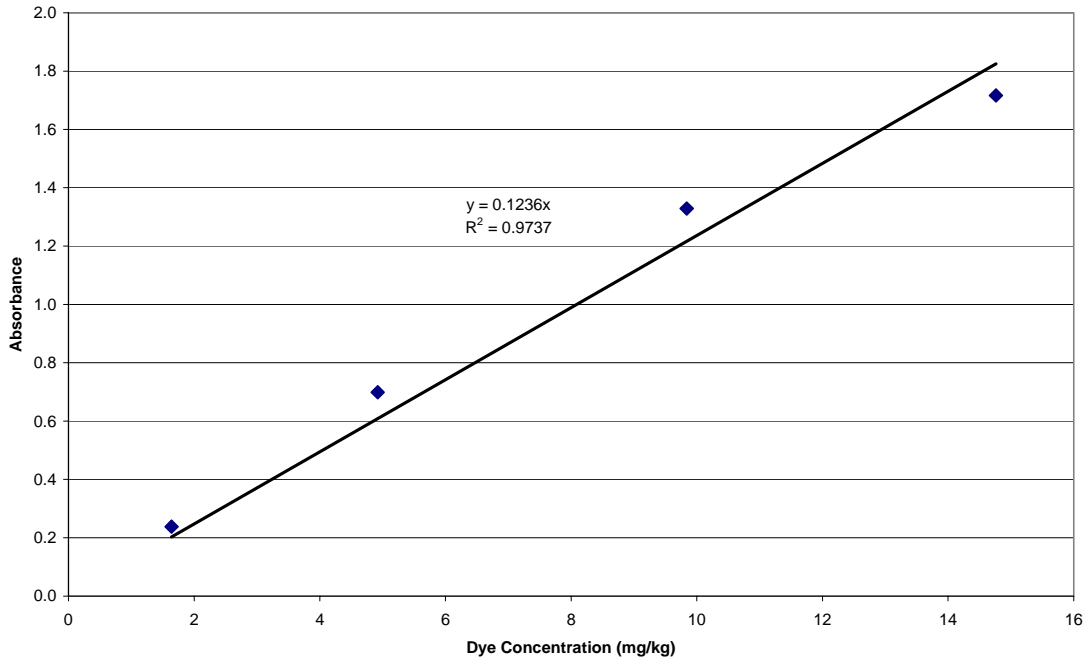


**Figure 4.6. Beer's Law Correlation of Optical Absorbance to Fluorescein Concentration in Laponite**

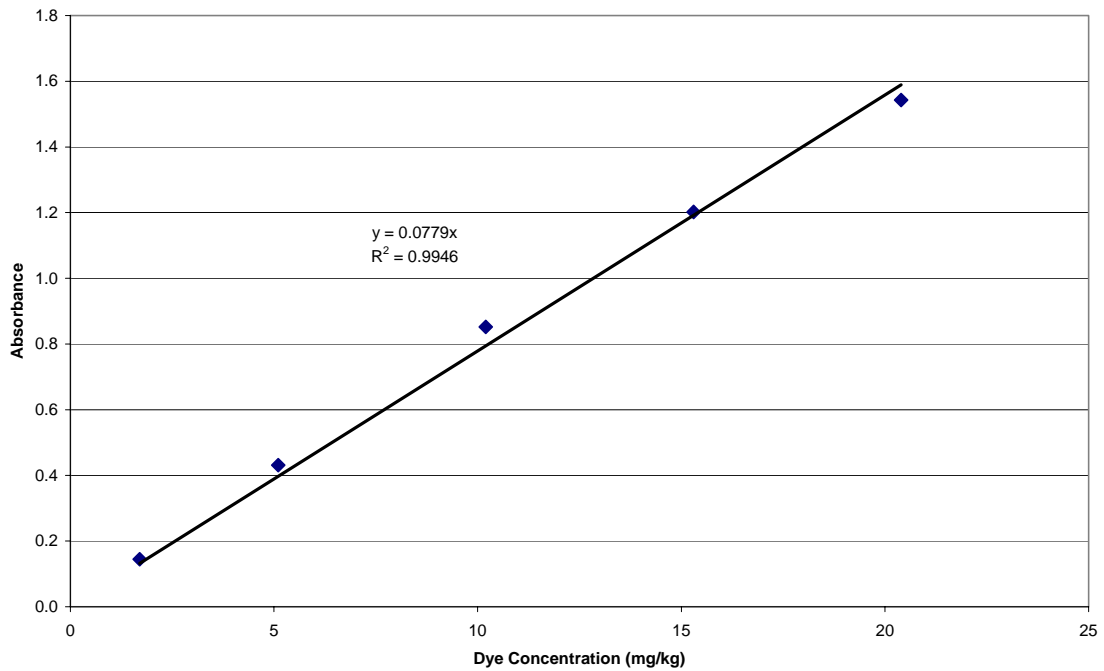


**Figure 4.7. Beer's Law correlation of optical absorbance to Ethyl Orange concentration in Laponite**

## **4.1 Tracer Development Conclusions**

Based on the absorbance result presented above, BB and Ethyl Orange are the primary tracer dyes recommended for percent mixed testing. This recommendation was based upon the linearity and reproducibility of the Beer's law results in water and laponite. The remaining dyes are recommended for visual indication of the cavern dimensions when using transparent simulants such as laponite.

## 5.0 Application to Opaque Simulants

This section extends the development of tracer methods for mixing performance to multiphase opaque simulants. The multiphase simulant used in the pulse jet mixing task was a suspension of kaolin and bentonite clays in water. This suspension was formulated such that certain rheological objectives were achieved. The basic formulation was a ratio of 3:1 dry kaolin:bentonite mixed to 27 wt% with water. The development of this simulant is discussed in detail in a separate report. This simulant is referred to as “kaolin:bentonite” throughout the report.

Because kaolin and bentonite clays are geological media, previous research on tracers in hydrology experiments could be used to shorten developmental efforts. A review of tracers for vadose zone hydrology is given by Flury and Wai (2003). Several tracers were discussed, including temperature, isotopes, inorganic ions, fluorocarbons, sulfur hexafluoride, ethanol, benzoate, fluorobenzoates, polyaromatic sulfonates, sulphonic acids, spores, microorganisms, and dyes. The discussion of these tracers involved ease of quantification, stability, interactions with other species, and toxicology. The authors recommend optical dyes and conclude that BB is the most prominent tracer dye for use in vadose zone hydrology and has been well investigated (Flury and Fluhler 1994; Flury and Fluhler 1995; Perillo et al. 1998; Fahrenhorst et al. 1999; Ketelsen and Meyer-Windel 1999). The authors also note that tracer dyes can be used in conjunction with other common inorganic ion tracers such as chloride and bromide. In this section, we discuss the use of BB and chloride ions as tracers for use with the kaolin:bentonite simulant.

### 5.1 Optical Dye

As discussed in Section 4.0, the concentration of optical dye was measured using a UV-vis spectrometer. This instrument requires that the sample be transparent. To overcome this limitation, the opaque kaolin:bentonite simulant was centrifuged, and the analysis was performed on the centrifuged liquid portion of the sample. This technique was also used by German-Heins and Flury (2000) to investigate the sorption properties of BB in soil samples. This produces the liquid-phase concentration of the tracer dye according to Beer’s law. Consequently, the concentration variables in Equation 3.6 can be replaced with absorbance.

$$X_j = \frac{Y_l(A_f - A_o) + Y_s(K_{df}A_f - K_{do}A_o)}{Y_l(A_j - A_o) + Y_s(K_{dj}A_j - K_{do}A_o)} \quad (5.1)$$

where  $K_{df}$  is the distribution coefficient at the homogenized tank tracer concentration,  $K_{do}$  is the distribution coefficient at the initial baseline tracer concentration, and  $K_{dj}$  is the distribution coefficient at the  $j$ -th tank sample tracer concentration.

As seen above, the dye adsorption is a significant parameter in this equation that must be well understood for implementation. Dye adsorption is discussed in more detail in Section 5.3. The absorption properties of BB tracer dye were investigated in enough detail for use with the opaque kaolin:bentonite simulant.

## 5.2 NaCl Tracer

To overcome the difficulties associated with evaluating results with tracers that adsorb onto the solids phase of the simulant, a second tracer was developed. This tracer is the chloride ion ( $\text{Cl}^-$ ) typically added as NaCl. Fortunately, the chloride ion was not observed adsorbing onto the simulant particles, and Equation 3.3 can be used directly for the NaCl tracer. This is consistent with previous work in hydrology (Flury and Wai 2003) where  $\text{Cl}^-$  and  $\text{Br}^-$  are considered almost ideal conservative tracers since anions rarely sorb to soil particles.

For the NaCl tracer, a chloride ion selective electrode and ion chromatography techniques were used to measure the concentration of chloride present in the samples. The ion selective electrode measures the potential difference across an electrode that is surrounded by a membrane that allows chloride ions to pass from the sample material into the electrode cell. Unlike the UV-vis absorption method, this measurement was performed directly on the simulant with no required preparation steps. However, the ion chromatography technique required the use of the centrifuged mother liquor. The evaluation of these techniques to measure the concentration of the  $\text{Cl}^-$  tracer is ongoing, but current results using the  $\text{Cl}^-$  tracer are discussed in Section 8.0 and presented in Appendix B.

## 5.3 Dye Absorption Kinetics

Equilibrium time before centrifugation must be considered before implementing the technique. Determining the rate at which the dye adsorbs onto the clay simulant involved preparing batches of kaolin:bentonite simulant with BB at two different concentrations:  $4\text{E-}06$  mmol/g (3.2 ppm) and  $1\text{E-}05$  mmol/g (7.9 ppm). Note that the molecular weight of the BB dye is 792.84 g/mol. Large batches of each concentration were made, and aliquots (10 g) of each were placed into centrifuge cones and allowed to sit for varying contact times before centrifuging. All samples were re-mixed immediately before centrifuging. After centrifuging, the supernatant liquid was removed and the absorbance measured. For each concentration of dye, a plot was made of absorbance vs. contact time. From this data, it was determined that a contact time of 24 to 48 hours before centrifuging and measuring the absorbance would be adequate time to allow the dye to equilibrate within the clay. Table 5.1 shows the contact times and absorbance values obtained. Figure 5.1 and Figure 5.2 show the resulting plots.

**Table 5.1. Contact Times and Absorbance Values for Kinetics Study**

3.2 ppm (mg/kg)		7.9 ppm (mg/kg)	
Contact Time (hr)	Absorbance	Contact Time (hr)	Absorbance
0.25	0.091	0.25	0.407
0.50	0.091	0.50	0.407
1	0.091	1	0.398
2	0.077	2	0.382
4	0.077	4	0.378
24	0.060	24	0.327
48	0.064	48	0.324

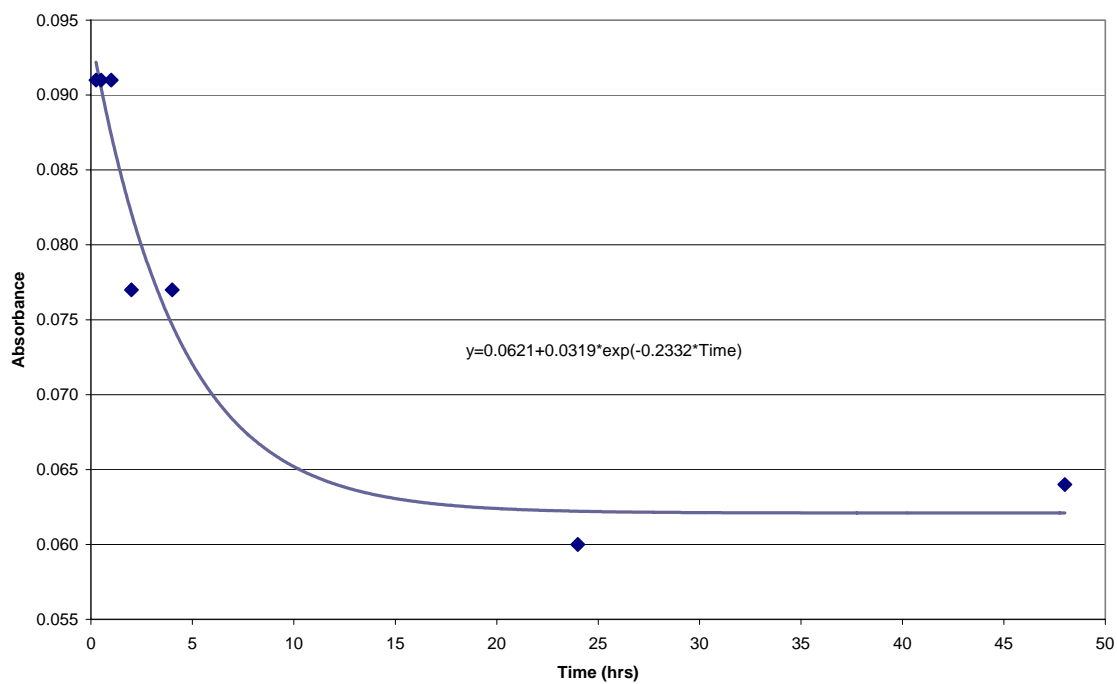


**Figure 5.1. Kinetics Plot for 3.2 ppm BB in Kaolin:Bentonite Clay**

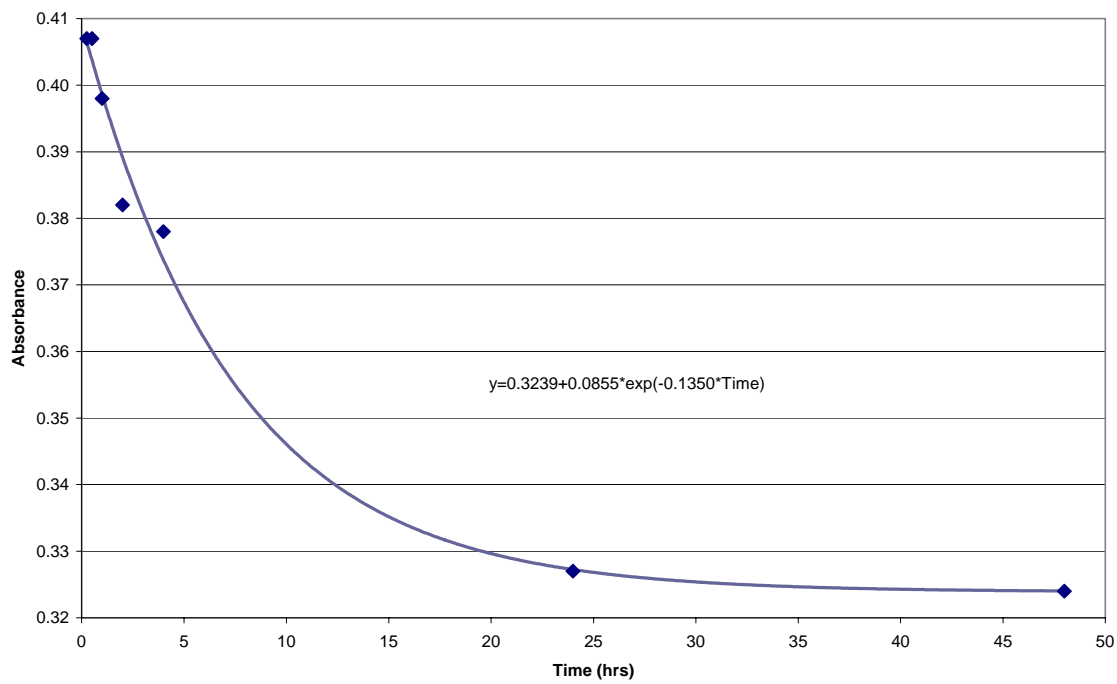


**Figure 5.2. Kinetics Plot for 7.9 ppm BB in Kaolin:Bentonite Clay**

As can be seen from the plots, there is an exponential decrease in absorbance. The absorbance levels stabilize between 24 and 48 hours. Consequently, a contact time of 24 to 48 hours will be sufficient to allow the dye to equilibrate with the clay. This conclusion is consistent with the observations of other researchers (German-Heins and Flury 2000; Roy 1993) of the sorption properties of BB with soil samples. These researchers observed that little difference (<1%) in the amount of dye sorbed to the soil between 24 and 48 hr contact times. Consequently, they concluded that a 24-hr contact period was sufficient to assume equilibrium.

## 5.4 Equilibrium Dye Absorption

BB Dye sorption onto soil media has been previously investigated by other researchers (German-Heins and Flury 2000; Fahrenhorst et al. 1999; Ketelsen and Meyer-Windel 1999). It was found that the sorption properties of the BB dye followed the Langmuir isotherm model as given by:

$$C_s = \frac{bK_L C_l}{1 + K_L C_l} \quad (5.2)$$

where  $C_s$  = concentration of dye sorbed onto the solid phase  
 $b$  = maximum amount of dye that can be adsorbed per unit mass of adsorbent  
 $K_L$  = constant relating to the affinity between the sorbate and sorbent  
 $C_L$  = concentration of dye in liquid phase.

At low dye concentrations,  $1 \gg K_L C_L$ , and Equation 5.2 reduces to  $C_s = b K_L C_L$ , which is equivalent to Equation 3.5 where  $K_d = b K_L$ . Consequently, at low dye concentrations, the isotherm predicts a linear region. At high dye concentrations, the L'Hopitals rule can be applied to show that  $\lim_{C_L \rightarrow \infty} C_s = b$ .

Consequently, when one plots  $C_L$  against  $C_s$ , the shape of the Langmuir isotherm is a linear region going through the origin that transforms to a constant value at high dye concentrations.

BB dye adsorption isotherms were prepared at ambient temperature (nominally 20 to 25°C) in a temperature-controlled room. This was achieved by performing a mass balance on several sets of samples described below. The first step in this mass balance was to prepare a stock solution of 1.69E-02 mmol/g BB in water. This stock solution was mixed with clay to make a stock solution of 3.85E-03 mmol/g BB in kaolin:bentonite simulant. This stock solution was then used to make several samples of dye in clay. Each sample was weighed and the mass recorded. After allowing all the samples to sit for 48 hours<sup>(a)</sup> for the dye to equilibrate with the clay, the samples were centrifuged and the liquid decanted. The absorbance of the liquid was then measured. Using the absorbance of each sample and the equation from the linear fit, we obtained from the Beer's Law plot of BB,

$$ab = 0.157 \text{ kg/mg} \quad (5.3)$$

The concentration in the liquid was determined as follows:

---

(a) This time frame was chosen based on results shown in Section 5.3.

$$C_L = \frac{A}{ab} \quad (5.4)$$

where  $C_L$  is the concentration of dye in liquid fraction (mg/kg), and  $A$  is the absorbance (dimensionless).

Using this equation, the concentration of dye in the liquid fraction (in mg dye/kg clay) of the sample can be calculated. From the simulant recipe, the clay simulant is approximately 75% water and 25% solids; the mass of each sample can be used to determine the mass of water and solids in each sample.

$$M_w = 0.75 \times M_C \quad (5.5)$$

$$M_s = 0.25 \times M_C \quad (5.6)$$

where  $M_w$  is the mass of H<sub>2</sub>O (g),  $M_s$  is the mass of solids (g), and  $M_C$  is the mass of clay sample (g).

The initial mass of dye in each sample can be calculated by using the concentration of dye in the original sample, the mass of the original sample, and the molecular weight of the dye:

$$M_{D,i} = \frac{C_i M_w}{1000} \quad (5.7)$$

where  $M_{D,i}$  is the initial mass of dye in the sample (mg) and  $C_i$  is the concentration of dye in the original sample (mg/kg).

Next, we need to calculate the mass of dye in water after the sample was centrifuged:

$$M_{D,W} = C_L M_w \quad (5.8)$$

where  $M_{D,W}$  is the final mass of dye in water fraction (mg).

Then the mass of dye in the solid fraction of the sample can be determined as follows:

$$M_{D,S} = M_{D,i} - M_{D,W} \quad (5.9)$$

where  $M_{D,S}$  is the final mass of dye in solid fraction (mg).

Finally, the concentration of dye in the solid and liquid fractions needs to be determined to plot the isotherm. This value,  $C_L$ , has already been calculated for the liquid fraction. For the solid fraction,

$$C_S = \frac{M_{D,S}}{M_S} \quad (5.10)$$

where  $C_S$  is the concentration of dye in solid fraction (mg/kg).

By plotting the dye concentration in the solid fraction vs. dye concentration in the liquid fraction over our experimental operating range<sup>(a)</sup>, we obtain the isotherm, plotted in Figure 5.3. Distribution coefficients ( $K_d$ ) needed for the calculation of extent of mixing from Equation 3.6 are simply the ratio of  $C_S$  to  $C_L$  at each point on the curve. Examination of the curves in Figure 5.3 reveals that absorption of dye onto the surface of the clay particles can be estimated through a linear approximation. Because of batch-to-batch variations of the clay composition, small differences in the amount of dye absorbed were measured from sample to sample. The linear-isotherm assumption allows for the calculation of percent mixed in a PJM test using the simplified Equation 4.2.

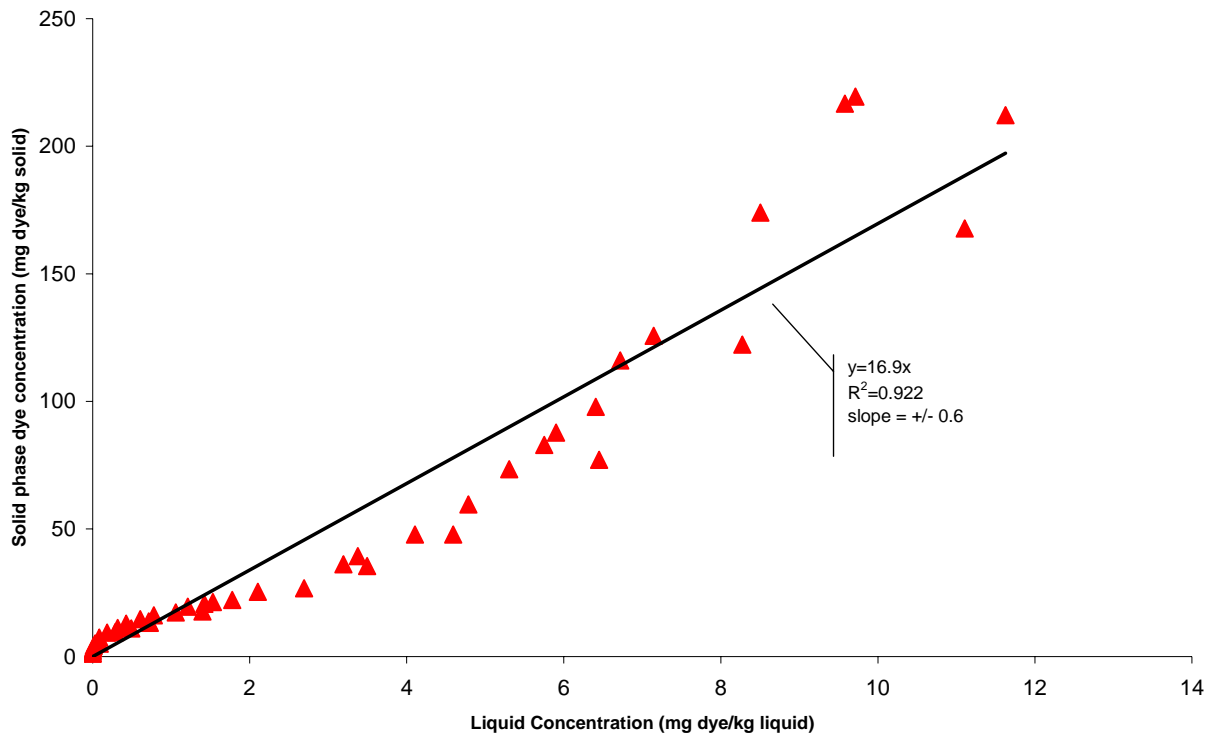


**Figure 5.3. Linear Fit of Isotherm Data over the Linear Beer's Law Region**

This isotherm result is consistent with previously published data on dye absorption in soils. German-Heins and Flury (2000) present Langmuir isotherm parameters for several sets of soil samples and BB dye solution. These results are plotted against the isotherm data for the BB and Kaolin:Bentonite system discussed above (this includes data that extends beyond the experimental operating range; see Figure 5.4). This figure illustrates that the dye concentrations used during the experiment (0 to 10 ppm in the liquid phase) are in the linear region approximation of the Langmuir isotherm model. Ketelsen and Meyer-Windell (1999) observe that for soil samples, the parameter  $b$  increases with clay concentration. Since the kaolin:bentonite simulant is 100% clay, one would expect a relatively large value for  $b$ . From the data point at a liquid-phase concentration of approximately 1200 ppm BB, one can see that the parameter  $b$  is

(a) 0 to 10 ppm BB in the liquid phase; this experimental operating range was established due to waste disposal and Beer's Law considerations.

large compared to the other soil samples. Based on these data, one can conclude that the assumption of a linear isotherm in the region of liquid phase dye concentrations between 0 to 100 ppm is reasonable. Again, Equation 4.2 can be used with the BB dye and the kaolin:bentonite simulant with acceptable error.

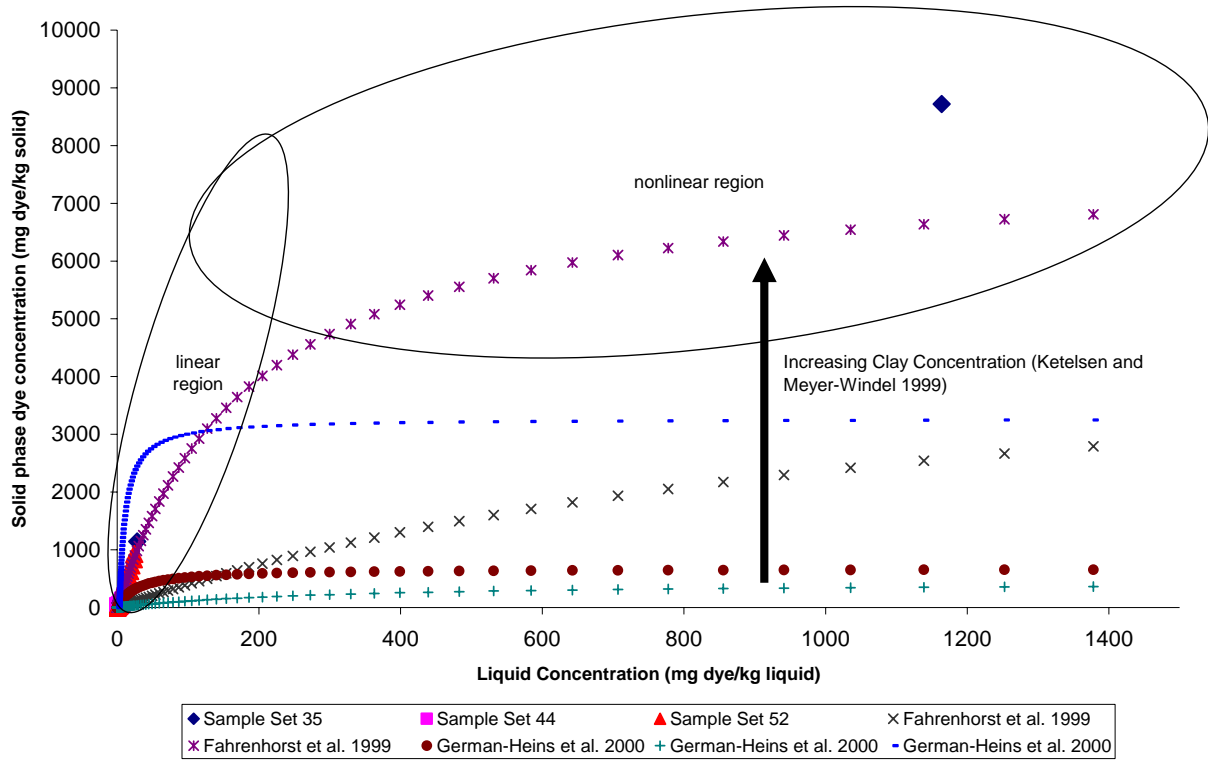


**Figure 5.4. Comparison of Measured to Published Isotherms**

## 6.0 Error Analysis

In order to analyze the data gathered from a test using the BB/kaolin:bentonite system, an estimate of the error incurred through the use of Equations 4.2 and 5.1 should be calculated. This is performed by estimating the error associated with each variable in equation 5.2 and propagating the error through the equation. After propagating the error through Equation 5.2, the following equation results,

$$\Delta X = X \left[ \frac{2(1-Y_s)^2 \Delta A^2 + Y_s^2 (A_f - A_0)^2 \Delta K_d^2 + 2Y_s^2 \Delta A^2 K_d^2}{[(1-Y_s)(A_f - A_0) + Y_s K_d (A_f - A_0)]^2} + \frac{2(1-Y_s)^2 \Delta A^2 + Y_s^2 (A_j - A_0)^2 \Delta K_d^2 + 2Y_s^2 \Delta A^2 K_d^2}{[(1-Y_s)(A_j - A_0) + Y_s K_d (A_j - A_0)]^2} \right]^{0.5} \quad (6.1)$$

where

- $\Delta X$  = error in the fraction mixed value
- $X$  = fraction mixed value
- $Y_s$  = mass fraction of solids in the slurry
- $\Delta A$  = error in absorbance measurements
- $A_0$  = initial absorbance measurement
- $A_f$  = final absorbance measurement
- $A_j$  =  $j^{\text{th}}$  sample absorbance measurement
- $\Delta K_d$  = error in the linear distribution coefficient
- $K_d$  = linear distribution coefficient

Sampling and measurement errors were estimated simultaneously by taking several samples from the tank in the same experimental fashion. The contents of the tank were homogenized such that measured differences were the result of sampling and measurement error. Using the BB dye with kaolin:bentonite simulant, in two different PJM vessels the standard deviation of the absorbance from these samples,  $\Delta A$ , was determined as shown below:

$$\Delta A = 0.008 \quad (6.2)$$

The error in the distribution coefficient can be estimated from Figure 5.3 as follows:

$$\Delta K_d = 0.6 \quad (6.3)$$

In addition, the distribution coefficient value from Figure 5.3 is approximately 16.9; the mass fraction of solids can be conservatively estimated at 0.3. The remaining variables are measured separately for each test condition.

The equations presented in this section can also be applied to different simulants and tracers. For the transparent simulant Laponite, dye adsorption is not significant, so the isotherm error can be neglected. Sampling and measurement techniques are similar, and these terms can be used as discussed above. For the Cl<sup>-</sup> tracer, sorption is not an issue as with the kaolin:bentonite simulant. Again, the isotherm terms are negligible and Equation 3.3 is used. Propagating errors through Equation 3.3 produces the following:

$$\Delta X = X \left[ \frac{\Delta(C_f - C_0)^2}{(C_f - C_0)^2} + \frac{\Delta(C_j - C_0)^2}{(C_j - C_0)^2} \right]^{0.5} \quad (6.4)$$

where  $\Delta X$  = error in the fraction mixed value  
 $X$  = fraction mixed value  
 $\Delta(C_f - C_0)$  = error in difference between final and initial concentration measurements  
 $\Delta(C_j - C_0)$  = error in difference between  $j^{\text{th}}$  sample and initial concentration measurements  
 $C_f$  = final concentration measurement  
 $C_0$  = initial concentration measurement  
 $C_j$  =  $j^{\text{th}}$  sample concentration measurement.

In a fashion similar to the estimation of error in the dye absorbance values, sampling and measurement errors were estimated simultaneously by taking several samples from the tank in the same experimental fashion. The contents of the tank were homogenized such that measured differences were the result of sampling and measurement error. Samples were measured using the ion chromatography (IC) technique. Using the chloride tracer with kaolin:bentonite simulant in two different PJM vessels, the standard deviation of the absorbance from these samples,  $\Delta C_{IC}$ , was determined as shown below:

$$\Delta C_{IC} = 4.5 \text{ ppm} \quad (6.5)$$

When IC is used as the analytical technique, Equation 6.5 can be applied in Equation 6.4 as follows:

$$\Delta X = X \left[ \frac{2\Delta C_{IC}^2}{(C_f - C_0)^2} + \frac{2\Delta C_{IC}^2}{(C_j - C_0)^2} \right]^{0.5} \quad (6.6)$$

Since the average deviation between duplicate measurements,  $\Delta C_{IC, meas}$ , is 1 ppm, this error measurement can be decoupled into a contribution due to sampling errors and measurement errors. The sampling error,  $\Delta C_{sam}$ , is calculated as:

$$\Delta C_{sam} = \sqrt{\Delta C_{IC}^2 - \Delta C_{IC, meas}^2} = 4.4 \text{ ppm} \quad (6.7)$$

For the ion-specific electrode (ISE) technique, the concentration of the tracer is calculated by fitting a set of calibration data to the following equation:

$$C_{ISE} = e^{\frac{P-b}{a}} \quad (6.8)$$

where  $C_{ISE}$  = concentration of chloride  
 $P$  = measured potential difference across ISE electrode  
 $b$  = fitting parameter  
 $a$  = fitting parameter.

Since the error due in the fitting parameters is small relative to the error in the potential measurement,  $\Delta P$ , of  $\pm 2$  mV, the resulting propagated error is as shown below:

$$\Delta C_{ISE,meas} = \frac{C}{a} \Delta P \quad (6.9)$$

The total error of using the ISE is a combination of the measurement error described by Equation 3.8 and the sampling error shown in Equation 6.7. This combined sampling and measurement error is shown below:

$$\Delta C_{ISE} = \sqrt{\left(\frac{C}{a} \Delta P\right)^2 + \Delta C_{sam}^2} \quad (6.10)$$

Using this equation, the error in the fraction mixed value can be calculated as follows:

$$\Delta X = X \left[ \frac{\left(\frac{\Delta P}{a}\right)^2 (C_f^2 + C_0^2) + 2\Delta C_{sam}^2}{(C_f - C_0)^2} + \frac{\left(\frac{\Delta P}{a}\right)^2 (C_j^2 + C_0^2) + 2\Delta C_{sam}^2}{(C_j - C_0)^2} \right]^{0.5} \quad (6.11)$$

## 7.0 Data Analysis

Using the fraction mixed equations requires that the 2-region model of a well formed turbulent mixing cavern and quiescent region hold. If samples are not taken from a turbulent mixing cavern region from either a sample location outside the mixing cavern or through a mechanism of laminar mixing cavern with concentration gradients, Equation 3.3 will produce results inconsistent with a practical fraction mixed value. For instance, when the sample concentration,  $C_j$ , is less than the final sample concentration,  $C_f$ , the fraction mixed value is greater than unity, which is not realistic. When the sample concentrations are equal to the initial test concentration,  $C_j$ , the fraction mixed approaches infinity. On a plot, these values are large enough that they cannot be observed with other samples with higher tracer concentrations. To simplify the data analysis in these situations, these data can be computed as a normalized concentration ratio referred to as the “mixing ratio.” The equation for the mixing ratio,  $MR$ , is shown below:

$$MR_j = \frac{C_f - C_j}{C_f - C_0} \quad (7.1)$$

When the sample tracer concentration is equal to the initial test concentration, the mixing ratio is unity. When the sample tracer concentration is equal to the final test concentration, the mixing ratio is zero. Lastly, when the sample tracer concentration is above the final test concentration, the mixing ratio is negative. This corresponds to a situation where the sample location is within the mixing cavern, and the fraction mixed calculation may be performed. From this information, the data analysis of mixing-ratio data is summarized by Table 7.1.

**Table 7.1. Mixing-Ratio Data Interpretation**

Mixing-Ratio Values	Description
~1	Tracer concentration near initial tracer test concentration; tracer has not reached sample location.
~0 to 1	Tracer concentration between initial and final tracer test concentration; tracer has begun to reach sample location or slow laminar mixing is occurring with large concentration gradients.
~0	Tracer concentration is near final tracer test concentration; vessel is nearly homogenous.
< ~0	Tracer concentration is above final tracer test concentration; sample location is within the mixing cavern. Fraction mixed values can be calculated.
High degree of noise	Noisy results indicate that tracer concentrations are varying in a temporal manner. This occurs when simulant with a small amount of tracer is mixing with high tracer simulant. Such results indicate transient behavior where the mixing cavern is growing or the vessel is micro-mixing previously quiescent simulant.
Low degree of noise	As micro-mixing proceeds, local concentration gradients within the vessel disappear, and samples will reach stable values. This indicates that mixing has reached a steady-state value.

Since the mixing ratio contains the same variables and information as the fraction mixed values, a transformation function between fraction mixed space and mixing-ratio space exists. This transformation function is shown below:

$$MR = 1 - \frac{1}{X} \quad (7.2)$$

A transformation function of the propagated error between fraction mixed and mixing ratio is shown below:

$$\Delta MR = \frac{\Delta X}{X^2} \quad (7.3)$$

The equations for fraction mixed described in Sections 5.4 and 6.0 can be applied to calculate mixing ratio and the corresponding errors from Equations 7.2 and 7.3, respectively.

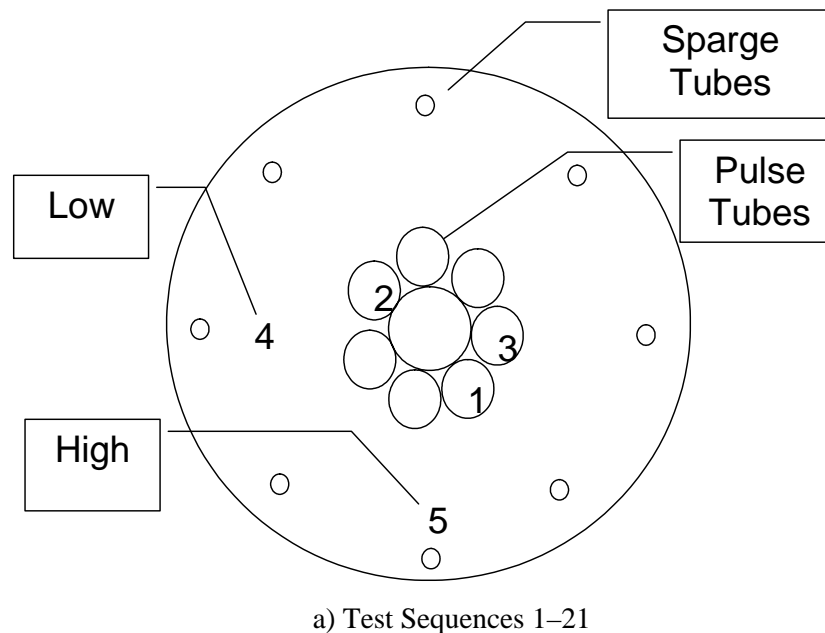
## 8.0 Test Results and Method Evaluation

Results from several PJM tests are given in Appendix A and Appendix B. Appendix A presents results from the transparent simulant tests while Appendix B presents results from the opaque simulant tests. Only raw non-interpreted data are presented in this report. Subsequent reports will describe the test conditions for each test result in Appendices A and B and evaluate the results with respect to test objectives. Such discussion is beyond the scope of this document.

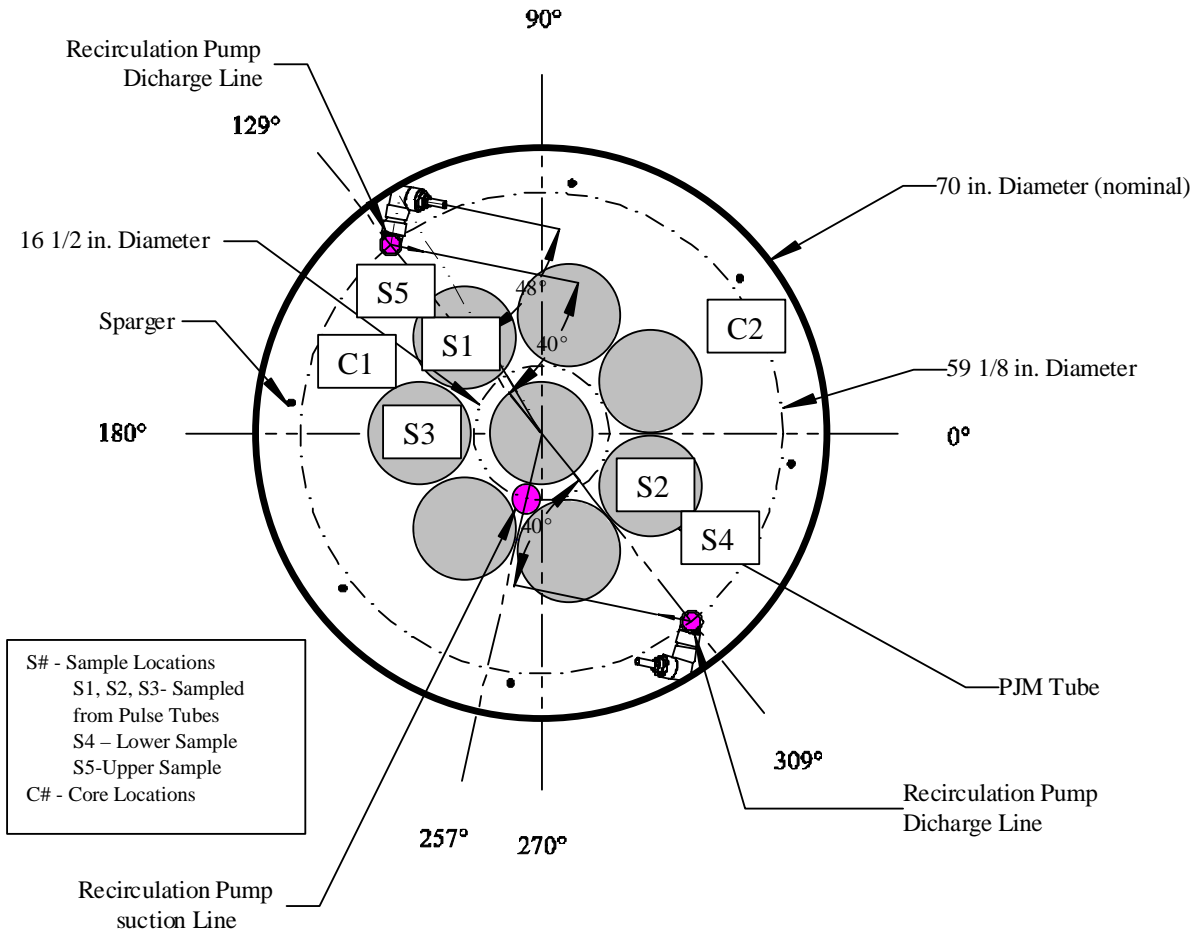
However, Appendix B presents results from a WTP-scaled prototype design effort (Phase II Scaled Test Platform Tests) that was focused on discovering configurations that will produce a fully mobilized and homogeneous vessel with kaolin:bentonite clay simulant. Results from this testing effort represent an opportunity to evaluate the performance of the tracer method in practice.

In this testing, a stock solution of the tracer is prepared by dissolution in water. This stock solution is then blended with a sample of the test simulant to raise the rheological properties close to the actual test simulant. This solution is introduced into the center PJM tube during operation through a sample injection line and peristaltic pump.

After the tracer is injected, the experimental clock starts, and samples are drawn from several locations in each test vessel. Locations 1, 2, and 3 are samples taken directly from three separate pulse tubes. These samples represent the contents of the well mixed cavern. Sample locations 4 and 5 are placed between the pulse tubes and the tank wall. Location 4 is at a low elevation, and location 5 is at a high elevation. Schematic diagrams of the tracer sampling locations are shown in Figure 8.1 and Figure 8.2 for the lag storage (LS) vessel and ultrafiltration process (UFP) vessel, respectively.

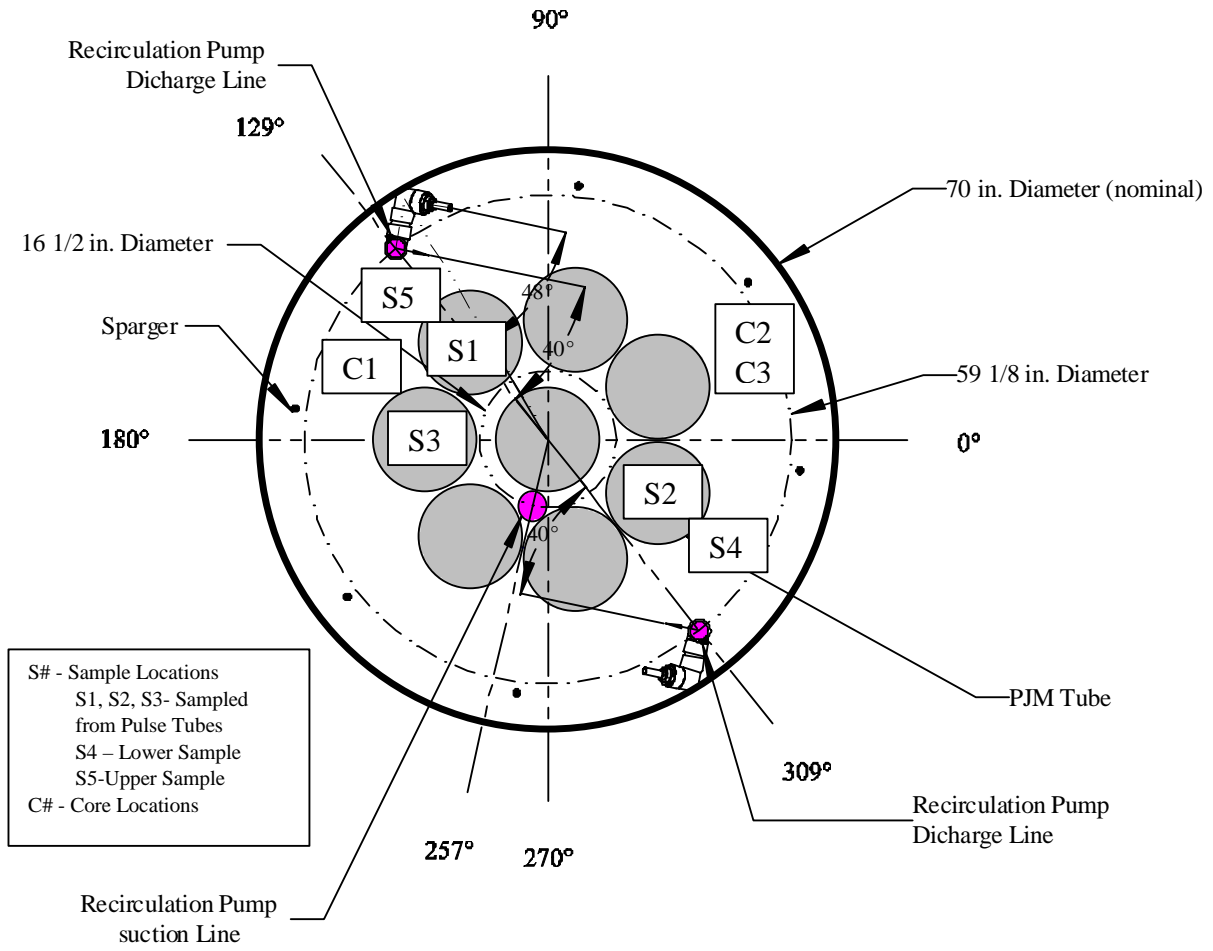


**Figure 8.1. Schematic of Lag Storage Vessel Tracer Sampling Locations During Phase II Scaled Test Platform Tests**



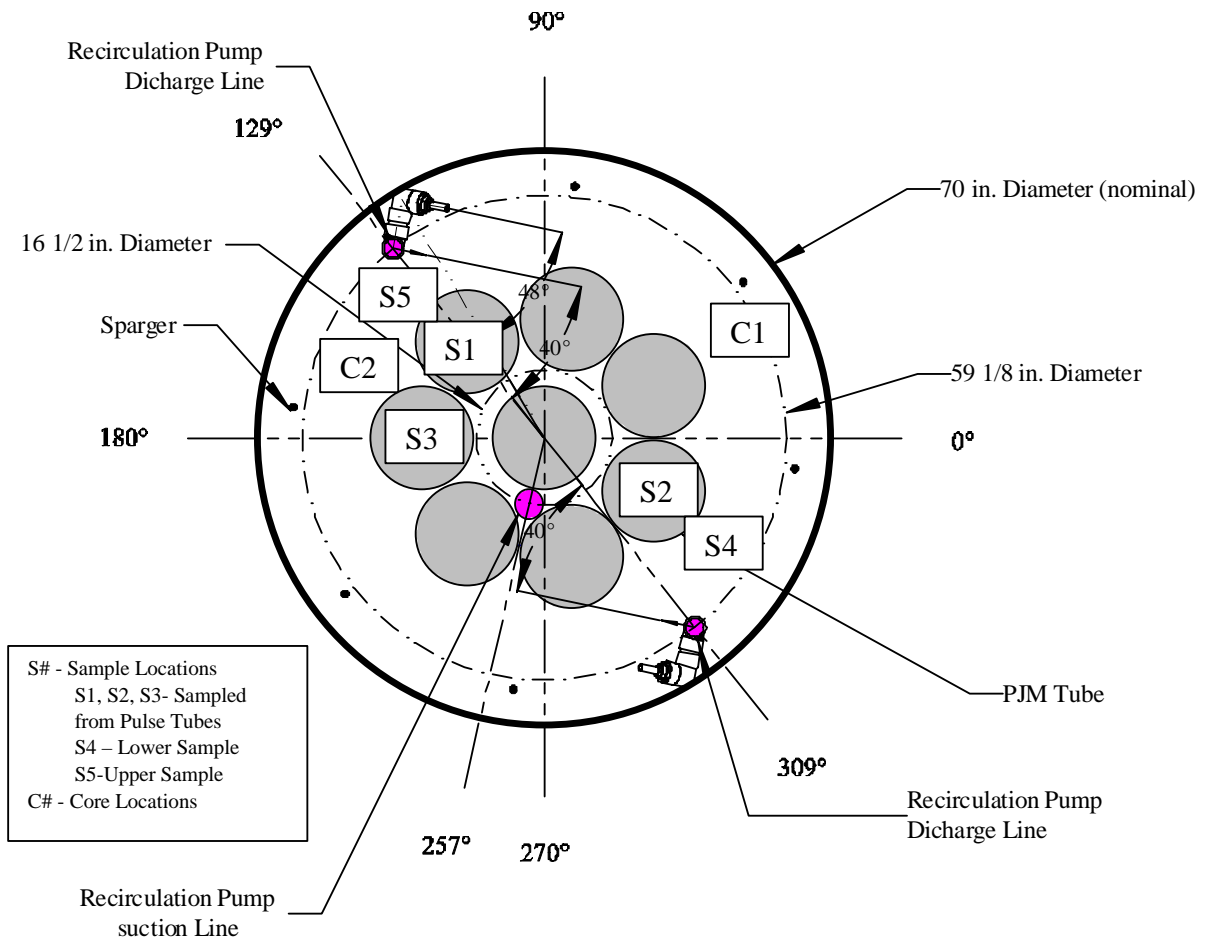
b) Test Sequence 26

Figure 8.1 (contd)



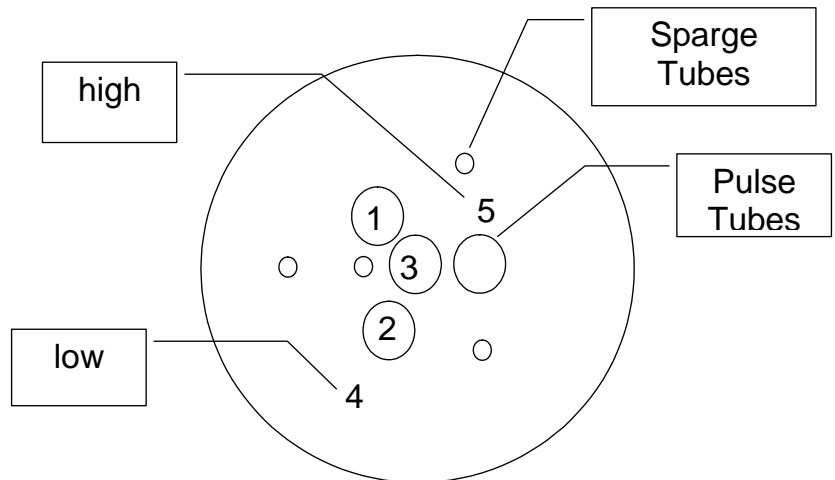
c) Test Sequence 27

Figure 8.1 (contd)

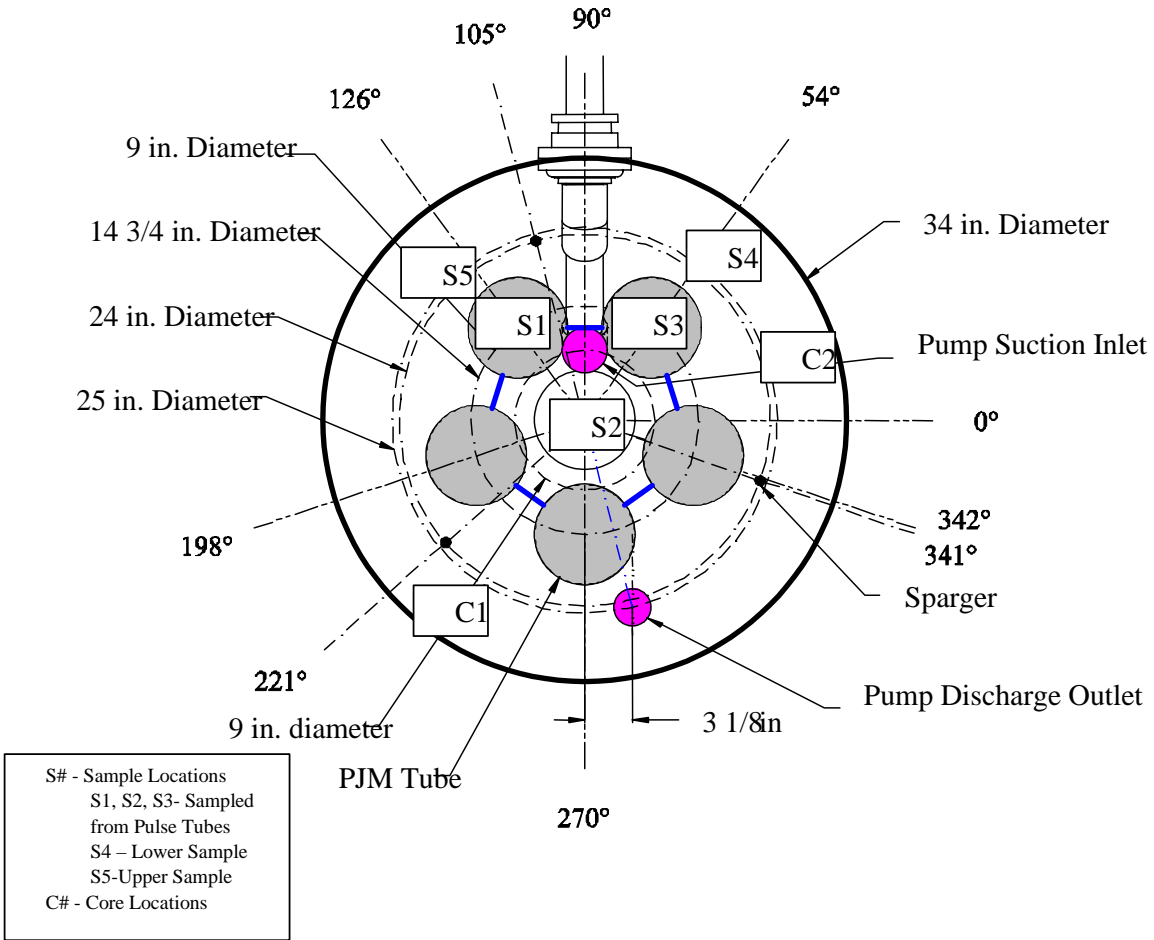


d) Test Sequence 28

**Figure 8.1 (contd)**

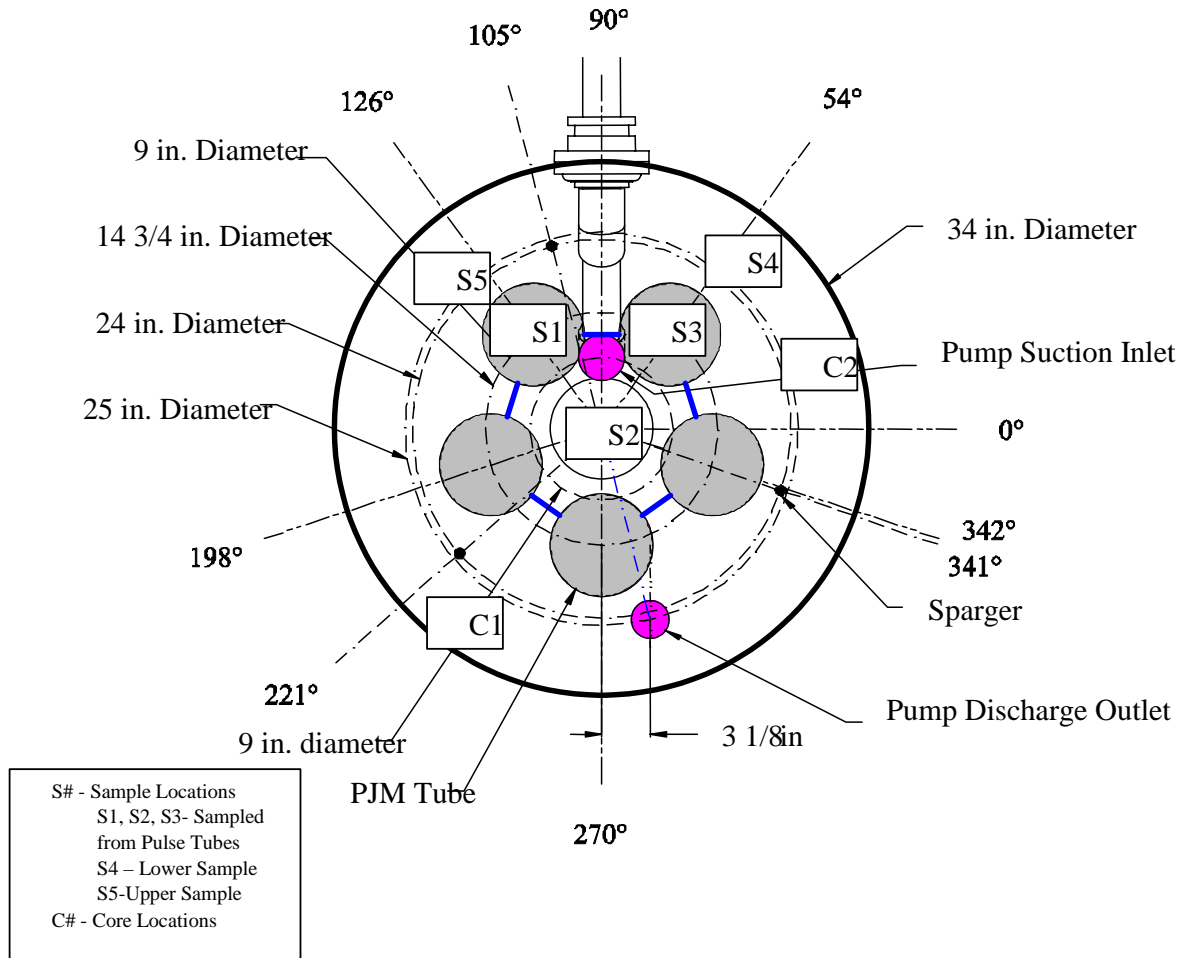


a) Test Sequences 1-13



b) Test Sequence 15

**Figure 8.2. Schematic of Ultrafiltration Process Vessel Tracer Sampling Locations During Phase II Scaled Test Platform Tests**



c) Test Sequence 16

**Figure 8.2 (contd)**

A set of tracer tests starts with the lowest mixing energy condition to form the initial well mixed cavern. Additional systems, such as recirculation pumps or sparging tubes, or increased pulse tube velocities are then used as subsequent operating conditions to form larger mixing caverns. By increasing the mixing energy through these additional systems, several operating conditions are tested with a single tracer addition. Each operating condition is termed a “run,” and samples in each run were taken at approximately 10-minute intervals for the initial run and 15 minutes for subsequent runs. This resulted in a total run time of 50 minutes for the first run and 45 minutes for the subsequent runs. Each set of runs is referred to as a “test sequence.” Note that on runs where the recirculation pump system was used, an additional volume of simulant was present in the system. Therefore, the volume of the tank as described by the equations in Section 5.4 is considered to be the tank and recirculation system contents. For run conditions before turning on the recirculation pump, the maximum fraction mixed value is below unity because the volume of the recirculation system contents is not being engaged in the mixing process.

The objective of these tests was to find the PJM configuration and operating conditions that leads to a fully mobilized, homogenous vessel. Two steps are performed to evaluate a tank as homogenous. The first step is to see if the results from each sample location for a run are consistent. This involves

calculating the mixing ratio and corresponding uncertainty for the final sample set in a run. Test results are shown in Appendix B. The test results are termed “consistent” if the range of mixing ratios with the associated error for each location contains zero:

$$MR - 2\Delta MR \leq 0 \leq MR + 2\Delta MR \quad (8.1)$$

The consistency test can be applied to one or two standard deviations for different confidence levels. If the results are consistent within two standard deviations, the test is termed consistent. A summary of this evaluation for the LS and UFP tests for each tracer is shown in Table 8.1 and Table 8.2, respectively. The consistency test identifies the test configurations (i.e., test sequences) that are likely to produce a well-mixed homogenous condition.

Table 8.1. Mixing-Ratio Consistency Test for Lag Storage Vessel During Phase II Scaled Test Platform Tests

		Run											
		1		2		3		4		5		6	
		Dye	Chloride										
Test Sequence	<b>1</b>	0	n/m	0	n/m	0	n/m	0	n/m	n/a	n/a	n/a	n/a
	<b>2</b>	0	n/m	0	n/m	0	n/m	0	n/m	n/a	n/a	n/a	n/a
	<b>2A</b>	0	n/m	0	n/m	0	n/m	1	n/m	n/a	n/a	n/a	n/a
	<b>3</b>	0	n/m	0	n/m	0	n/m	1	n/m	n/a	n/a	n/a	n/a
	<b>4</b>	0	n/m	0	n/m	1	n/m	2	n/m	n/a	n/a	n/a	n/a
	<b>5</b>	0	n/m	1	n/m	n/a	n/a	n/a	n/a	n/a	n/a	n/a	n/a
	<b>6</b>	0	n/m	2	n/m	2	n/m	n/a	n/a	n/a	n/a	n/a	n/a
	<b>7</b>	0	n/m	1	n/m								
	<b>8</b>	0	n/m	0	n/m	n/a	n/a	n/a	n/a	n/a	n/a	n/a	n/a
	<b>9</b>	0	n/m	0	n/m	0	n/m	n/a	n/a	n/a	n/a	n/a	n/a
	<b>10</b>	0	n/m	1	n/m	n/a	n/a	n/a	n/a	n/a	n/a	n/a	n/a
	<b>11</b>	0	n/m	0	n/m	n/a	n/a	n/a	n/a	n/a	n/a	n/a	n/a
	<b>12</b>	0	2	0	2	n/a	n/a	n/a	n/a	n/a	n/a	n/a	n/a
	<b>13</b>	0	2	0	2	n/a	n/a	n/a	n/a	n/a	n/a	n/a	n/a
	<b>19</b>	0	0	0	0	n/a	n/a	n/a	n/a	n/a	n/a	n/a	n/a
	<b>20</b>	1	1	1	2	n/a	n/a	n/a	n/a	n/a	n/a	n/a	n/a
	<b>21</b>	0	0	1	0	2	1	n/a	n/a	n/a	n/a	n/a	n/a
	<b>26</b>	1	0	0	2	n/a	n/a	n/a	n/a	n/a	n/a	n/a	n/a
<b>27</b>	0	2	n/a	n/a									
<b>28</b>	2	2	n/a	n/a									
0	inconsistent results												
1	consistent results to 2s												
2	consistent results to 1s												
n/a	not applicable												
n/m	not measured												

**Table 8.2. Mixing-Ratio Consistency Test for Ultrafiltration Process Vessel During Phase II Scaled Test Platform Tests**

		Run							
		1		2		3		4	
		Dye	Chloride	Dye	Chloride	Dye	Chloride	Dye	Chloride
Test Sequence	1	0	n/m	0	n/m	1	n/m	2	n/m
	2	0	n/m	0	n/m	0	n/m	0	n/m
	3	0	n/m	0	n/m	0	n/m	0	n/m
	3B	0	0	2	2	2	2	2	2
	11	0	0	0	1	n/a	n/a	n/a	n/a
	12	0	0	2	2	n/a	n/a	n/a	n/a
	13	0	0	0	0	2	1	n/a	n/a
	15	0	0	2	2	n/a	n/a	n/a	n/a
	16	n/m	2	n/a	n/a	n/a	n/a	n/a	n/a
0	inconsistent results								
1	consistent results to 2s								
2	consistent results to 1s								
n/a	not applicable								
n/m	not measured								

With the consistent set of results identified, the results are further scored by calculating an average mixing ratio and associated propagated error as shown by the Equations 8.2 and 8.3 below:

$$\overline{MR} = \frac{\sum_{i=1}^N MR_i}{N} \quad (8.2)$$

$$\Delta\overline{MR} = \frac{\left[ \sum_{i=1}^N (\Delta MR_i)^2 \right]^{0.5}}{N} \quad (8.3)$$

where  $\overline{MR}$  = average mixing ratio

$MR_i$  = mixing ratio of  $i^{\text{th}}$  sample location

$N$  = total number of sample locations

$\Delta\overline{MR}$  = error associated with the average mixing ratio

$\Delta MR_i$  = error associated with the mixing ratio of the  $i^{\text{th}}$  sample location.

Assuming that the error associated with each result is Gaussian, the cumulative probability density function can be used as a scoring function to identify the test results with a high probability of being fully homogenous (i.e., the mixing ratio is zero). The cumulative Gaussian probability function,  $P$ , with a mean mixing-ratio value,  $\overline{MR}$  and associated error  $\Delta\overline{MR}$  is calculated at mixing-ratio values of 0.1 and -0.1. The difference between these two values represents the probability of the actual mean value being between mixing ratios in the range of (0.1,-0.1) is shown in Equation 8.4.

$$P(\overline{MR}, \Delta\overline{MR})_{0.1} - P(\overline{MR}, \Delta\overline{MR})_{-0.1} \quad (8.4)$$

For reference purposes, an average mixing ratio of zero with an error of 0.1 corresponds to a probability score of 68%. Probability scores greater than 68% are considered high confidence while values below 68% are considered lower confidence. Results for the LS and UFP tests are shown in Table 8.3 and Table 8.4, respectively.

From these test results, a high confidence (>68% probability score) can be placed that the following tests fully mix the PJM test vessels:

1. LS Test Sequence 2A Run 4
2. LS Test Sequence 3 Run 4
3. LS Test Sequence 4 Run 3
4. LS Test Sequence 6 Run 3
5. LS Test Sequence 20 Run 1
6. LS Test Sequence 20 Run 2
7. LS Test Sequence 21 Run 2
8. UFP Test 1 Run 4
9. UFP Test 3B Run 2
10. UFP Test 3B Run 3
11. UFP Test 3B Run 4
12. UFP Test 12 Run 2
13. UFP Test 16 Run 1

**Table 8.3. Mixing-Ratio Probability Score for Lag Storage Vessel During Phase II Scaled Test Platform Tests**

		Run											
		1		2		3		4		5		6	
		Dye	Chloride	Dye	Chloride	Dye	Chloride	Dye	Chloride	Dye	Chloride	Dye	Chloride
<b>Test Sequence</b>	<b>1</b>	inc	n/m	inc	n/m	inc	n/m	inc	n/m	n/a	n/a	n/a	n/a
	<b>2</b>	inc	n/m	inc	n/m	inc	n/m	inc	n/m	n/a	n/a	n/a	n/a
	<b>2A</b>	inc	n/m	inc	n/m	inc	n/m	99%	n/m	n/a	n/a	n/a	n/a
	<b>3</b>	inc	n/m	inc	n/m	inc	n/m	100%	n/m	n/a	n/a	n/a	n/a
	<b>4</b>	inc	n/m	inc	n/m	97%	n/m	0%	n/m	n/a	n/a	n/a	n/a
	<b>5</b>	inc	n/m	2%	n/m	n/a	n/a	n/a	n/a	n/a	n/a	n/a	n/a
	<b>6</b>	inc	n/m	45%	n/m	80%	n/m	n/a	n/a	n/a	n/a	n/a	n/a
	<b>7</b>	inc	n/m	inc	n/m	inc	n/m	inc	n/m	inc	n/m	71%	n/m
	<b>8</b>	inc	n/m	inc	n/m	n/a	n/a	n/a	n/a	n/a	n/a	n/a	n/a
	<b>9</b>	inc	n/m	inc	n/m	inc	n/m	n/a	n/a	n/a	n/a	n/a	n/a
	<b>10</b>	inc	n/m	3%	n/m	n/a	n/a	n/a	n/a	n/a	n/a	n/a	n/a
	<b>11</b>	inc	n/m	inc	n/m	n/a	n/a	n/a	n/a	n/a	n/a	n/a	n/a
	<b>12</b>	inc	62%	inc	60%	n/a	n/a	n/a	n/a	n/a	n/a	n/a	n/a
	<b>13</b>	inc	4%	inc	35%	n/a	n/a	n/a	n/a	n/a	n/a	n/a	n/a
	<b>19</b>	inc	inc	inc	inc	n/a	n/a	n/a	n/a	n/a	n/a	n/a	n/a
	<b>20</b>	91%	2%	98%	9%	n/a	n/a	n/a	n/a	n/a	n/a	n/a	n/a
	<b>21</b>	inc	inc	85%	inc	67%	0%	n/a	n/a	n/a	n/a	n/a	n/a
	<b>26</b>	12%	inc	inc	59%	n/a	n/a	n/a	n/a	n/a	n/a	n/a	n/a
<b>27</b>	inc	15%	n/a	n/a	n/a	n/a	n/a	n/a	n/a	n/a	n/a	n/a	
<b>28</b>	60%	62%	n/a	n/a	n/a	n/a	n/a	n/a	n/a	n/a	n/a	n/a	
n/a	not applicable												
n/m	not measured												
inc	inconsistent results												

**Table 8.4. Mixing-Ratio Probability Score for Ultrafiltration Process  
Vessel During Phase II Scaled Test Platform Tests**

Test Sequence	Run							
	1		2		3		4	
	Dye	Chloride	Dye	Chloride	Dye	Chloride	Dye	Chloride
<b>1</b>	inc	n/m	inc	n/m	66%	n/m	95%	n/m
<b>2</b>	inc	n/m	inc	n/m	inc	n/m	inc	n/m
<b>3</b>	inc	n/m	inc	n/m	inc	n/m	inc	n/m
<b>3B</b>	inc	inc	98%	58%	97%	77%	95%	69%
<b>11</b>	inc	inc	inc	inc	n/a	n/a	n/a	n/a
<b>12</b>	inc	inc	97%	55%	n/a	n/a	n/a	n/a
<b>13</b>	inc	inc	inc	inc	42%	35%	n/a	n/a
<b>15</b>	inc	inc	67%	62%	n/a	n/a	n/a	n/a
<b>16</b>	n/m	86%	n/a	n/a	n/a	n/a	n/a	n/a
n/a	not applicable							
n/m	not measured							
inc	inconsistent results							

Examining these results reveals that a wide range or noisy set of mixing-ratio data may increase the probability score by averaging the data closer to a mixing ratio of zero. This problem is minimized by the consistency test screening process but occurred in LS test sequence 21 (see Figure 8.3). In this test, the dye results from Run 2 were consistent to two standard deviations while Run 3 was consistent to one standard deviation. Although the mixing energy was increased from Run 2 to Run 3, the probability score from Run 2 to Run 3 decreased. This is because the average value from Run 2 is closer to zero than Run 3, resulting in an inflated probability score. Consequently, probability scores need to be augmented with the raw data from a test for proper interpretation of the results.

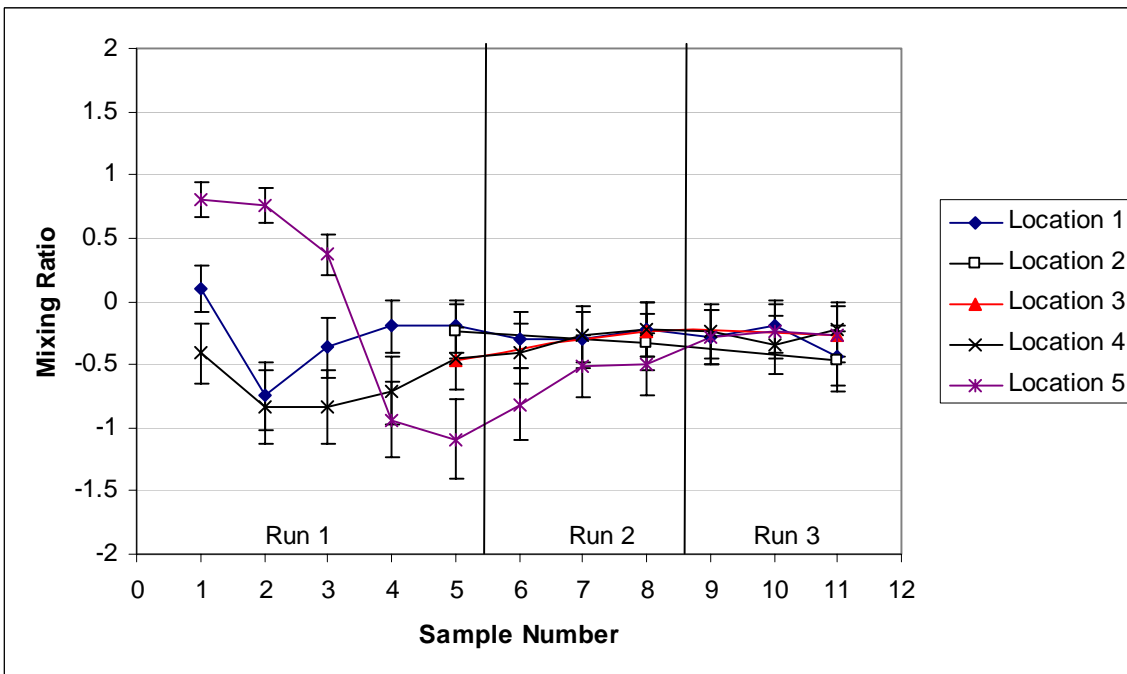
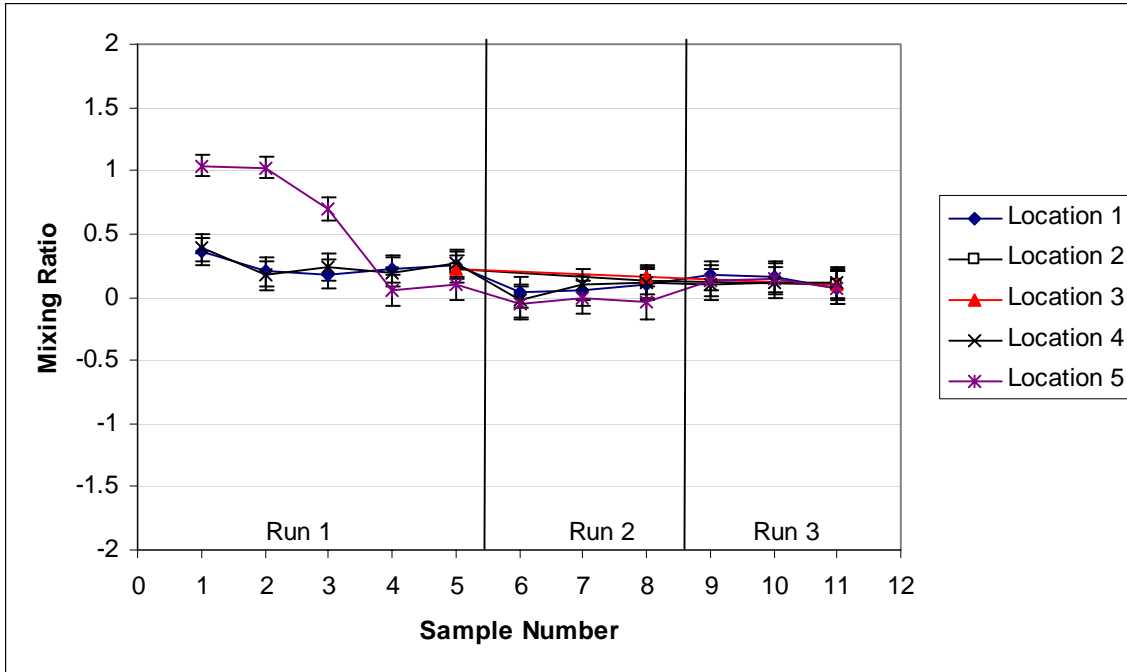


**Figure 8.3. Mixing-Ratio Results from LS Test Sequence 21 Using BB Tracer (top) and Chloride Tracer Using IC Technique (bottom)**

When the BB dye results are compared to the chloride results, the dye-mixing-ratio values are consistently biased towards greater values than the chloride results. This can be seen in Figure 8.4 through Figure 8.6. In many instances, the final mixing ratio for the BB dye exceeds zero while the chloride tracer results rarely exceed zero. These data suggest that a systemic issue with the BB dye exists where the 2-phase model of a well-mixed cavern and quiescent phase does not hold. However, this model appears to hold for the chloride tracer. This behavior may be explained by the dye sorbing onto the clay particles in the stock solution while the chloride remains in solution. The stock solution clay particles loaded with BB dye may adhere to the tank walls more readily than the low-dye clay. This behavior is consistent with observations of streaking along the tank walls during some tests. Conversely, the chloride remains mobile within the mixing cavern. During the tests, samples are taken and dye concentrations are reduced compared to the chloride measurements. During the final homogenization step, enough energy is supplied to incorporate the adhered dye into the simulant, resulting in greater-than-zero mixing-ratio values for the BB dye. Because BB dye adherence was not observed when used with laponite and other simulants it can be concluded that the combination of BB dye and kaolin:bentonite clay simulant rather than the BB dye alone appears to possess this adherence behavior.

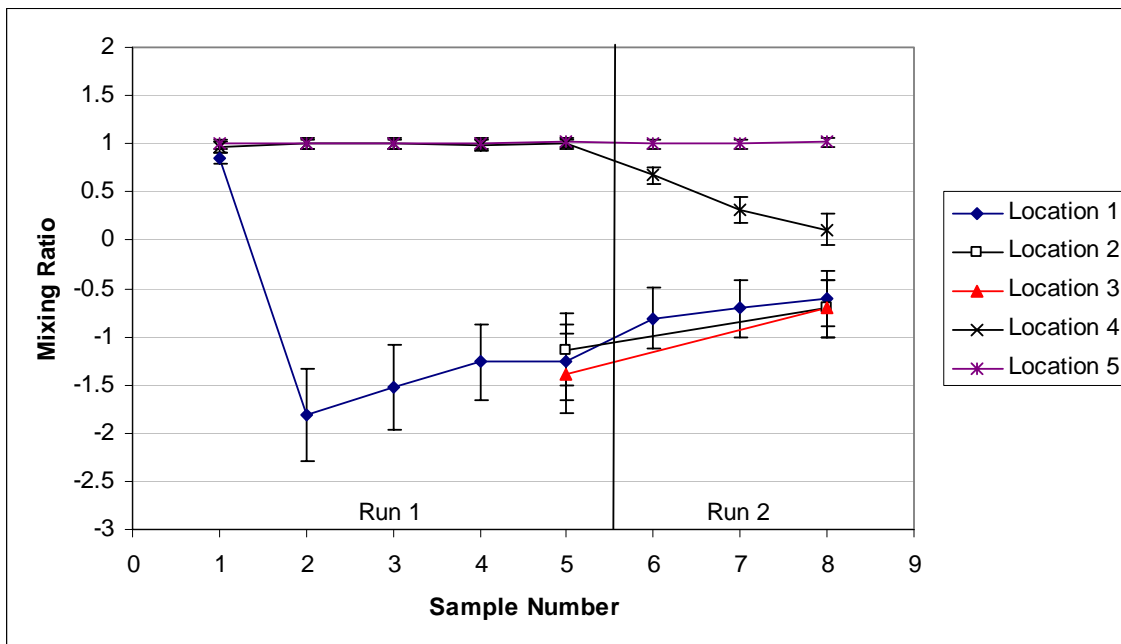
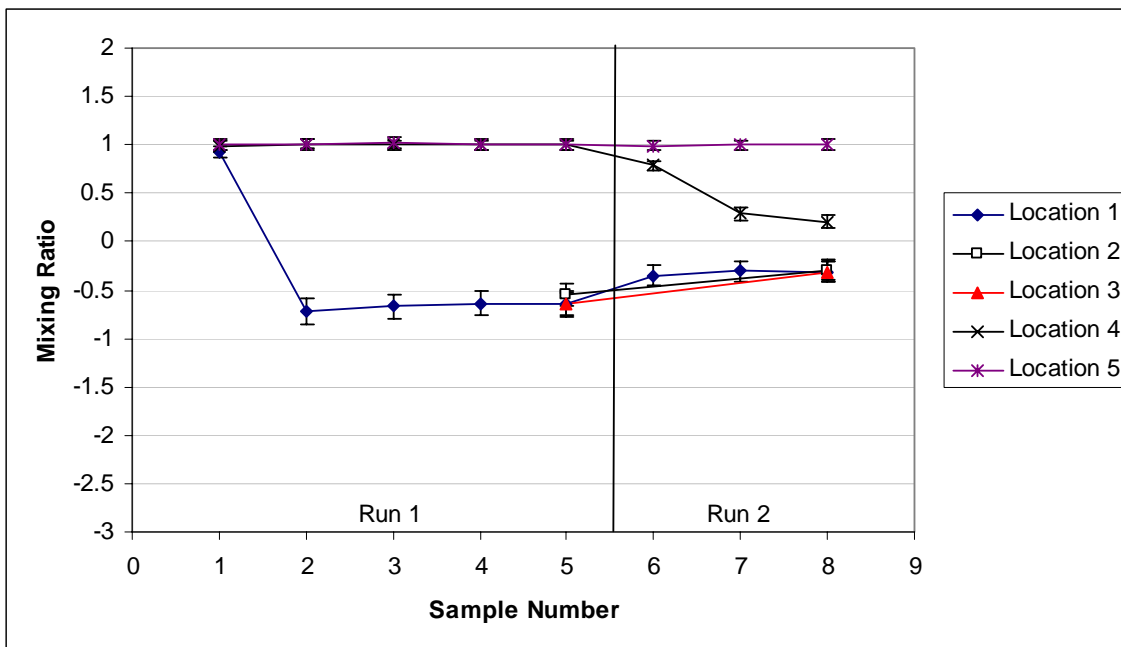
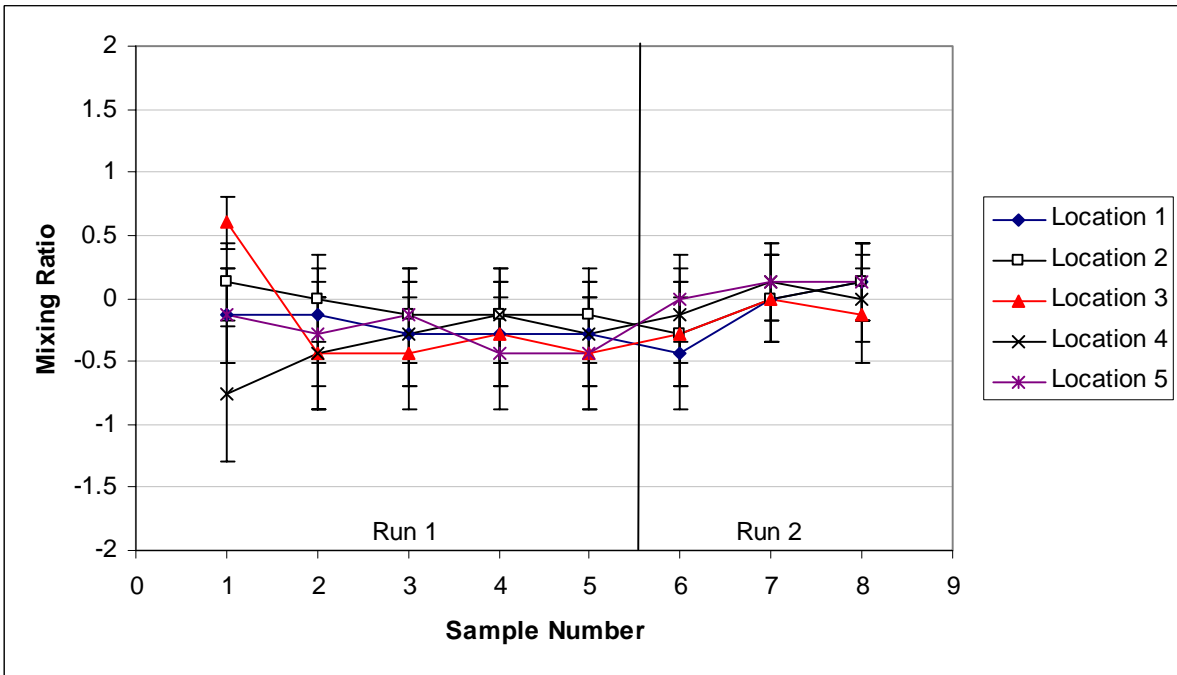
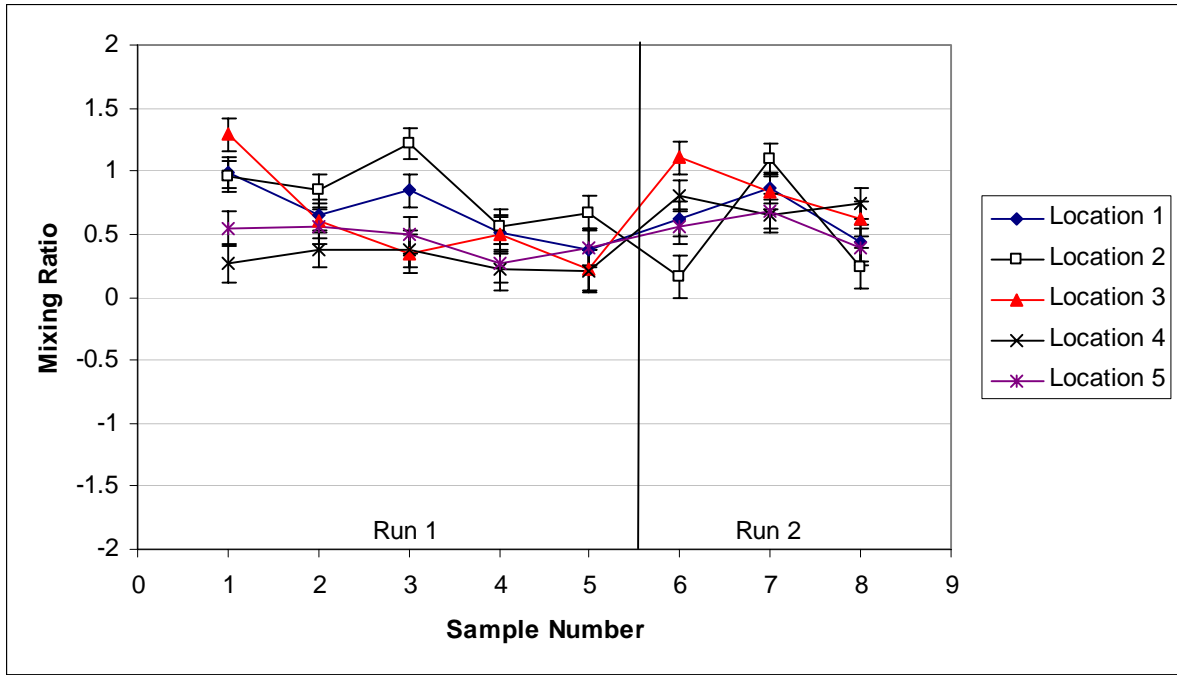


Figure 8.4. Mixing-Ratio Results from LS Test Sequence 19 Using BB Tracer (top) and Chloride Tracer Using ISE Technique (bottom)



**Figure 8.5. Mixing-Ratio Results from LS Test Sequence 13 Using BB Tracer (top) and Chloride Tracer Using IC Technique (bottom)**

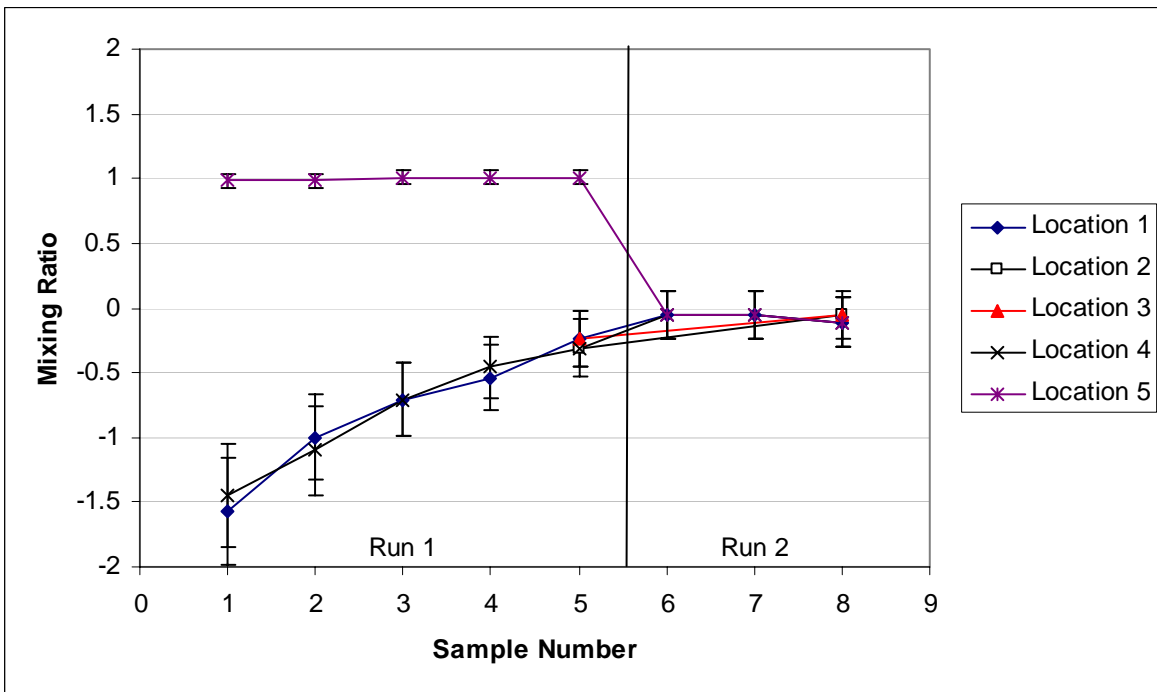
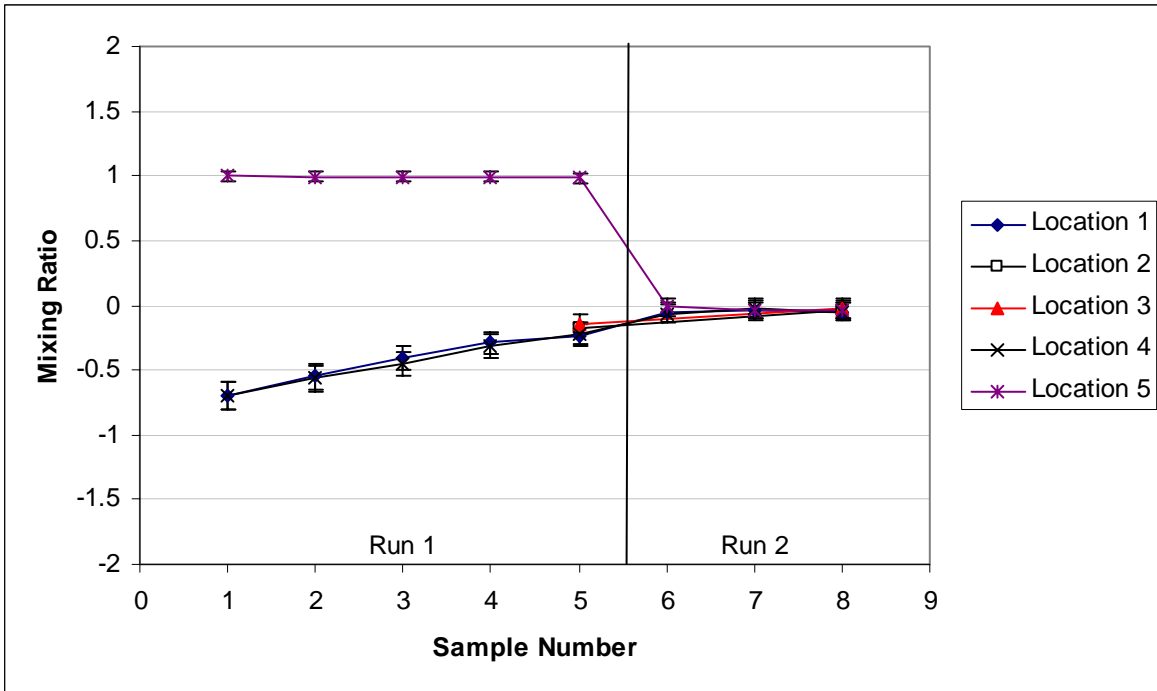


Figure 8.6. Mixing-Ratio Results from UFP Test Sequence 12 Using BB Tracer (top) and Chloride Tracer Using ISE Technique (bottom)

During the initial use of the BB dye, this bias was observed to be a function of how the tracer was introduced into the mixing cavern. When the dye is injected in one large pulse as a water-based stock solution, the observed bias is large, and greater-than-zero mixing ratios are produced. When the dye is injected slowly over many cycles in a stock solution of clay simulant, the bias is much lower, and mixing ratios near zero are produced. If the degree of BB dye adherence increases with dye concentration, then more dye holdup along the vessel walls would be expected when the dye is injected as a pulse, and this observation is consistent with the previous hypothesis. An example of dye adherence as a function of tracer-injection procedure is shown in Figure 8.7.

To eliminate this problem, an obvious solution is to only use the chloride data for evaluating the tests. Unfortunately, the chloride analytical techniques possess a higher degree of measurement error compared to the dye techniques. This can be seen by comparing the size of the error bars in Figure 8.8 and Figure 8.9. Therefore, if the biased results are neglected, the corresponding probability scores for the chloride tracer are significantly lower than the BB dye tracer scores. The current evaluation strategy is to use both techniques and interpret the results with the knowledge that bias may be present in the BB dye results. If a configuration is tested that possesses enough mixing energy, the adhered dye is removed, and zero mixing-ratio values are obtained. This situation is seen in Figure 8.8 where the BB dye and chloride results are in good agreement. When a promising configuration is identified, multiple tests should be performed with the chloride tracer. These multiple tests should allow for the error bars to be computed experimentally. With high test repeatability, confidence in the mixing potential for a given test configuration can be increased.



**Figure 8.7. BB Dye Adherence to Vessel Wall**

**Dye is injected as a pulse at the top of the vessel (top). After several hours of additional mixing (middle), the dye is injected directly into the mixing cavern (bottom).**

Selecting the analytical technique used also has an impact on the chloride results. This is caused by the large instrument error of  $\pm 2$  mV on the ISE system potentiometer. Under typical circumstances, an injection of 30 ppm of chloride tracer (final homogenized concentration difference) results in an error of approximately  $\pm 0.2$  mixing-ratio units. Because several minutes are required for the potentiometer reading to stabilize, ISE results may also be biased by the length of time used for each measurement. This occurred in UFP test 3B (see Figure 8.8) where the chloride ISE results were shifted downward, resulting in negative mixing-ratio values for runs 2, 3, and 4. Since no increase in mixing was observed in these results and the mixing energy was increasing significantly, these values appear to be erroneous. The samples were reanalyzed with the ISE for a longer analysis time, and the current plot shown in Figure 8.8 was obtained. This issue is also suspected in LS test 20 (see Figure 8.9).

For these reasons, the IC technique is preferred to the ISE technique and was used in LS Tests 21 through 28 and UFP Tests 13 through 16. However, the ISE technique was used directly on clay slurry samples that were not centrifuged. Measurement time for the ISE method is expected to decrease significantly if the ISE probe is used with the centrifuged liquid from each sample. Implementing this additional centrifugation step may eliminate previous issues with the technique.

The amount of chloride tracer used in each test may be increased to reduce uncertainty. Typically, a final concentration increase of 30 ppm chloride is used. Increasing this value to 100 ppm should reduce the associated error significantly. However, tradeoffs such as wastewater limitations for chloride ions and simulant rheological properties changes with salt concentration should to be considered.

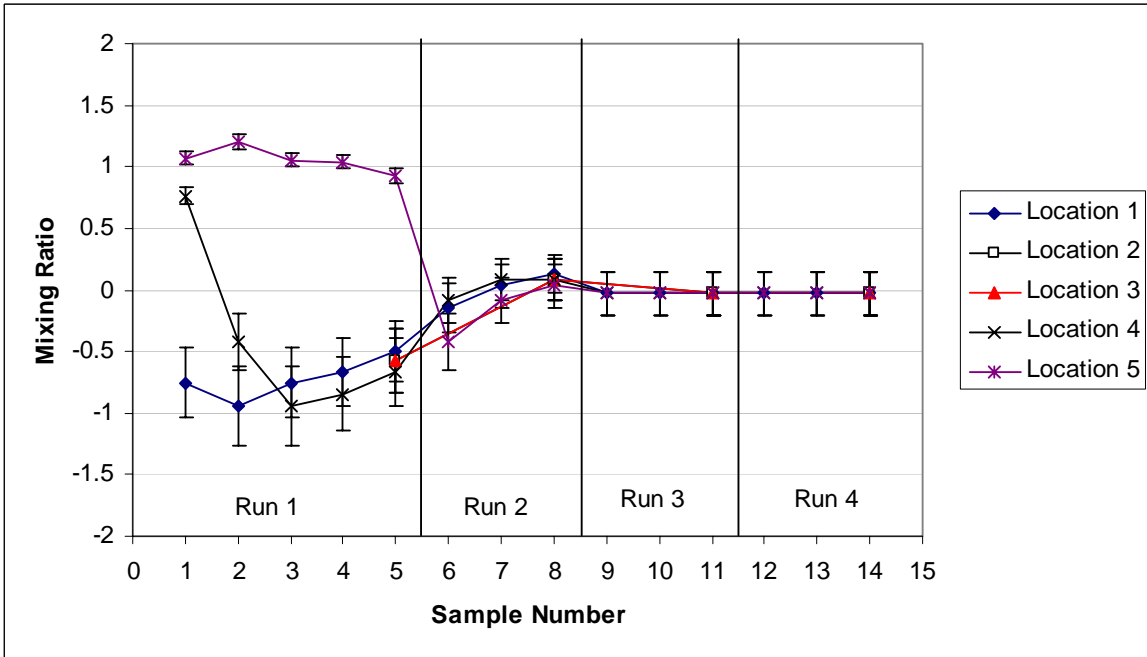
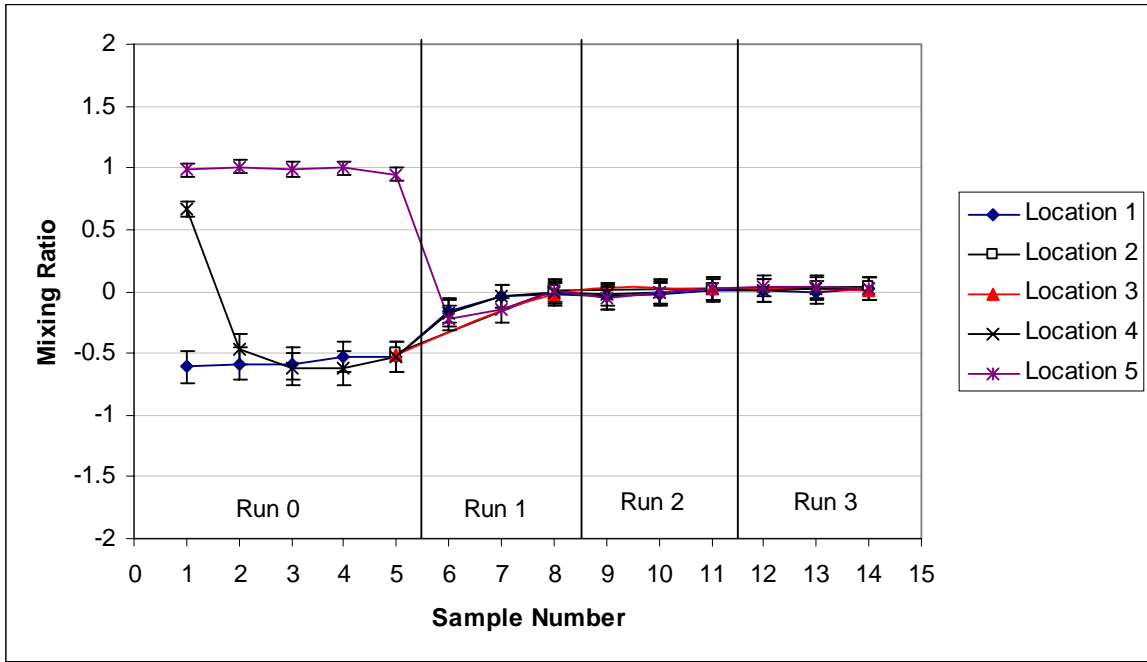


**Figure 8.8. Mixing-Ratio Results from UFP Test Sequence 3B Using BB Tracer (top) and Chloride Tracer Using ISE Technique (bottom)**

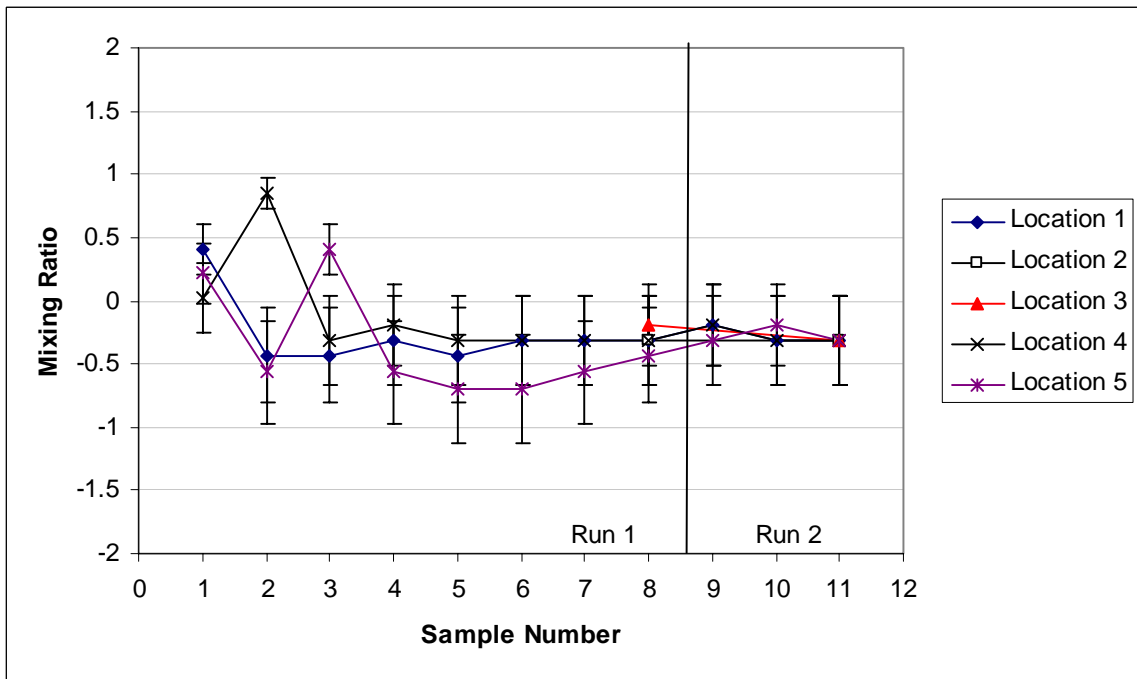
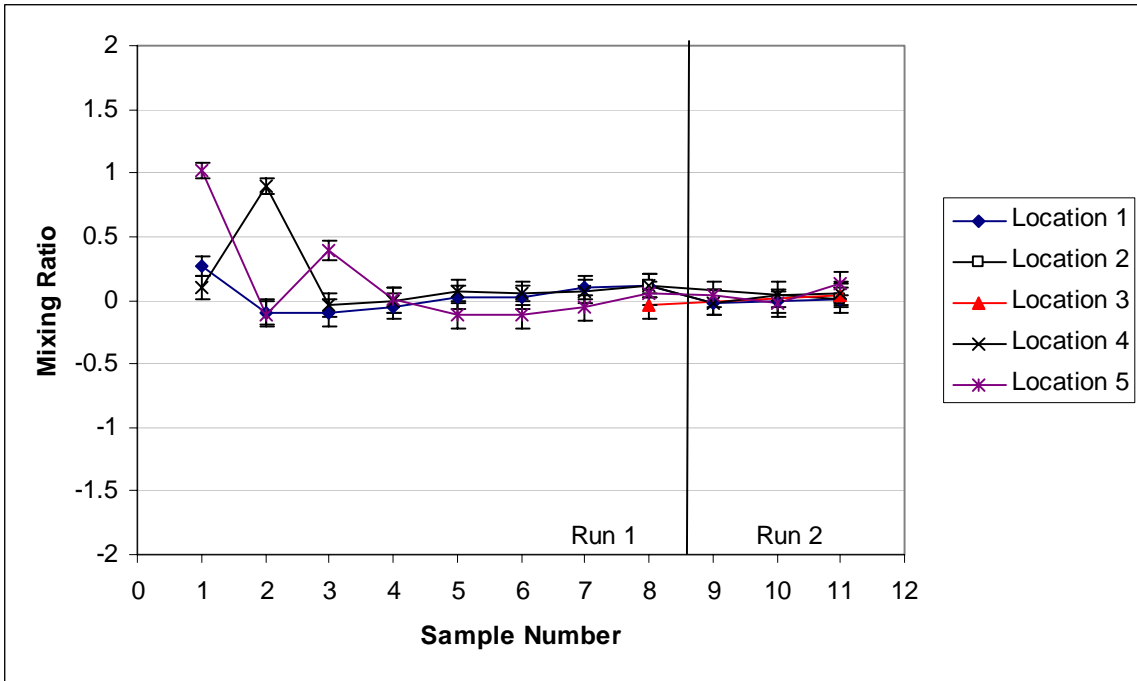


**Figure 8.9. Mixing-Ratio Results from LS Test Sequence 20 Using BB Tracer (top) and Chloride Tracer Using IC Technique (bottom)**

Core samples were taken in several tank locations for LS Tests 26, 27, and 28 and UFP Tests 15 and 16. The core samples were taken after the mixing test was complete with all mixing equipment off.<sup>(a)</sup> Because of the non-Newtonian nature of the simulant, these core samples represent a snapshot of the tracer concentration profile at the conclusion of the mixing test. For LS Test 26 and UFP Test 16, core samples were also taken at the beginning of the test before adding tracer<sup>(b)</sup> and after the final homogenization step.<sup>(c)</sup> Core sample locations can be seen schematically in Figure 8.1 and Figure 8.2 for the LS vessel and UFP vessel prototypes, respectively.

The core samples were segmented into 2-inch segments that were analyzed for chloride concentration using the IC technique. Using initial and final tracer concentrations from the sample tube samples discussed above, mixing-ratio calculations were performed on each core sample segment. In the case of LS Test 26 and UFP Test 16, the average concentrations of the initial and final core samples were used in the calculation. The average mixing ratio for each core segment and associated error was calculated using Equations 7.3 and 7.4. Results from this calculation are shown in Table 8.5. With the exception of core 2 from LS Test 27 and 28, every core sample mixing ratio with error creates a range of values that contain zero mixing ratio. The average value of core 2 from LS Test 27 and 28 is still relatively close to zero but of lower confidence. This can also be seen by the probability scores (calculated using Equation 7.5) for these core samples shown in Table 8.6.

**Table 8.5. Mixing-Ratio Values from Chloride IC Data for Core Samples Taken During Phase II Scaled Test Platform Tests**

		Core 1	Core 2	Core 3
Test Sequence	UFP-T15	0.03 ± 0.06	-0.01 ± 0.06	n/m ± n/m
	UFP-T16	0.05 ± 0.02	0.06 ± 0.02	n/m ± n/m
	LS-T26	-0.01 ± 0.05	-0.02 ± 0.05	n/m ± n/m
	LS-T27	-0.05 ± 0.05	-0.14 ± 0.06	-0.01 ± 0.05
	LS-T28	0.00 ± 0.05	-0.08 ± 0.06	n/m ± n/m
n/m	not measured			

**Table 8.6. Mixing-Ratio Probability Scores from Chloride IC Data for Core Samples Taken During Phase II Scaled Test Platform Tests**

		Core 1	Core 2	Core 3
Test Sequence	UFP-T15	85%	88%	n/m
	UFP-T16	99%	96%	n/m
	LS-T26	94%	92%	n/m
	LS-T27	82%	26%	94%
	LS-T28	94%	62%	n/m
n/m	not measured			

- 
- (a) Core samples taken after mixing tests at locations 1 and 2 are labeled as “Core 1”, “Core 2”, respectively.
  - (b) Core samples taken prior to tracer addition at locations 1 and 2 are labeled as “Core Initial”, “Core 2 Initial”, respectively.
  - (c) Core samples after final homogenization step at locations 1 and 2 are labeled as “Core 1 Final”, “Core 2 Final”, respectively.

To assess the tracer uniformity as a function of depth, the mixing-ratio depth profile for each core segment is shown in Figure 8.10 through Figure 8.14. In general, the data indicate that the tracer concentrations fluctuate close to a fraction mixed value of unity for all core samples. This behavior is characteristic of a fully mobilized system that is in the process of complete homogenization. As noted above, samples from core 2 in LS Tests 27 and 28 deviate from a zero mixing-ratio value more than core samples from other tests. Since these tracer results do not indicate the presence of stagnant regions, these data indicate that there are regions of the tank where the mixing process occurs at a slower rate.

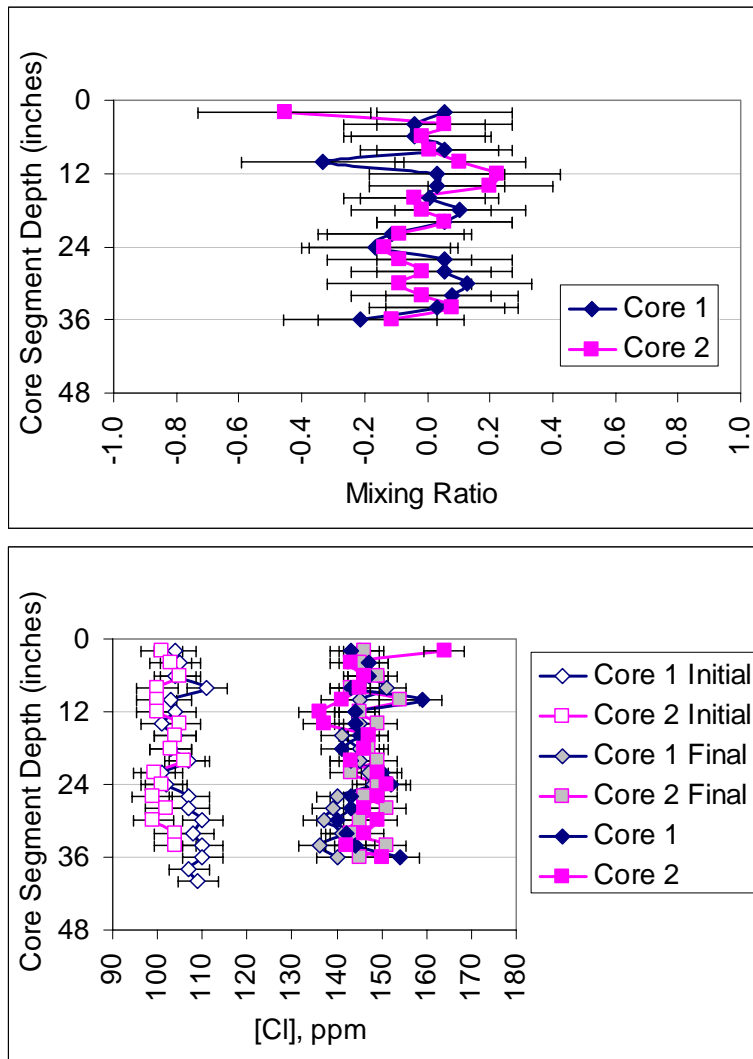


**Figure 8.10. Mixing-Ratio Results from LS Test Sequence 26 Core Samples using Chloride Tracer (top) and Chloride Concentration as a Function of Depth (bottom)**

Additional information on the mixing state of LS Test 27 can be inferred by comparing the core sample results to results from the sampling tubes (see Figure 8.11). Sampling-tube results indicate that locations 1, 2, and 3 have a higher tracer concentration than locations 4 and 5. Locations 1, 2, and 3 are samples taken directly from the pulse tubes while locations 4 and 5 are at low and high elevations near the sparge tubes. Core sample results are consistent with mixing-ratio data from locations 4 and 5 and do not

show increased tracer concentration near the bottom of the tank. This observation infers that increased tracer concentration should be present below the 36-inch depth of the core segments and represents the mixing cavern formed by the PJM operation. This test consists of PJMs operating with spargers and is consistent with a two-zone mixing model. In this model, the bottom of the tank is mixed by PJMs while the upper portion of the tank is mobilized by spargers. As material from the upper portion of the tank is mobilized and introduced into the PJM mixing region, the entire tank contents will eventually become homogenous. If the exchange rate between these two zones is small, the homogenization process will take a longer period of time to complete. LS Test 27 appears to follow this behavior, where the entire tank contents are mobilized but total tank homogenization occurs at a slower rate than the other tests.

Core Samples from UFP Test 16 show a pattern of slightly decreased tracer concentration in the midsection of each core. Increased tracer concentration is present at the top and bottom of each core. This test consists of PJMs operating with spargers and is consistent with a two-zone mixing model. This situation may occur if the sparging system is creating a relatively large circulation cell where the tracer injected in the pulse tubes is brought to the surface by the sparger system and then forced back to the bottom along the tank walls. Because of the location of tracer injection, increased tracer concentration would be present along the top, sides, and bottom of the tank. A core sample taken off of the tank wall would have a profile consistent with the observed profile.

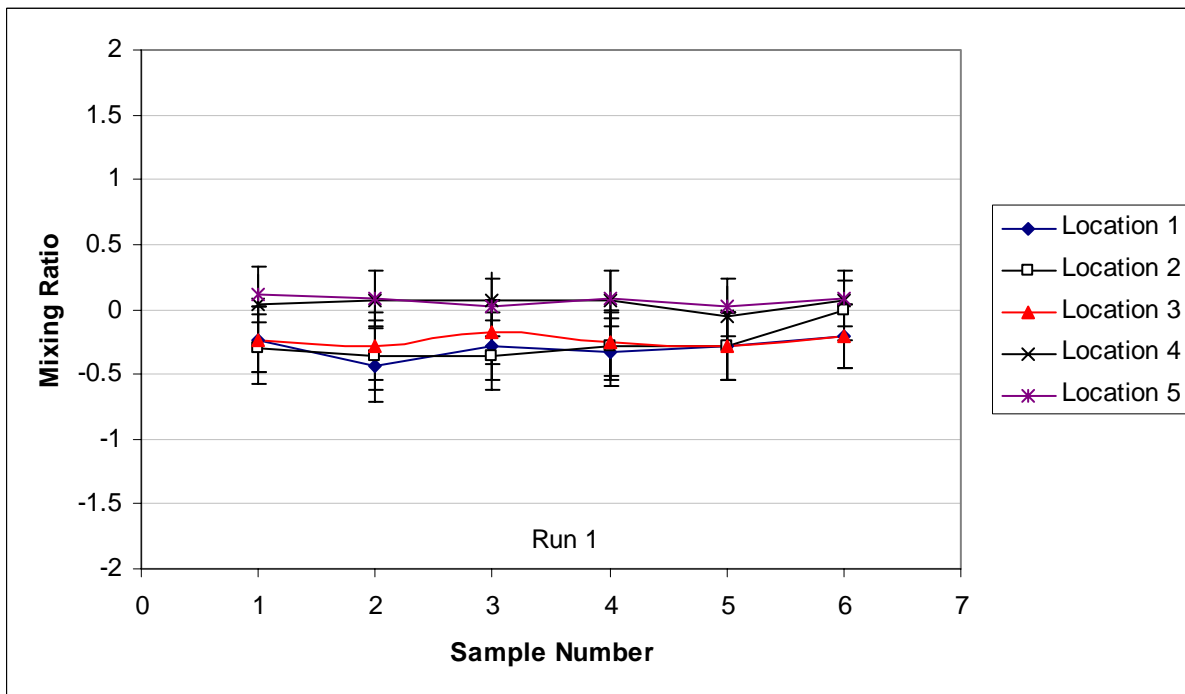
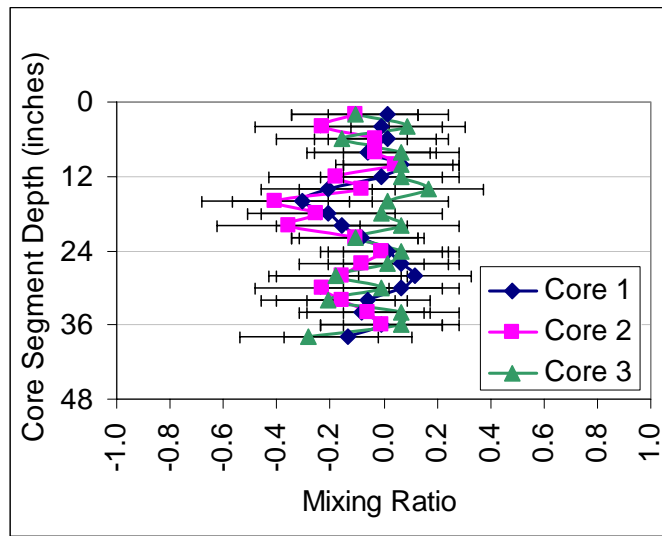


**Figure 8.11. Mixing-Ratio Results from LS Test Sequence 27 Core Samples Using Chloride Tracer (top) and Mixing-Ratio Results from Sampling Tubes (bottom)**

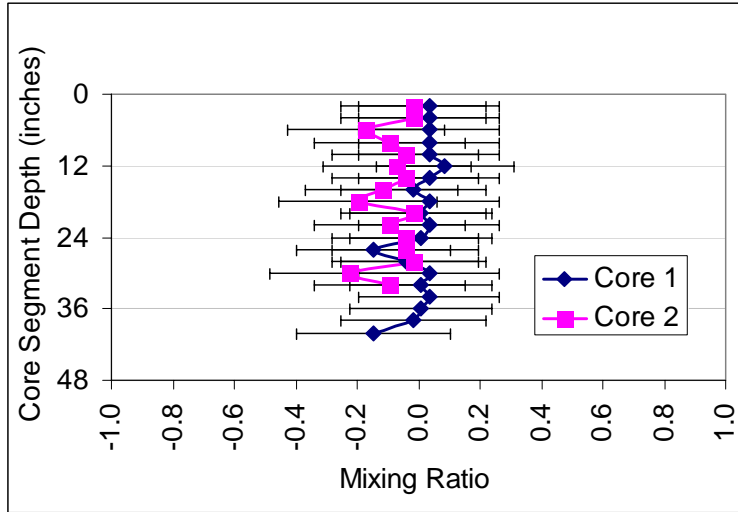


**Figure 8.12. Mixing-Ratio Results from LS Test Sequence 28  
Core Samples Using Chloride Tracer**

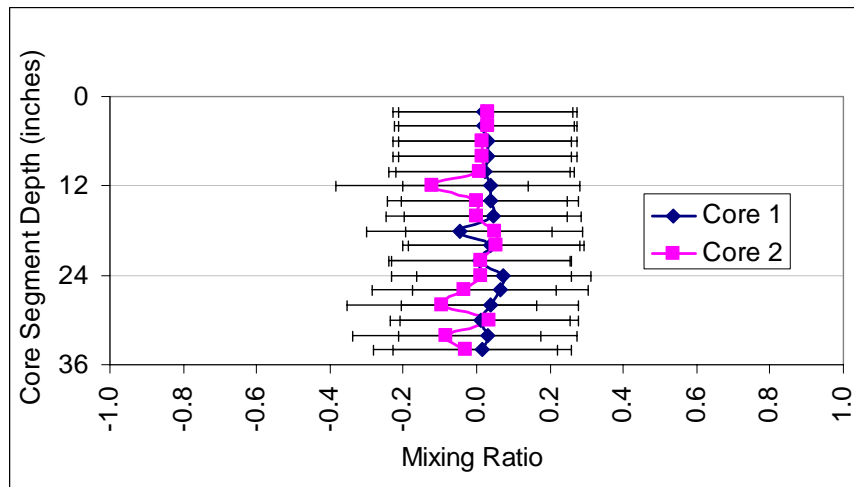


**Figure 8.13. Mixing-Ratio Results from UFP Test Sequence 15  
Core Samples using Chloride Tracer**

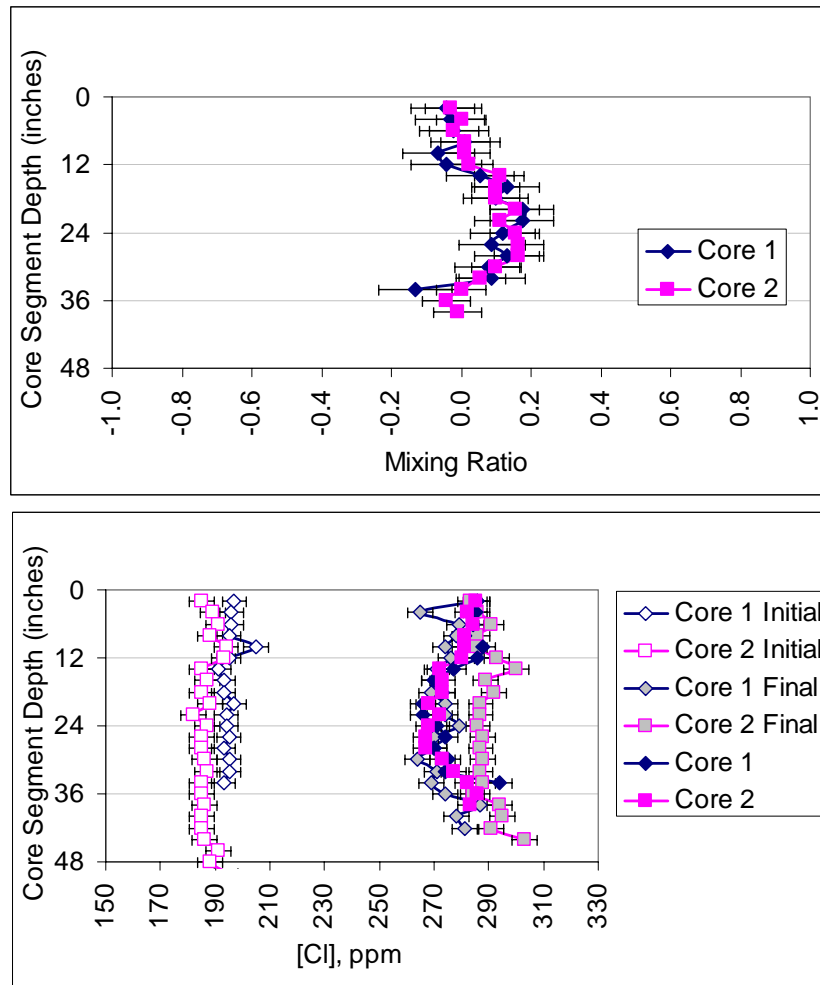


**Figure 8.14. Mixing-Ratio Results from UFP Test Sequence 16 Core Samples Using Chloride Tracer (top) and Chloride Concentration as a Function of Depth (bottom)**

Initial and final core samples were taken for LS Test 26 and UFP Test 16. The initial core sample profiles show uniform tracer concentrations at the start of each test. The final core samples were taken after additional mixing energy was used to completely mix the entire tank contents. Core results from LS Test 26 indicate a uniform concentration consistent with the core samples taken after the PJM mixing test. For UFP Test 15, final core samples show a small difference in concentration between locations 1 and 2. In this experiment, the tracer concentration was increased to approximately 100 ppm. This is a factor of two to three larger than the other experiments. Because of this salt addition, the Bingham Plastic yield stress value of the kaolin: bentonite simulant increases by several Pascal, hindering the final homogenization process and creating small concentration gradients. Nonetheless, the core samples taken after the PJM test agree well with the final homogenization samples and indicate near complete mixing.

A mass balance around the chloride added to the tank was calculated to confirm that the final homogenization procedure adequately mixed the tank contents before sampling. Even though the

mass of the salt solution added to each test was measured, this mass balance is an estimate because several variables, such as simulant volume, density of the simulant, and fraction of water in the simulant, need to be estimated to complete the calculation. The mass balance is performed in Table 8.7 with assumed values of these properties with associated uncertainty estimates. When these errors are propagated through the calculation, the results indicate that the tank is homogenized within an estimate uncertainty. Note that this volume estimate does not consider the volume of simulant displaced by a “shroud” encasement which was installed around the PJMs for these particular tests. The shroud volume is on the order of 10% of the tank volume. If the mass balance is recalculated with 10% less simulant volume, the deviation between predicted and measured concentrations is closer to 0%. Consequently, the final homogenization procedure for the LS and UFP vessels can be assumed to be adequate.

**Table 8.7. Mass Balance Estimation From Chloride IC Data After Final Homogenization Step for both the Lag Storage and Ultrafiltration Process Vessels During Phase II Scaled Test Platform Tests**

Description	LS T27		UFP T16		Units
	Value	Uncertainty	Value	Uncertainty	
<b>Mass Cl- Tracer Injected</b>	84.2	± 10%	43.7	± 10%	g
<b>Tank Simulant Volume</b>	774	± 10%	171	± 10%	gal
<b>Simulant Density</b>	1.18	± 0.03	1.20	± 0.03	g/mL
<b>Fraction of Liquid in Simulant</b>	0.73	± 0.02	0.73	± 0.02	n/a
<b>Measured Initial Conc</b>	140	± 4.5	190	± 4.5	ppm
<b>Measured Final Conc</b>	181	± 4.5	282	± 4.5	ppm
<b>Estimated Final Conc</b>	174	± 7	269	± 12	ppm
<b>Delta</b>	-7	± 8	-13	± 13	ppm
<b>% Deviation</b>	-4%	± 6%	-5%	± 5%	n/a
n/a not applicable					

## 9.0 Conclusions

Chemical tracer development studies for PJM mixing vessels have led to the following conclusions:

- BB and Ethyl Orange optical tracers are recommended for use with the transparent laponite simulant because of the reproducibility of the optical-absorbance values as a function of dye concentration.
- BB optical tracer is recommended for use as a tracer with the kaolin:bentonite opaque simulant. Samples should be centrifuged, and absorbance on the liquid phase should be analyzed. Dye adsorption isotherm data indicated that at low concentrations in the linear Beer's law region, the distribution coefficient can be considered a constant.
- NaCl is recommended as a tracer with the kaolin:bentonite opaque simulant. Samples should be centrifuged and the supernate liquid analyzed with ion chromatography techniques. Use of a chloride ion selective electrode with centrifuged supernate liquid is an option that should be further evaluated. Adsorption of the chloride ion on the solid phase did not appear significant.
- Although developed for use with the opaque simulant, the combination of NaCl and chloride ion selective electrode could be used with the laponite simulant. However, rheological changes may be produced when adding salts to laponite. These rheological changes should be evaluated before implementing a tracer.
- The equation  $MR_j = \frac{C_f - C_j}{C_f - C_0}$  where  $MR_j$  is the fraction mixed in the PJM vessel should be used for evaluating mixing performance with all recommended tracer/simulant combinations. This equation requires concentration determination in the liquid phase of an initial low-tracer baseline sample,  $C_0$ , a sample from the mixing cavern,  $C_j$ , and a sample from the vessel after complete homogenization,  $C_f$ . This equation requires an experimental method of homogenizing the tank contents. However, this equation has the advantage over alternative equations of not using isotherm, mass of tracer injected, or mass fraction of solids data. Such data are often difficult to obtain in an accurate manner and can lead to a high degree of uncertainty.
- When the sample tracer concentration is equal to the initial test concentration, the mixing ratio is unity, and the tracer has not reached sample location. When the sample tracer concentration is equal to the final test concentration, the mixing ratio is zero, and the vessel is nearly homogenous. Lastly, when the sample tracer concentration is above the final test concentration, the mixing ratio is negative. This corresponds to a situation where the sample location is within the mixing cavern, and the fraction mixed calculation may be performed.
- Two criteria for "good" mixing were established. The first criterion is that all samples at a particular time are consistent with a well mixed vessel condition (i.e., mixing ratio is zero) to two standard deviations on measurement error. The second criterion is to calculate the probability score of a well mixed vessel by calculating the probability of the mixing ratio being zero using the average mixing-ratio values and measurement error—the higher the probability score, the more confidence that a homogenous condition can be achieved in a PJM test vessel.
- When the BB dye results are compared to the chloride results, the dye mixing-ratio values are consistently biased towards greater values than the chloride results. In many instances, the final mixing ratio for the BB dye exceeds zero while the chloride tracer results rarely exceed zero. These

data suggest that a systemic issue with the BB dye exists where the 2-phase model of a well mixed cavern and quiescent phase does not hold. However, this model appears to hold for the chloride tracer. This behavior may be explained by the dye sorbing onto the clay particles in the stock solution while the chloride remains in solution. The stock solution clay particles loaded with BB dye may adhere to the tank walls more readily than the low dye clay. This behavior is consistent with observations of streaking along the tank walls during some tests. Conversely, the chloride remains mobile within the mixing cavern. During the tests, samples are taken and dye concentrations are reduced compared to the chloride measurements. During the final homogenization step, enough energy is supplied to incorporate the adhered dye into the simulant, resulting in greater-than-zero mixing-ratio values for the BB dye.

- To eliminate the BB dye bias problem, an obvious solution is to only use the chloride data for evaluating the tests. Unfortunately, the chloride analytical techniques possess a higher degree of error compared to the dye techniques. Therefore, the corresponding probability scores for the chloride tracer are significantly lower than the BB dye tracer scores. The current evaluation strategy is to use both techniques and interpret the results with the knowledge that bias may be present in the BB dye results. If a configuration is tested that possesses enough mixing energy, the adhered dye is removed, and zero mixing-ratio values are obtained. This situation is seen in Figure 8.8 where the BB dye and chloride results are in good agreement. When a promising configuration is identified, multiple tests should be performed with the chloride tracer. These multiple tests should allow for the error bars to be computed experimentally. With high test repeatability, confidence in the mixing potential for a given test configuration can be increased.
- The amount of chloride tracer used in each test may be increased to reduce uncertainty. Currently, a final concentration increase of 30 ppm chloride is used. Increasing this value to 100 ppm should reduce the associated error significantly. However, tradeoffs such as wastewater limitations for chloride ions and simulant rheological properties changes with salt concentration should be considered.

## 10.0 References

- Fahrenhorst C, J Botschek, A Skowronek, J Ferraz. 1999. "Application of gypsum and lime to increase cation adsorption of a Geric Ferralsol in the Brazilian Amazon region." *J. Plant Nutr. Soil Sci.* 162:41-47.
- Flury M, and NN Wai. 2003. "Dyes as tracers for vadose zone hydrology." *Reviews of Geophysics.* 41(1):1002.
- Flury M, and H Fluhler. 1994. "Brilliant Blue FCF as a dye tracer for solute transport studies – a toxicological overview." *J. Environ. Qual.* 23:1108-1112.
- Flury M, and H Fluhler. 1995. "Tracer characteristics of Brilliant Blue FCF." *Soil Sci. Soc. Am. J.* 59:22-27.
- German-Heins J, and M Flury. 2000. "Sorption of Brilliant Blue FCF in soils as affected by pH and ionic strength." *Geoderma.* 97:87-101.
- Green FJ. 1990. *The Sigma-Aldrich Handbook of Stains Dyes and Indicators.* Aldrich Chemical Company Milwaukee, Wisconsin. ISBN 0-941633-22-5
- Ketelsen H, and S Meyer-Windel. 1999. "Adsorption of Brilliant Blue FCF by soils." *Geoderma.* 90:131-145.
- Perillo CA, CS Gupta, EA Nater, JF Moncrief. 1998. "Flow velocity effects on the retardation of FD&C Blue No. 1 food dye in soil." *Soil Sci. Soc. Am. J.* 62:39-45.
- Roy WR. 1993. "Adsorption-desorption methodologies and selected estimation techniques for transport-modeling parameters." In: *Migration and Fate of Pollutants in Soils and Subsoils.* Petruzelli D, and FG Helfferich (Eds.), NATO ASI Series vol. g 32 Springer-Verlag, Berlin, pp 169-188.
- Skoog DA, DM West, and FJ Holler. 1988. *Fundamentals of Analytical Chemistry.* Saunders College Publishing, New York. ISBN 0-03-14828-6.

## **Appendix A**

### **Laponite Simulant Test Results**

## Appendix A: Laponite Simulant Test Results

For testing with laponite, dye-injection lines and sample ports were added via tubing into the bottom of the PJM tanks near the PJM nozzles. These lines were then used to inject dye and sample directly from the PJM cavern during operation. It was discovered that the injection with the pump had to be done at a slow pump speed. At high pump rates, the stock dye solution could jet out of the cavern and onto the surface of the tank, resulting in erroneous results. In addition, the air in the sample line needed to be purged by pumping simulant from the test vessel through the dye-injection line. Rising air bubbles would rise out of the mixing cavern and create a path for the dye to flow through the mixing cavern to the surface.

Samples were drawn from the sample lines in the bottom of the PJM vessel. The samples were taken without using a pump. The line valve was opened, and a sample was obtained via gravity draining. The sample line was purged of residual sample before collecting the sample for analysis.

Results using this method of dye injection/sampling with the transparent laponite simulant are described in the remainder of Appendix A.

### A.1 APEL Four PJM System

**Table A.1. Percent of Tank Mixed and Error Estimate APEL 4-PJM Tests**

Test Date	Dye Used	Initial Sample Absorbance	Cavern Sample Absorbance	Final Sample Absorbance	Percent of Tank Mixed	Estimated Error ( $\pm$ )
9/15/03	Brilliant Blue (633.3 nm)	-0.004	0.352	0.111	32	3.0
9/16/03	Fluorescein (489.4 nm)	0.775	1.880	1.201	38.6	1.1
9/18/03	Brilliant Blue (633.3 nm)	0.109	1.249	0.497	34.0	1.0
9/30/03 Run 1	Ethyl Orange (476.95 nm)	-0.002	1.218	0.271	22.4	1.0
9/30/03 Run 2	Ethyl Orange (476.95 nm)	-0.002	0.505	0.271	54	3.0

## A.2 336 Four PJM System

Figures A.1 through A.6 show results from 336 Laponite Cavern tests.

### 336 Laponite Cavern Test with Brilliant Blue Tracer Dye 10/28/03

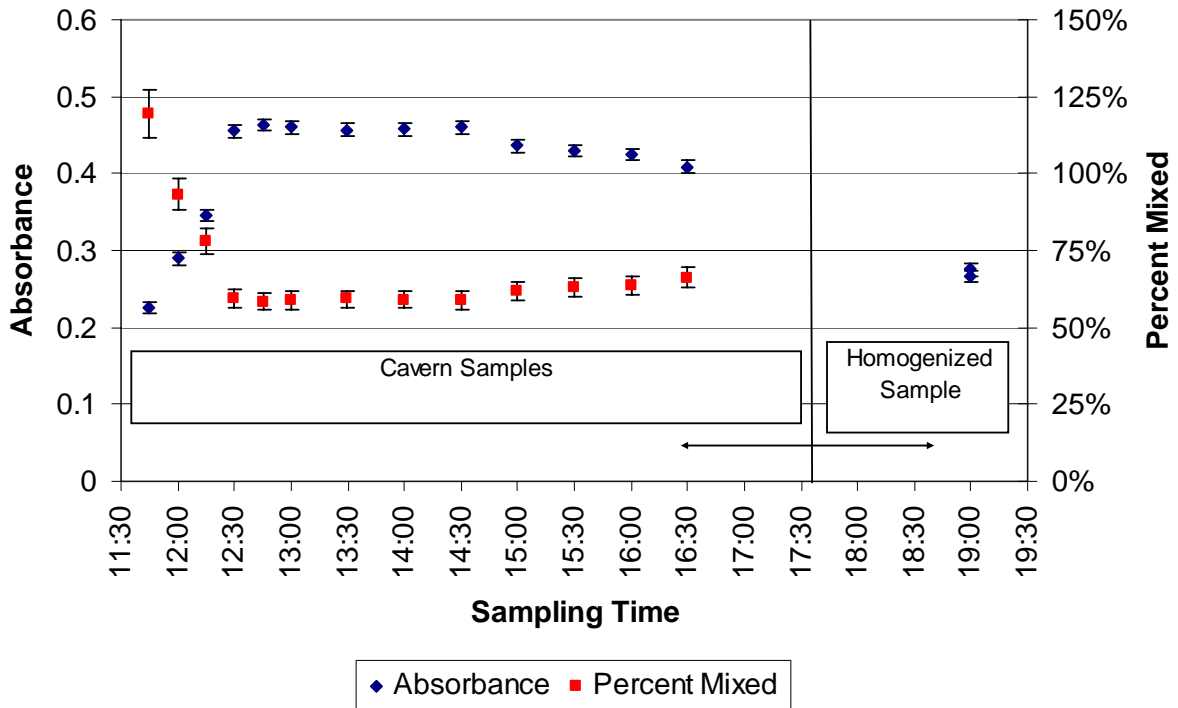


Figure A.1. Absorbance Plots for 10/28/03 336 4-PJM Test

## 336 Laponite Cavern Test with Brilliant Blue Tracer Dye 10/30/03

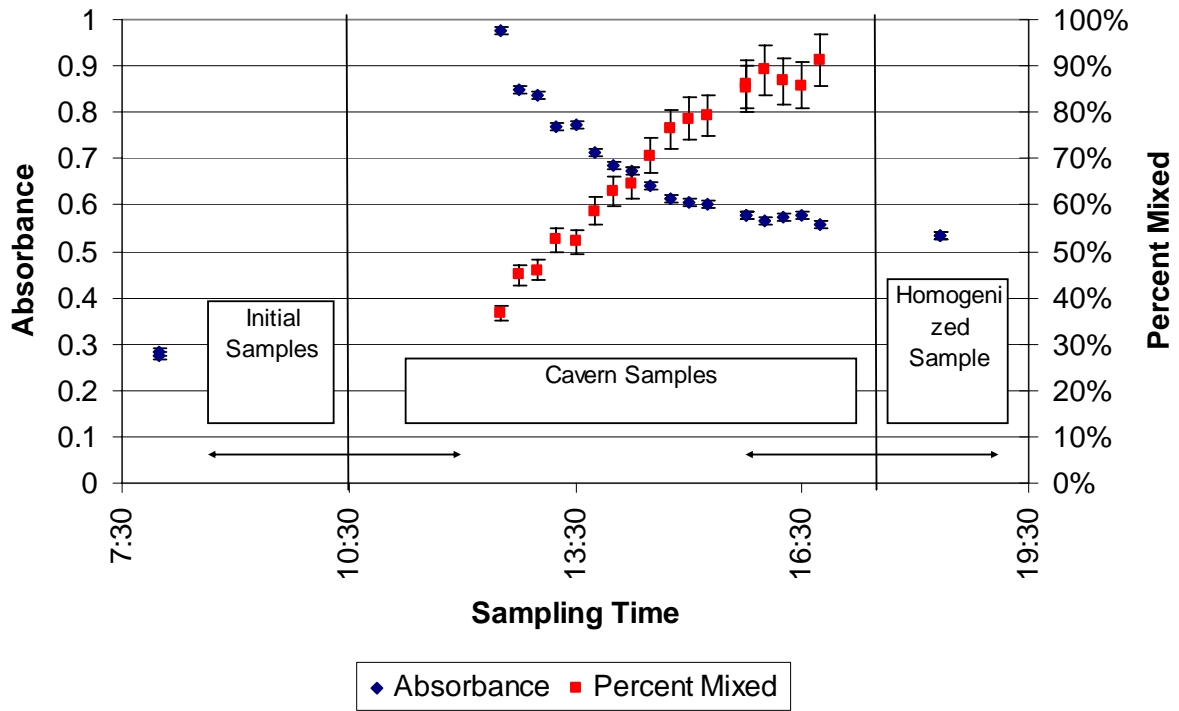


Figure A.2. Absorbance Plots for 10/30/03 336 4-PJM Test

### 336 Laponite Cavern Test with Brilliant Blue Tracer Dye 11/06/03 Run 1

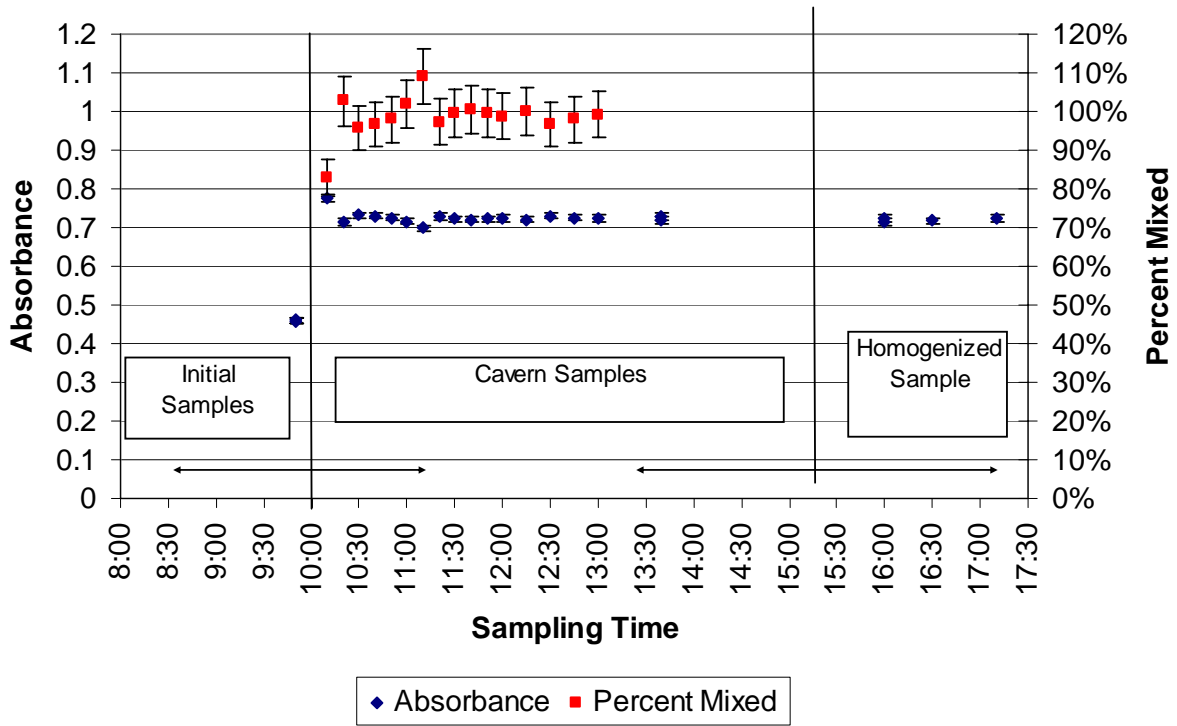


Figure A.3. Absorbance Plots for 11/06/03 336 4-PJM Test (Run 1)

### 336 Laponite Cavern Test with Brilliant Blue Tracer Dye 11/06/03 Run 3

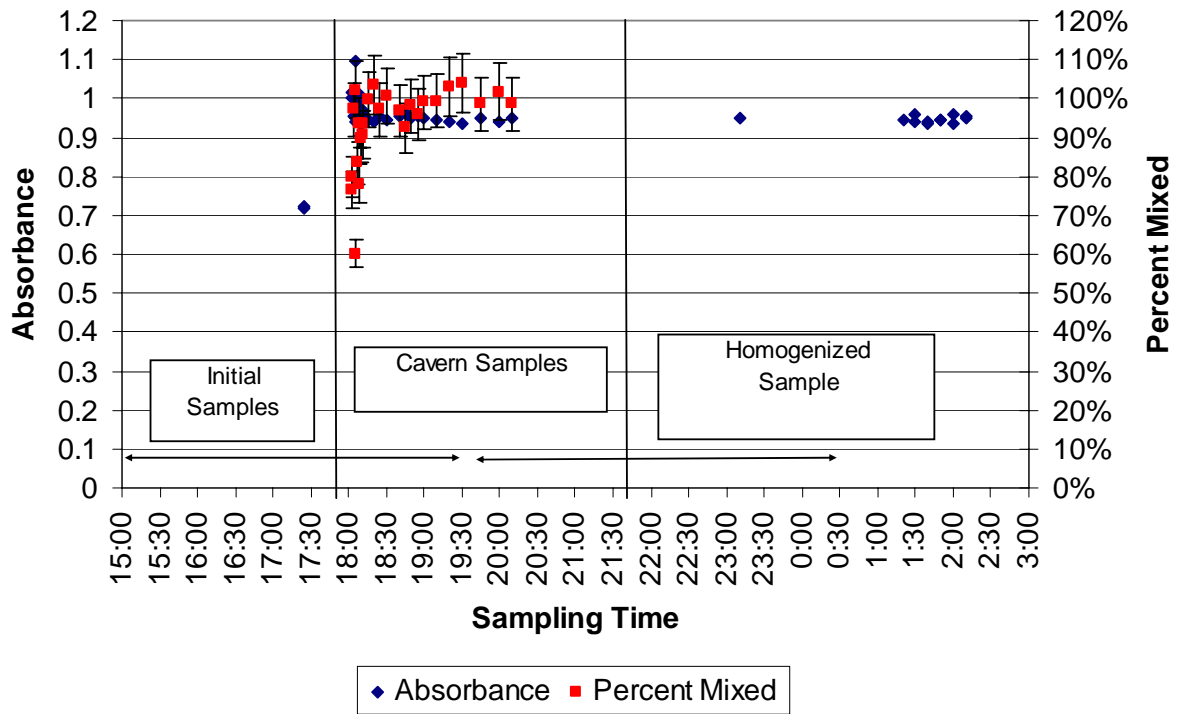


Figure A.4. Absorbance Plots for 11/06/03 336 4-PJM Test (Run 3)

## 336 Laponite Cavern Test with Brilliant Blue Tracer Dye 11/18/03

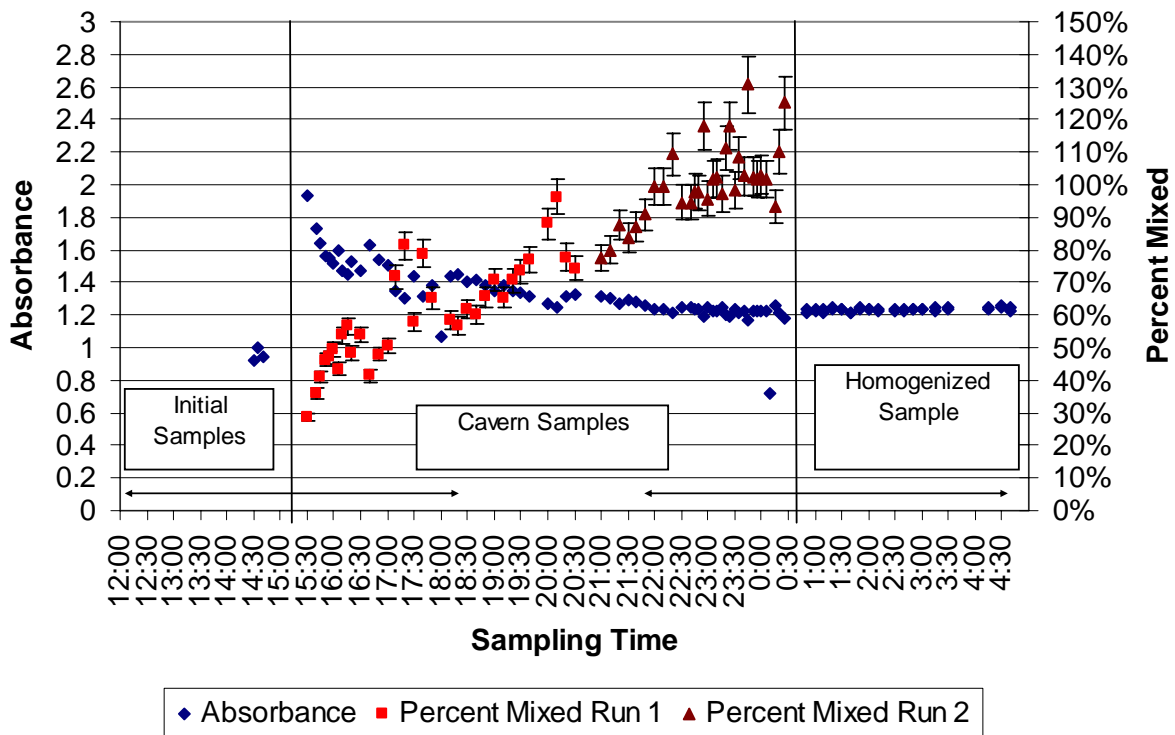


Figure A.5. Absorbance Plots for 11/18/03 336 4-PJM Test

### 336 Laponite Cavern Test with Brilliant Blue Tracer Dye 11/20/03

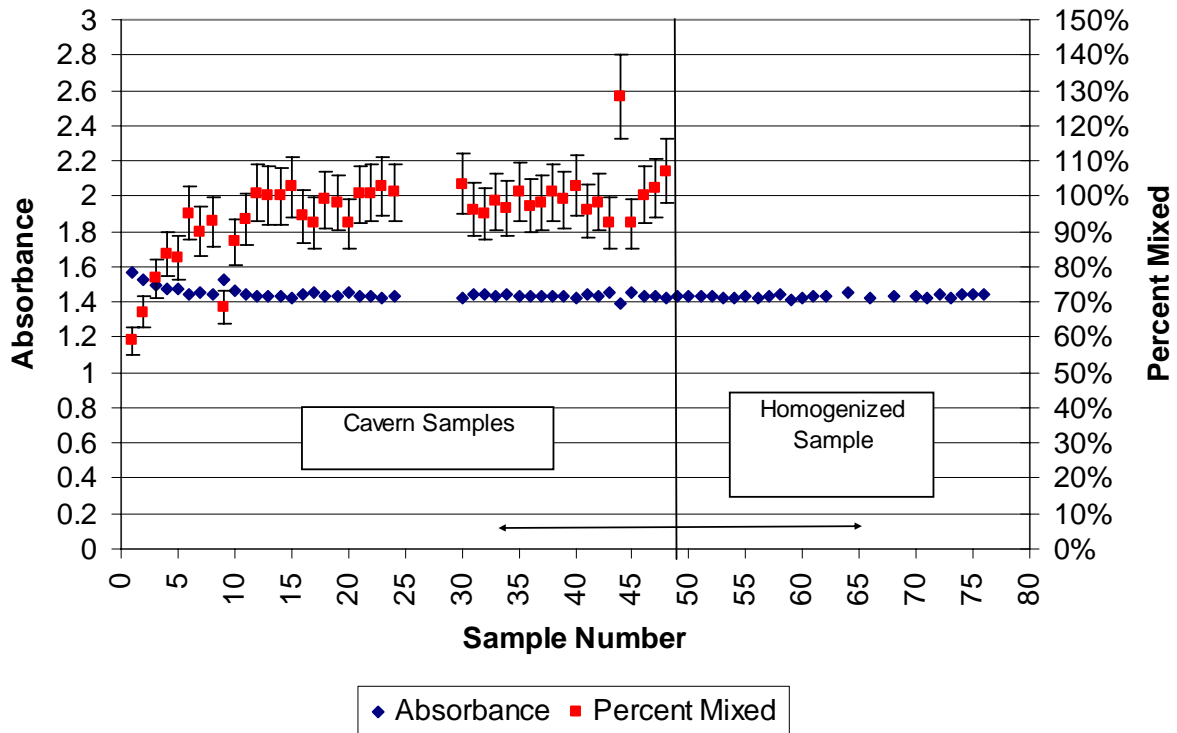


Figure A.6. Absorbance plots for 11/20/03 336 4-PJM Test

## **Appendix B**

### **Kaolin:Bentonite Simulant Test Results**

## Appendix B: Kaolin:Bentonite Simulant Test Results

When testing with the kaolin:bentonite simulant, a stock solution of the chemical being used was prepared by dissolution in water. This stock solution was then blended with a sample of the test simulant to raise the rheological properties close to the actual test simulant. This solution was introduced into the center PJM tube during operation by operating a pump on the sample injection line.

After the dye was injected, the experimental clock started, and samples were drawn from several locations in each test vessel. For example, during Phase II Scaled Test Platform Tests, locations 1, 2, and 3 were samples taken directly from three separate pulse tubes. These samples should represent the contents of the well mixed cavern. Sample locations 4 and 5 were placed between the pulse tubes and the tank wall. Location 4 was at a low elevation and location 5 was at a high elevation. Schematic diagrams of the tracer sampling locations during phase II are shown in Figures B.1 and B.2 for the lag storage (LS) vessel and ultrafiltration process (UFP) vessel, respectively.

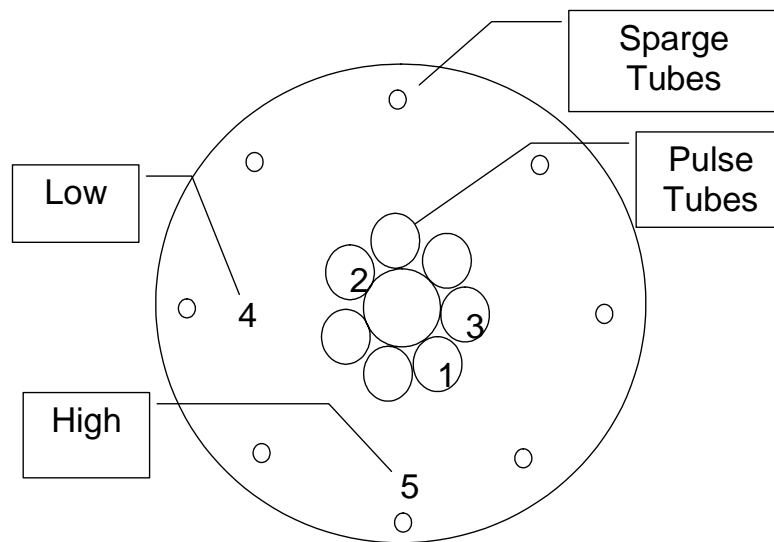


**Figure B.1. Schematic of Lag Storage Vessel Tracer Sampling Locations During Phase II Scaled Test Platform Tests**

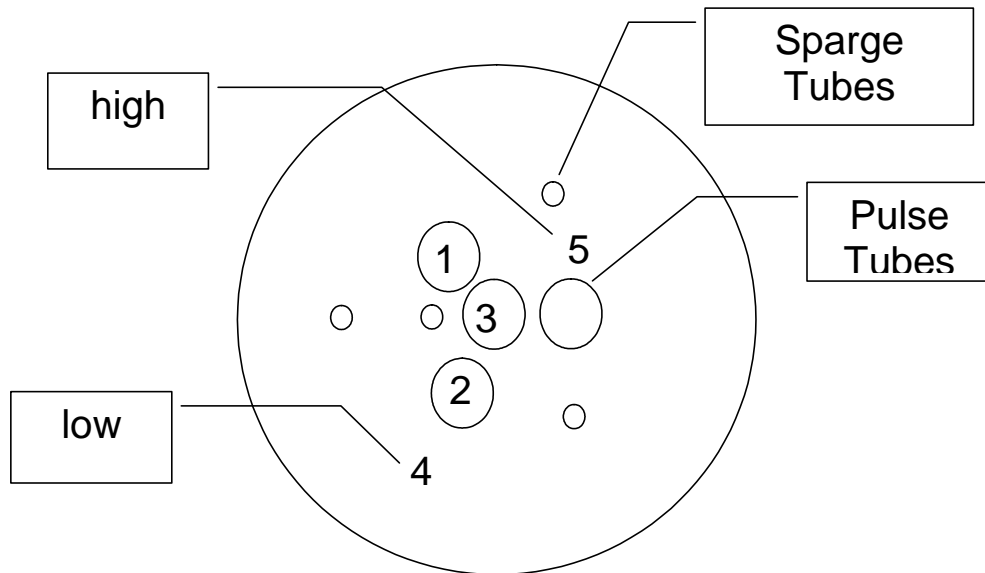


**Figure B.2. Schematic of Ultrafiltration Process Vessel Tracer Sampling Locations During Phase II Scaled Test Platform Tests**

Multiple-run conditions were typically achieved for each tracer injection. The tracer test started with the lowest mixing energy condition to form the initial well mixed cavern. Additional systems, such as recirculation pumps or sparging tubes, or increased pulse tube velocities were then used as subsequent run conditions to form larger mixing caverns.

Results of using this method of dye injection/sampling with the opaque kaolin:bentonite simulant are described in the remainder of Appendix B.

## B.1 Phase I Scaled Test Platform Tests

Figures B.3 through B.5 shows results from Phase I Scaled Test Platform Tests.

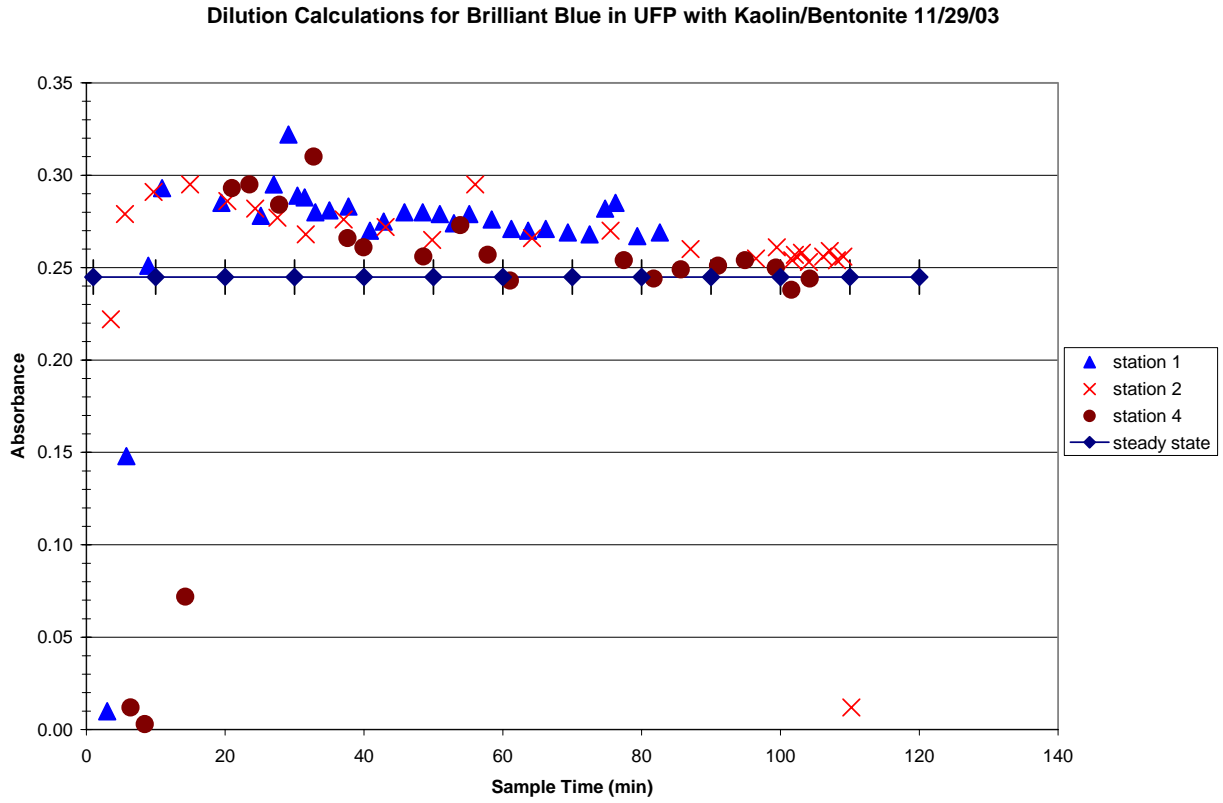


**Figure B.3. Dye Adsorption on Samples Taken from UFP All-in Test 11/29/03**

Absorption Calculations for Brilliant Blue in LS with Kaolin/Bentonite 12/04/03

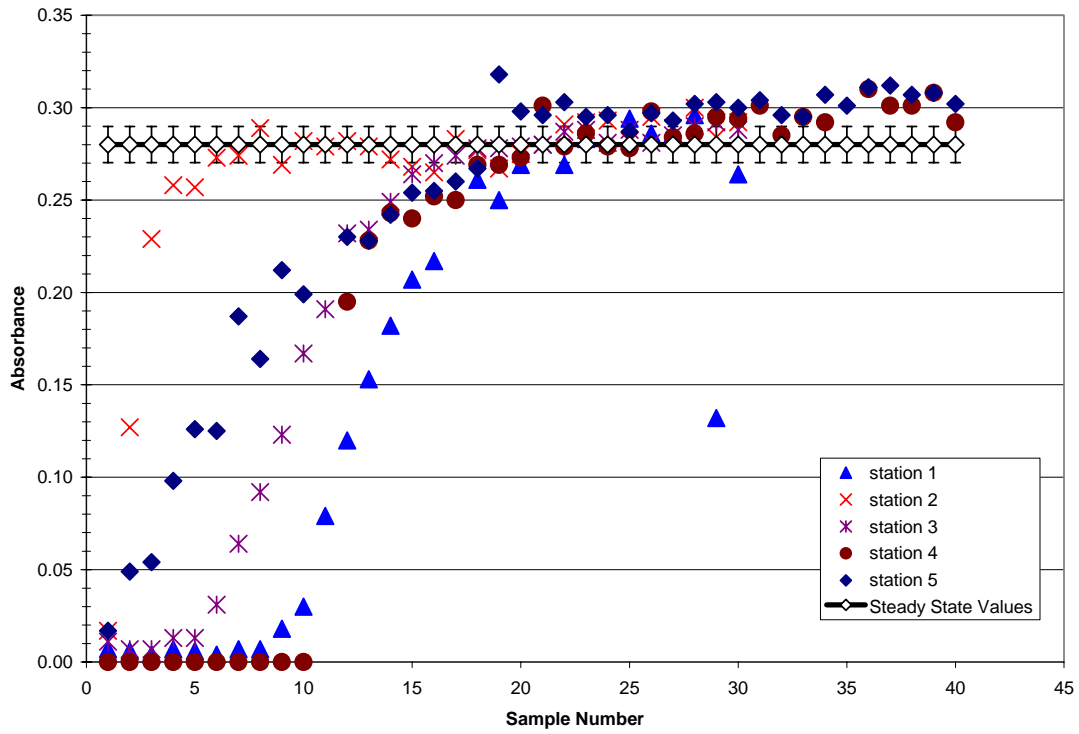


Figure B.4. Dye Adsorption on Samples Taken from LS All-in Test 12/04/03

Absorption Calculations for Brilliant Blue in LS with Kaolin/Bentonite 12/13/03

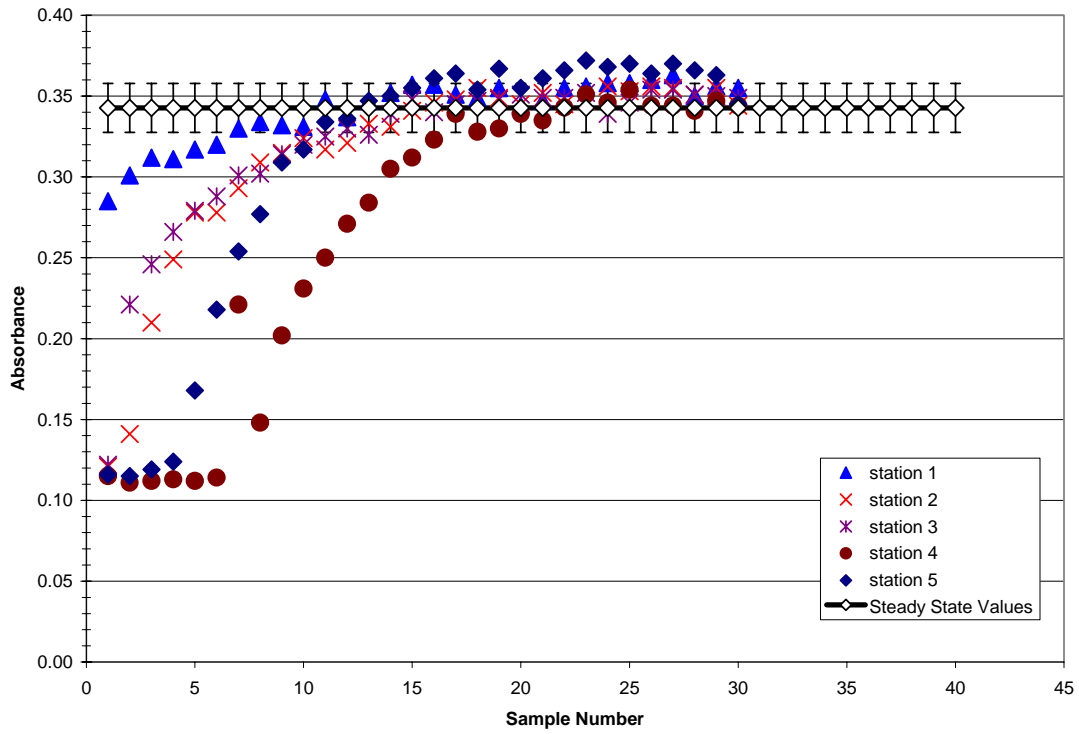


Figure B.5. Dye Adsorption on Samples Taken from LS All-in Test 12/13/03

## B.2 Phase II Scaled Test Platform Tests

Figures B.6 through B.29 shows results from Phase II Scaled Test Platform Tests.

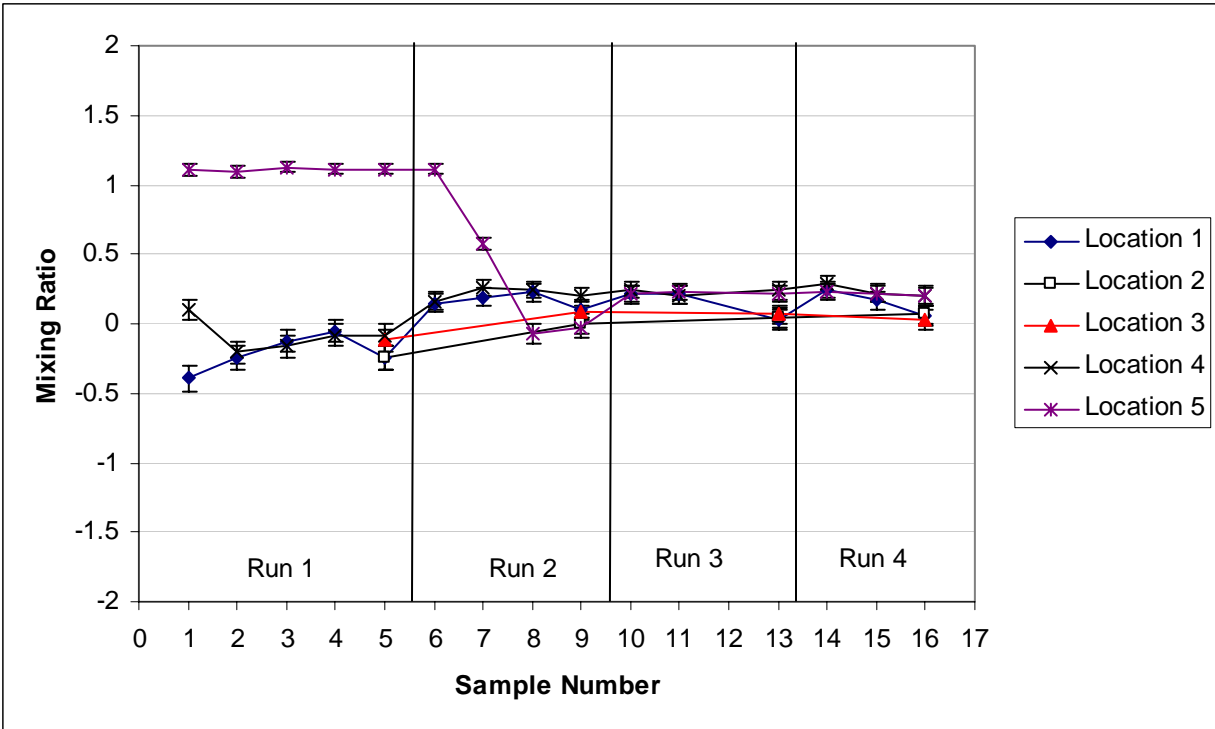
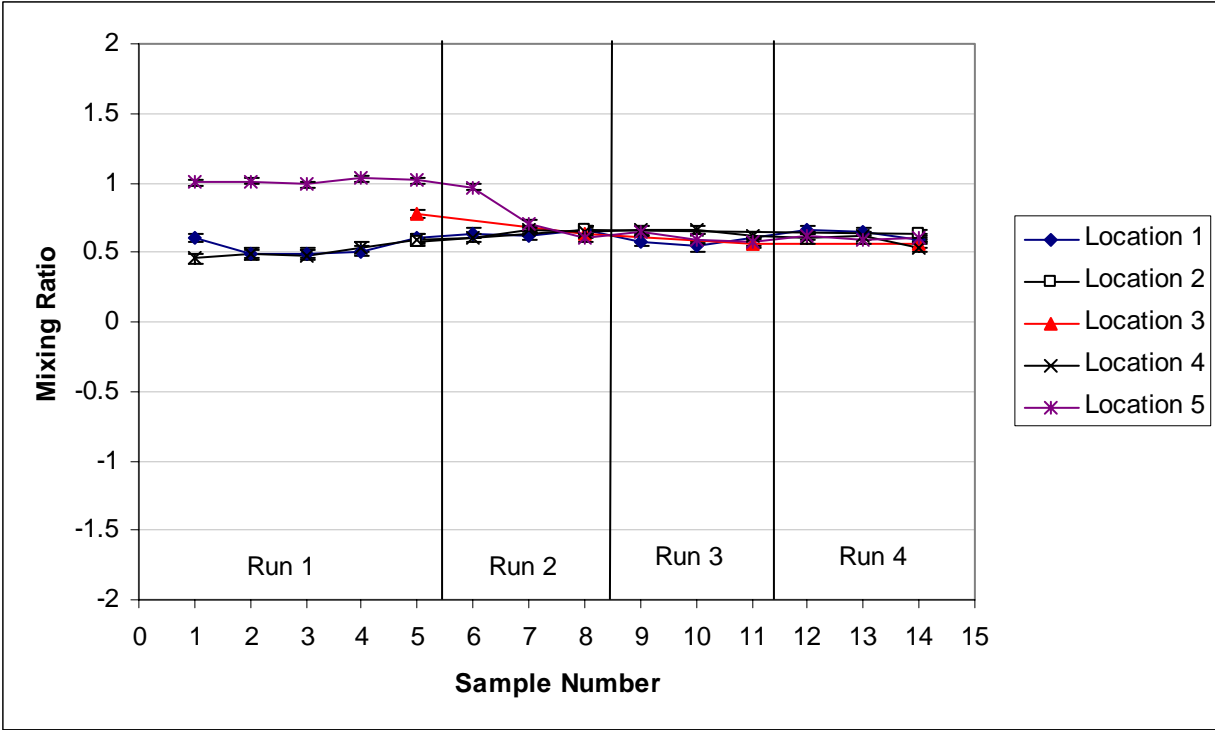
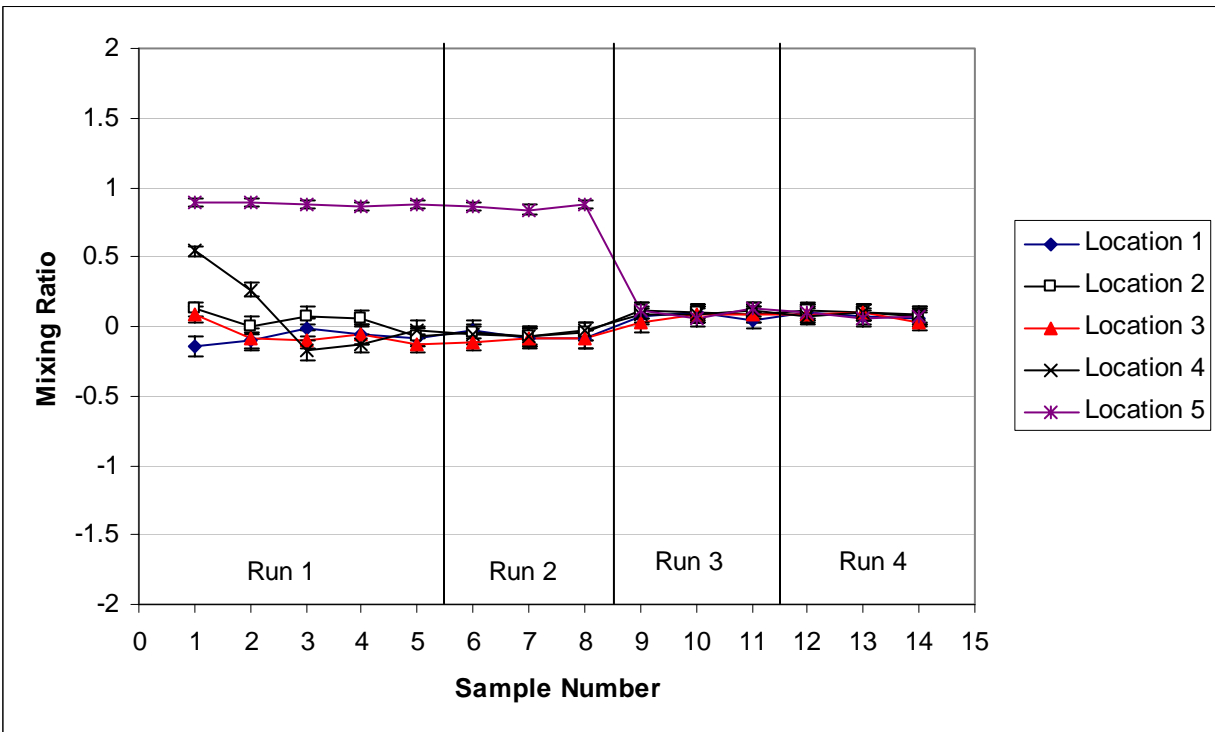


Figure B.6. Mixing-Ratio Results from LS Test Sequence 1 Using BB Tracer



**Figure B.7. Mixing-Ratio Results from LS Test Sequence 2 Using BB Tracer**



**Figure B.8. Mixing-Ratio Results from LS Test Sequence 2A Using BB Tracer**

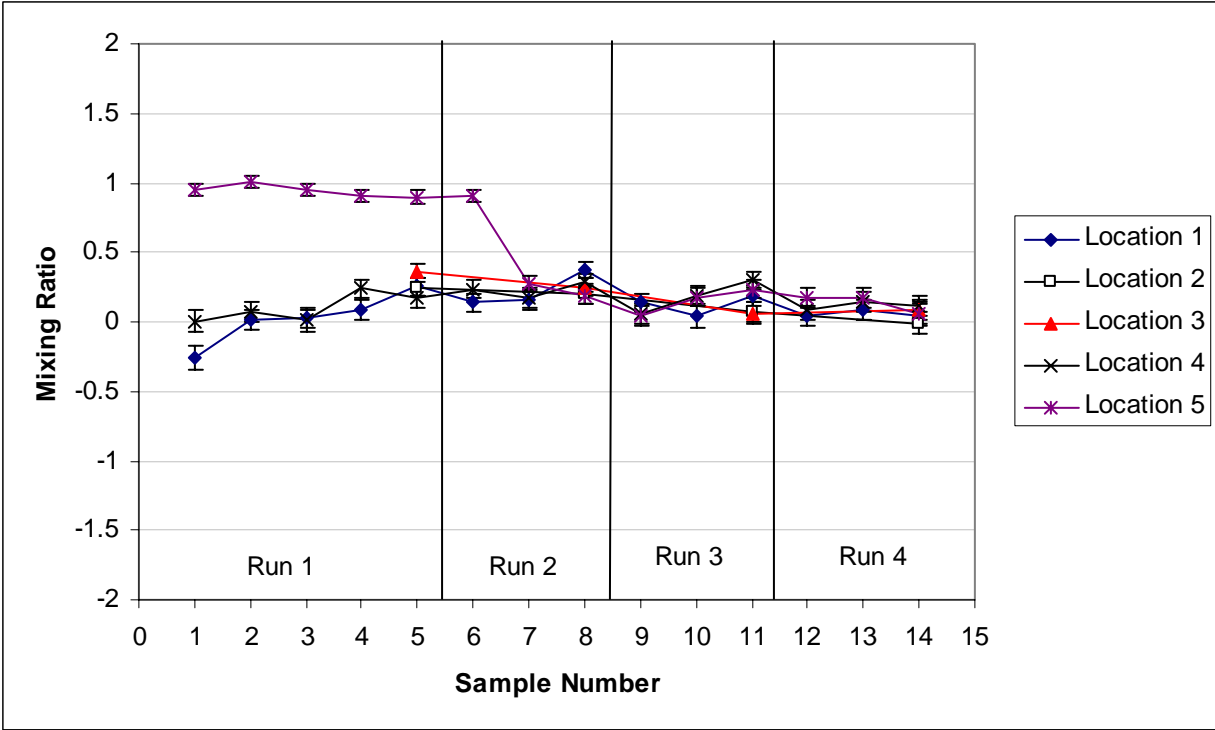


**Figure B.9. Mixing-Ratio Results from LS Test Sequence 3 Using BB Tracer**

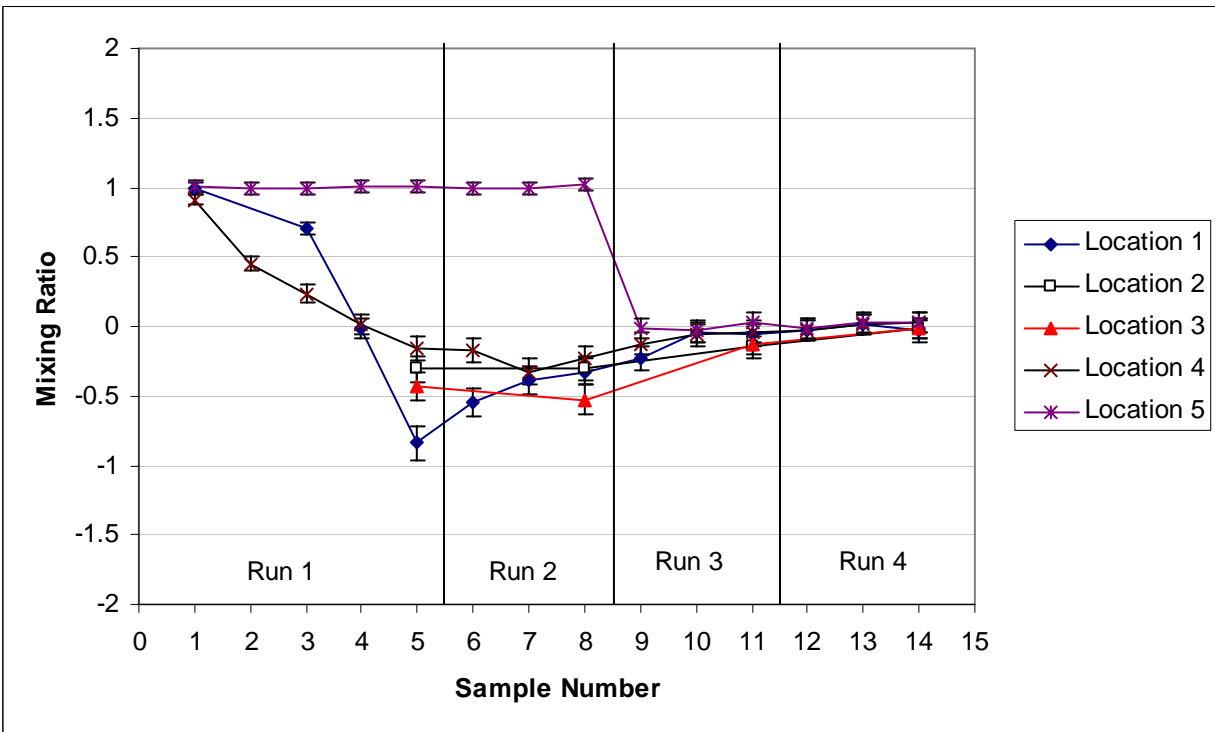


**Figure B.10. Mixing-Ratio Results from LS Test Sequence 4 Using BB Tracer**

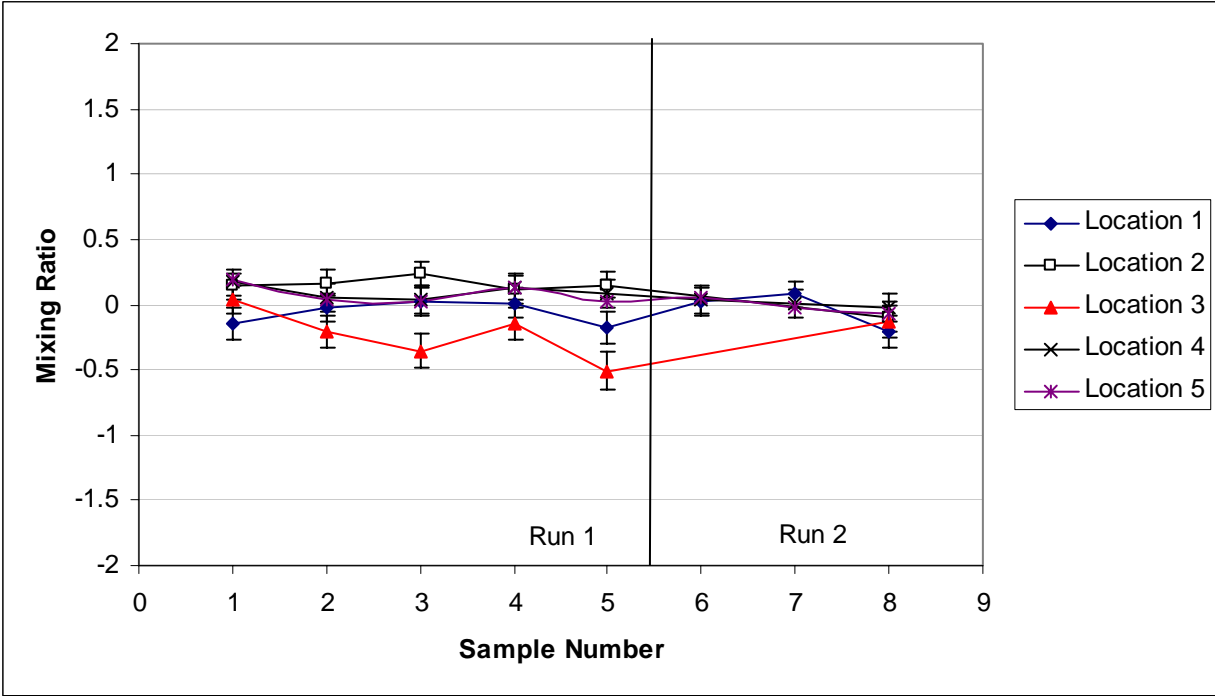


Figure B.11. Mixing-Ratio Results from LS Test Sequence 5 Using BB Tracer

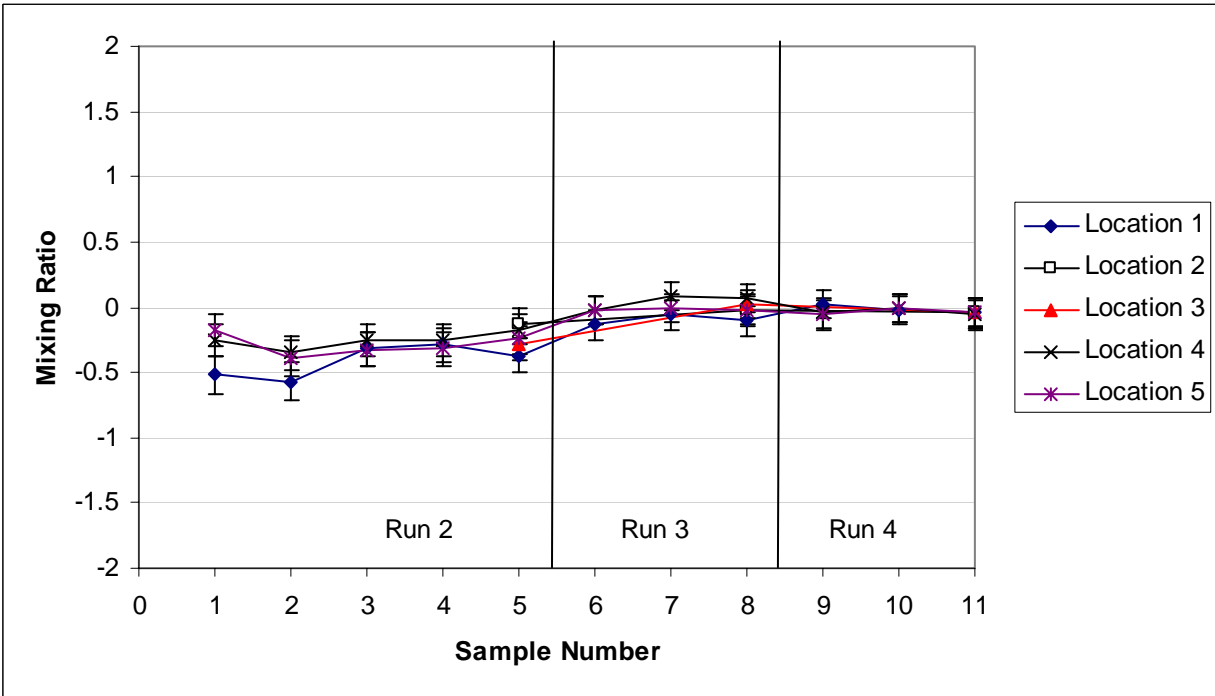


Figure B.12. Mixing-Ratio Results from LS Test Sequence 6 Using BB Tracer

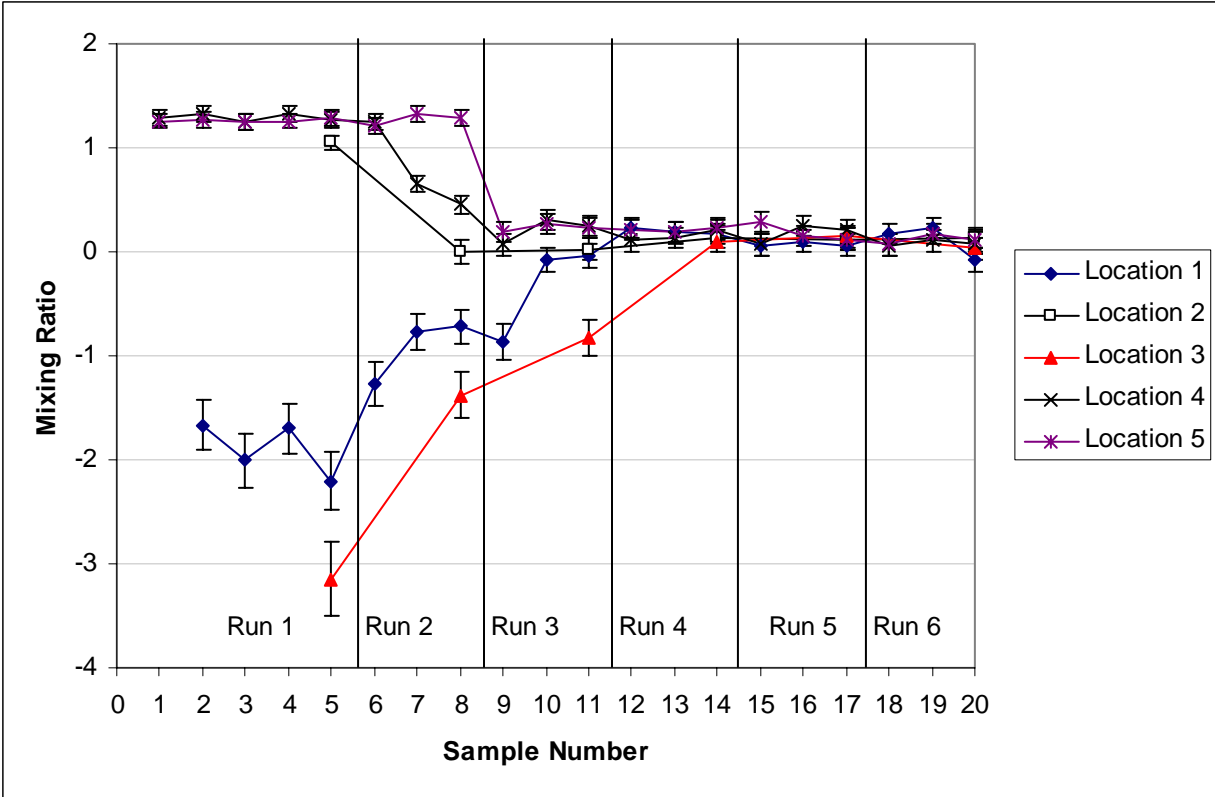


Figure B.13. Mixing-Ratio Results from LS Test Sequence 7 Using BB Tracer

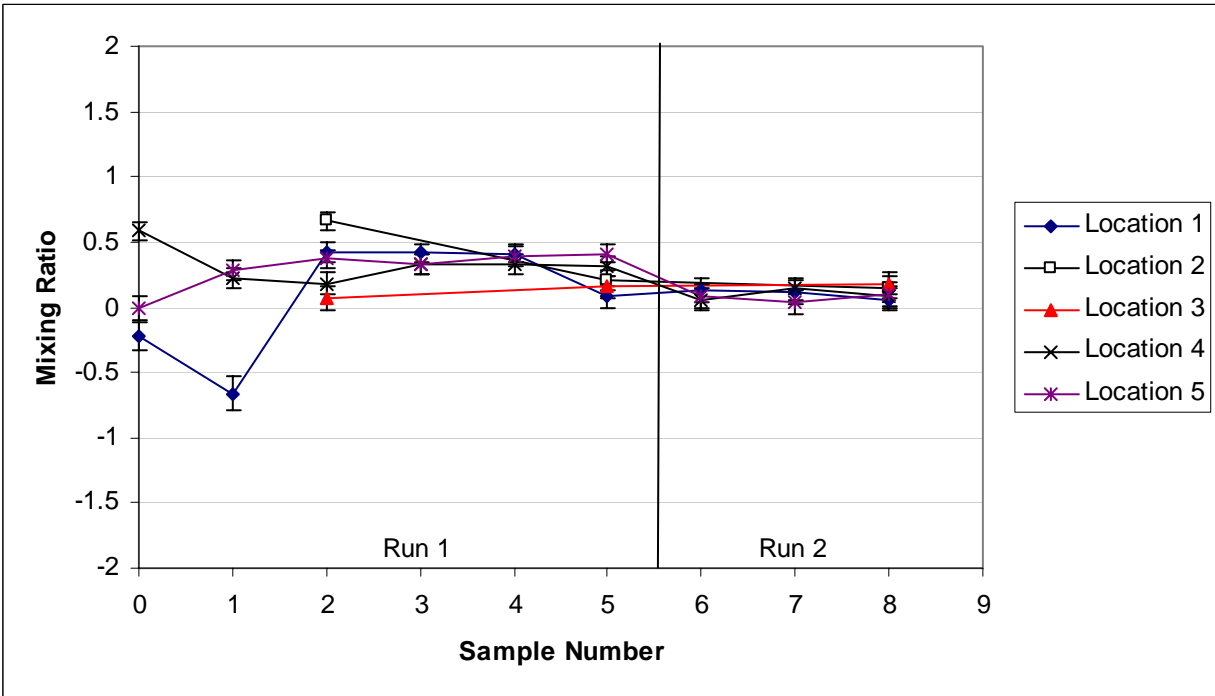


Figure B.14. Mixing-Ratio Results from LS Test Sequence 8 Using BB Tracer

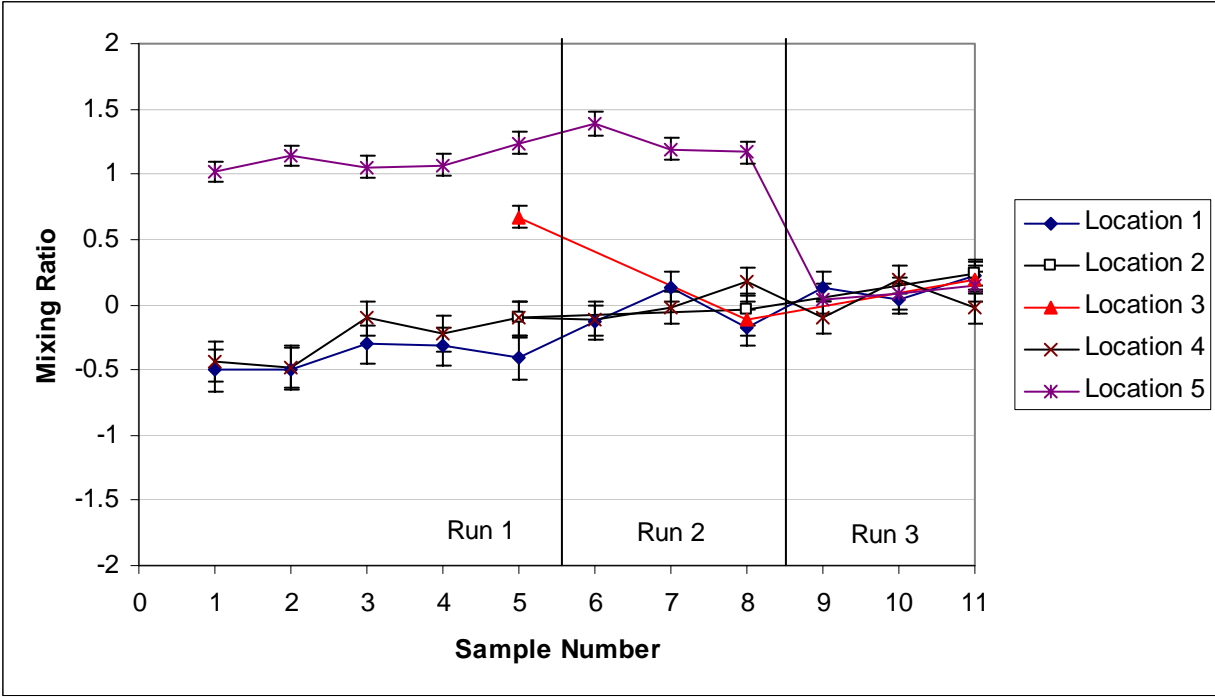


Figure B.15. Mixing-Ratio Results from LS Test Sequence 9 Using BB Tracer

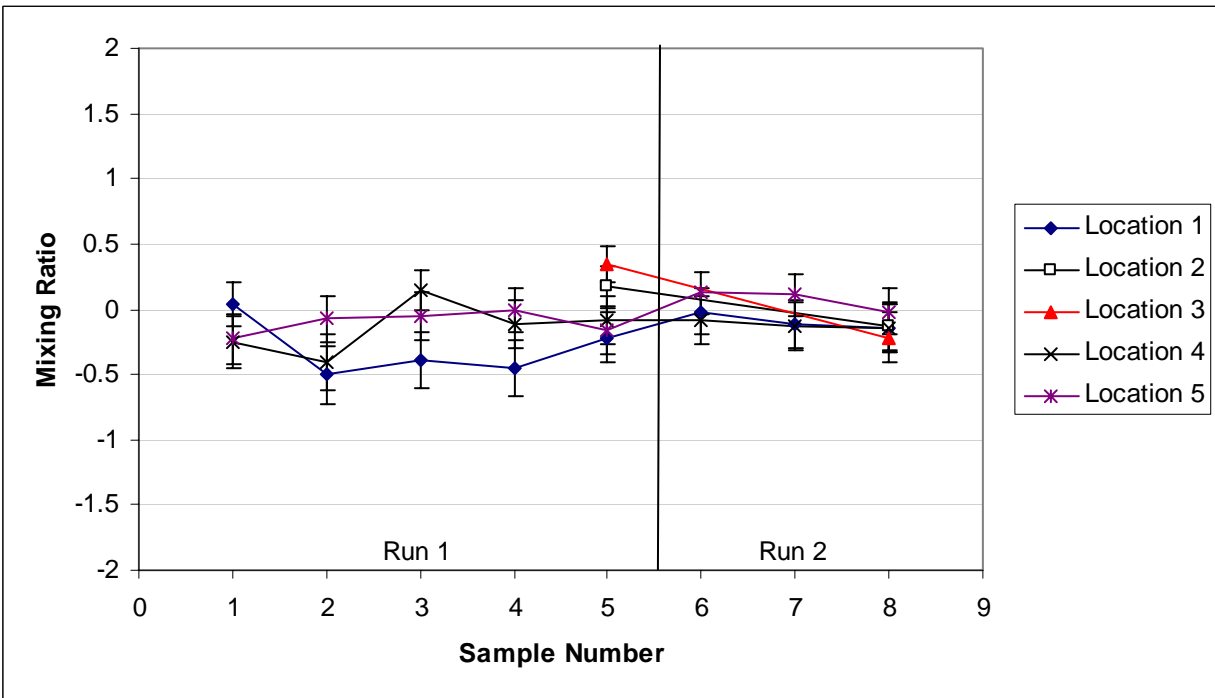


Figure B.16. Mixing-Ratio Results from LS Test Sequence 10 Using BB Tracer

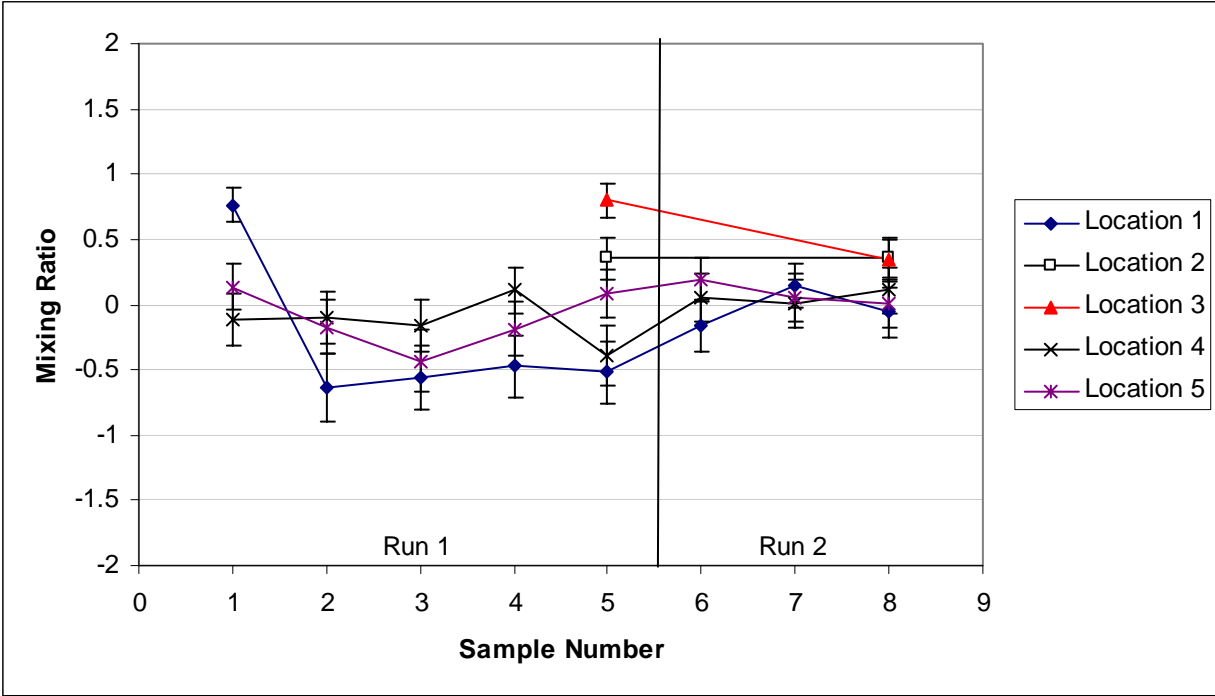


Figure B.17. Mixing-Ratio Results from LS Test Sequence 11 Using BB Tracer

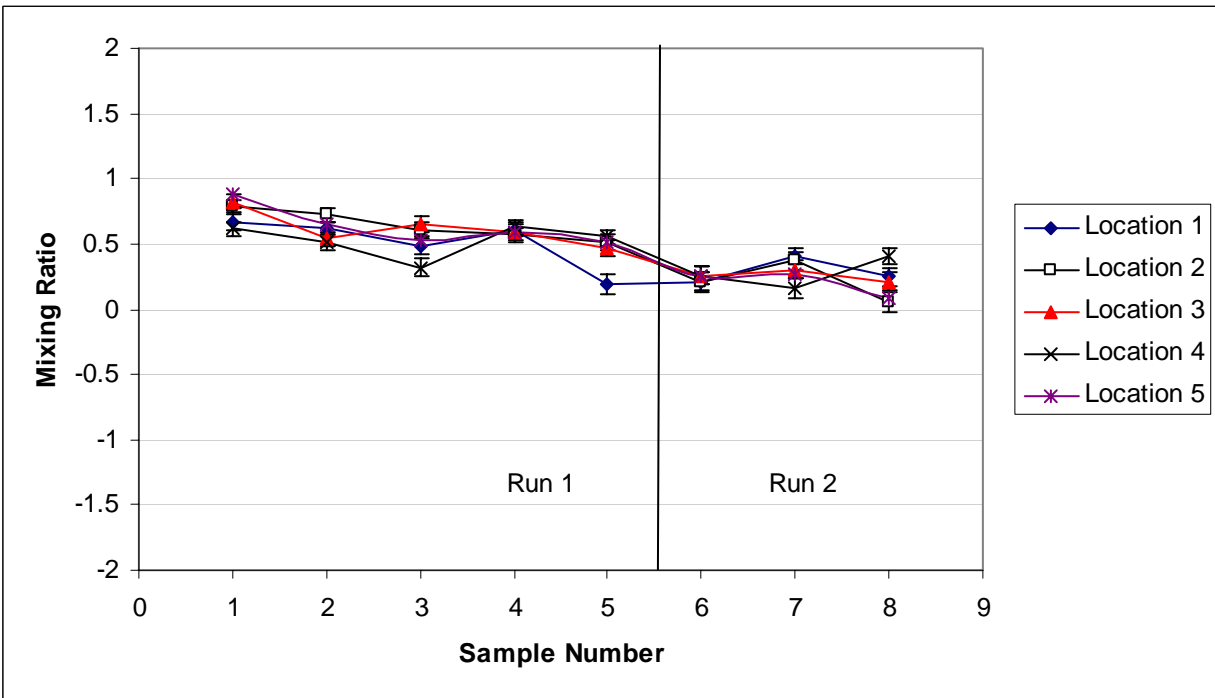


Figure B.18. Mixing-Ratio Results from LS Test Sequence 12 Using BB Tracer

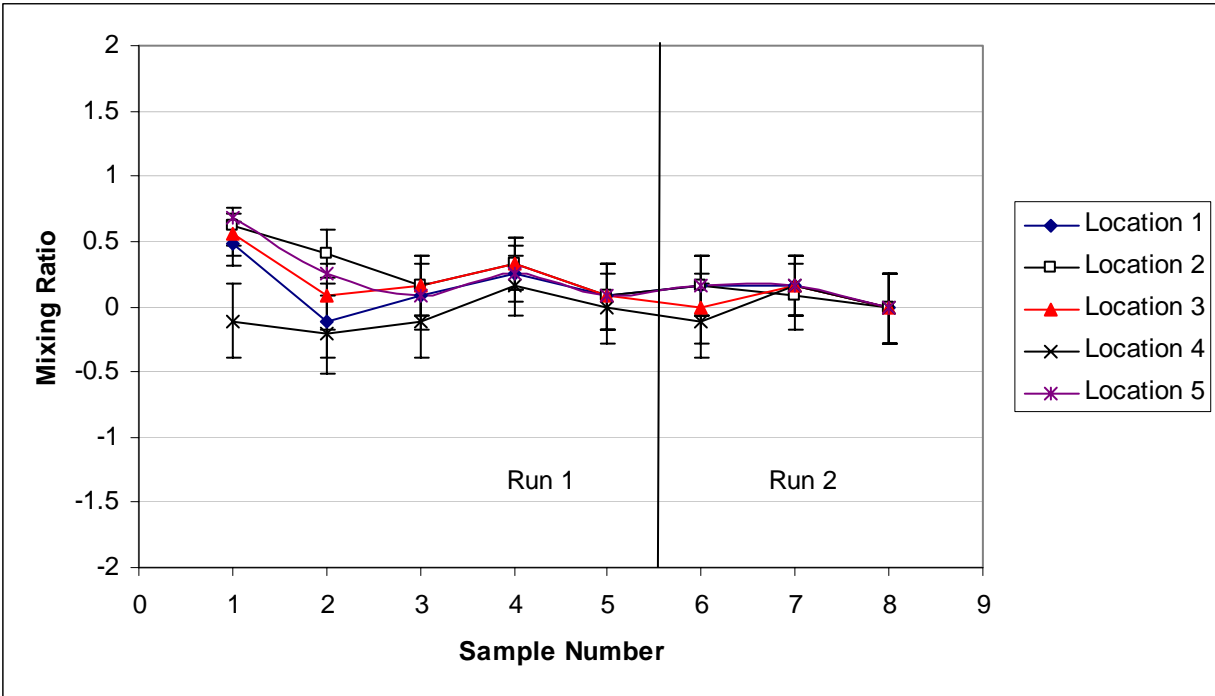


Figure B.19. Mixing-Ratio Results from LS Test Sequence 12 Using Chloride Tracer with ISE

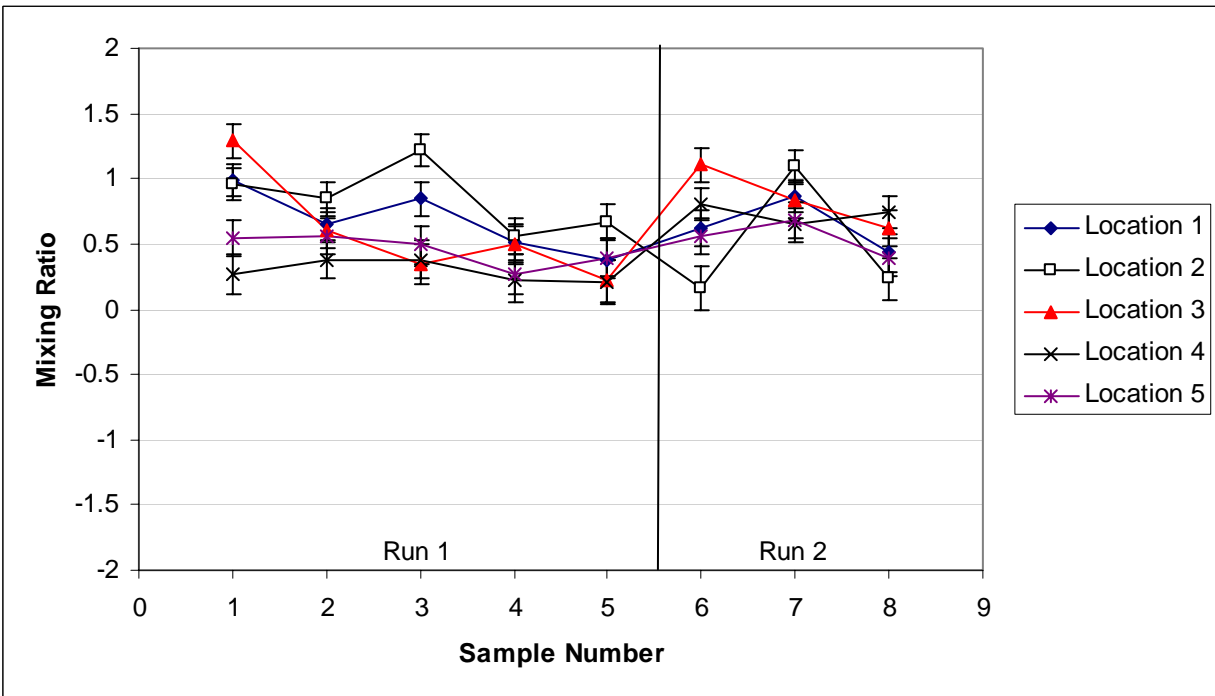


Figure B.20. Mixing-Ratio Results from LS Test Sequence 13 Using BB Tracer

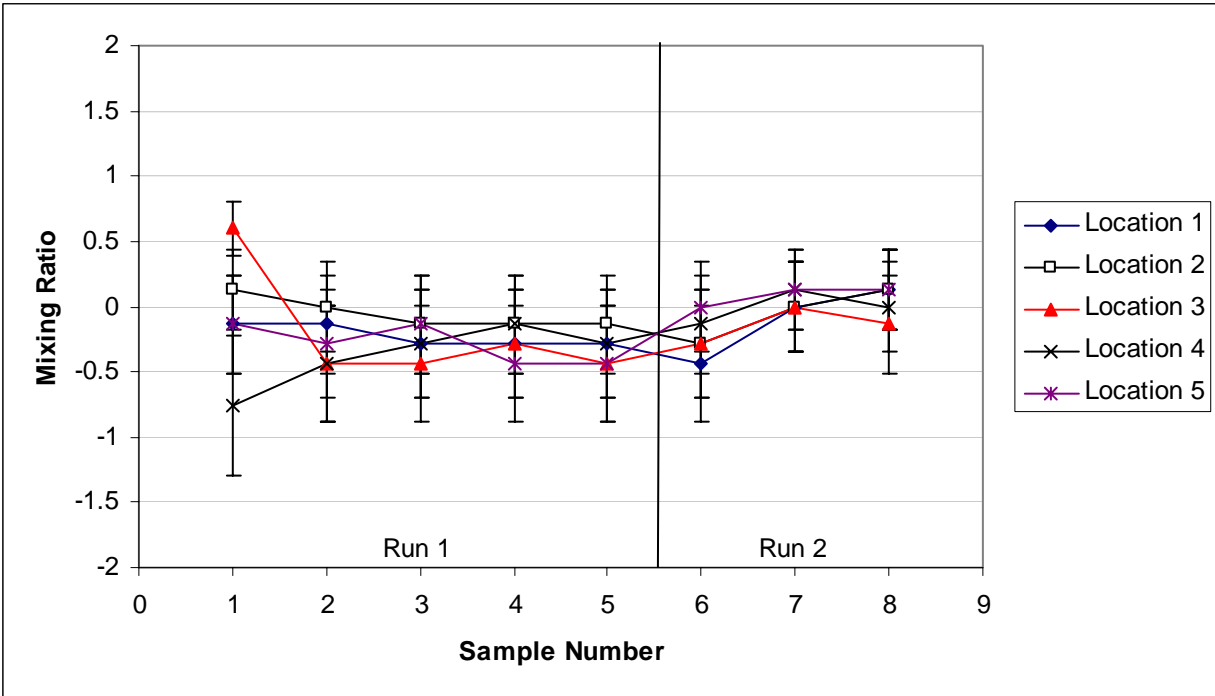


Figure B.21. Mixing-Ratio Results from LS Test Sequence 13 Using Chloride Tracer with ISE

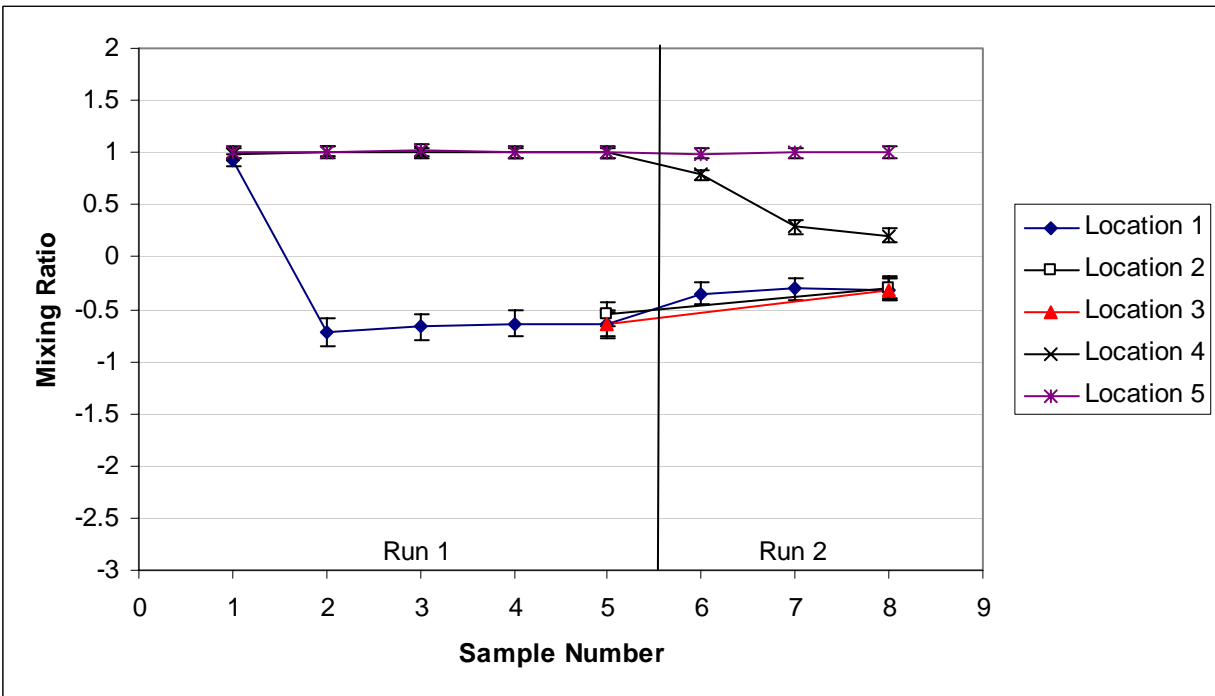


Figure B.22. Mixing-Ratio Results from LS Test Sequence 19 Using BB Tracer

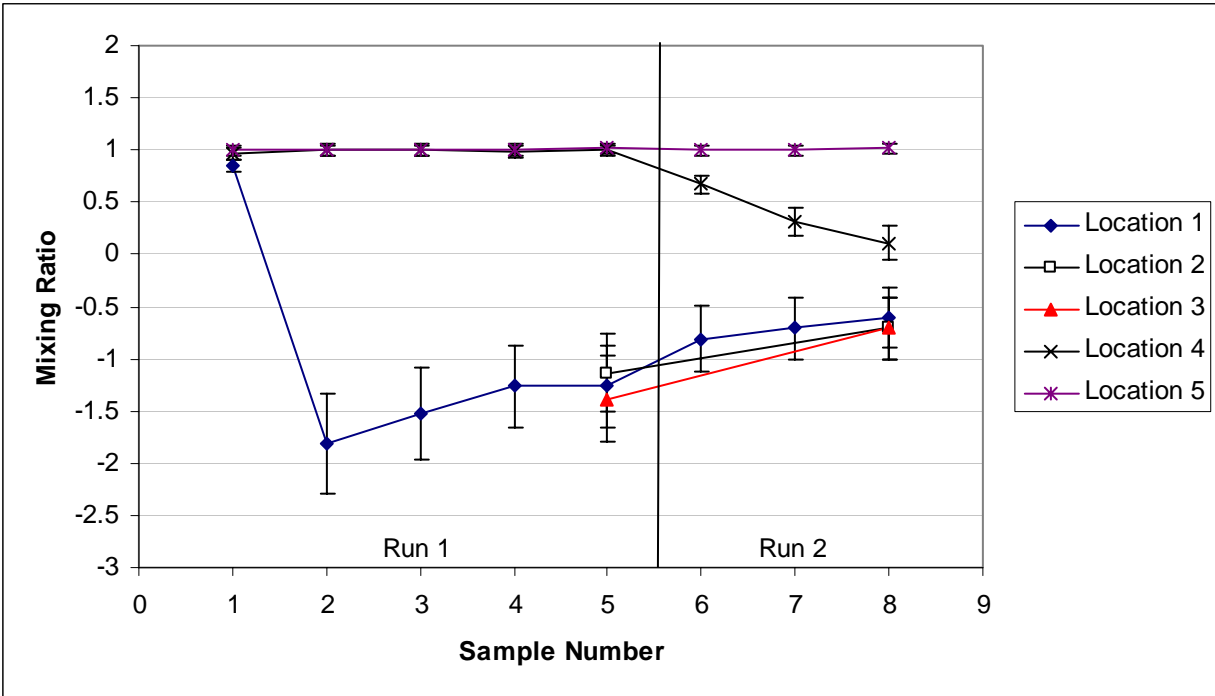


Figure B.23. Mixing-Ratio Results from LS Test Sequence 19 Using Chloride Tracer with ISE

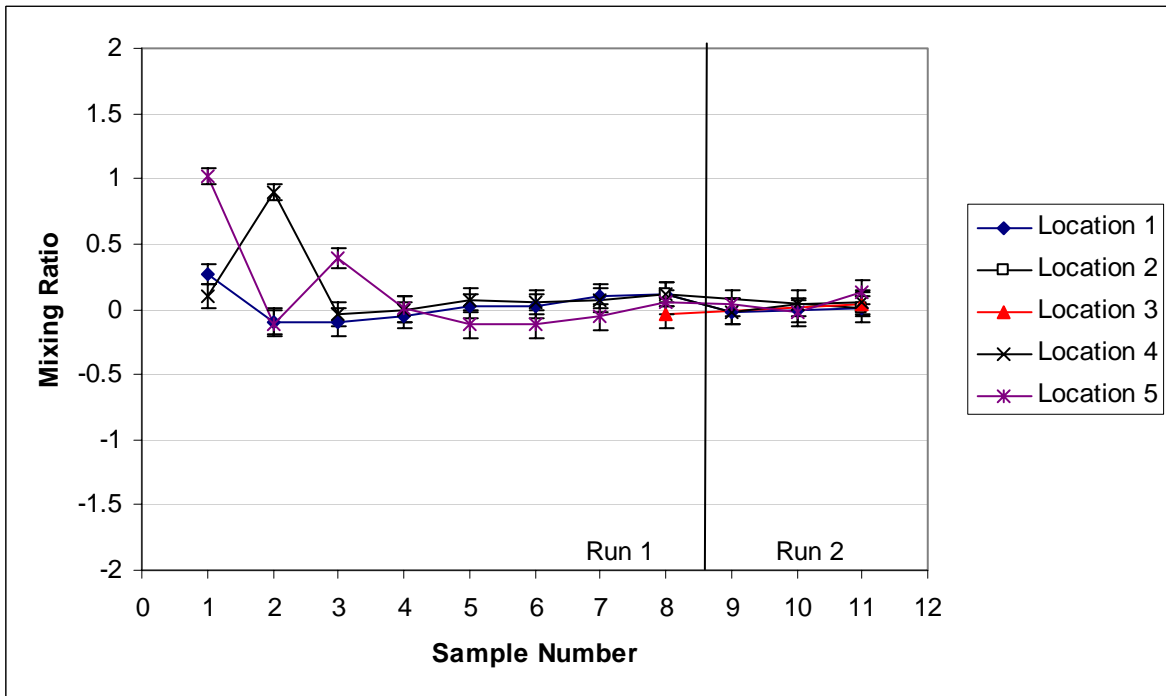


Figure B.24. Mixing-Ratio Results from LS Test Sequence 20 Using BB Tracer

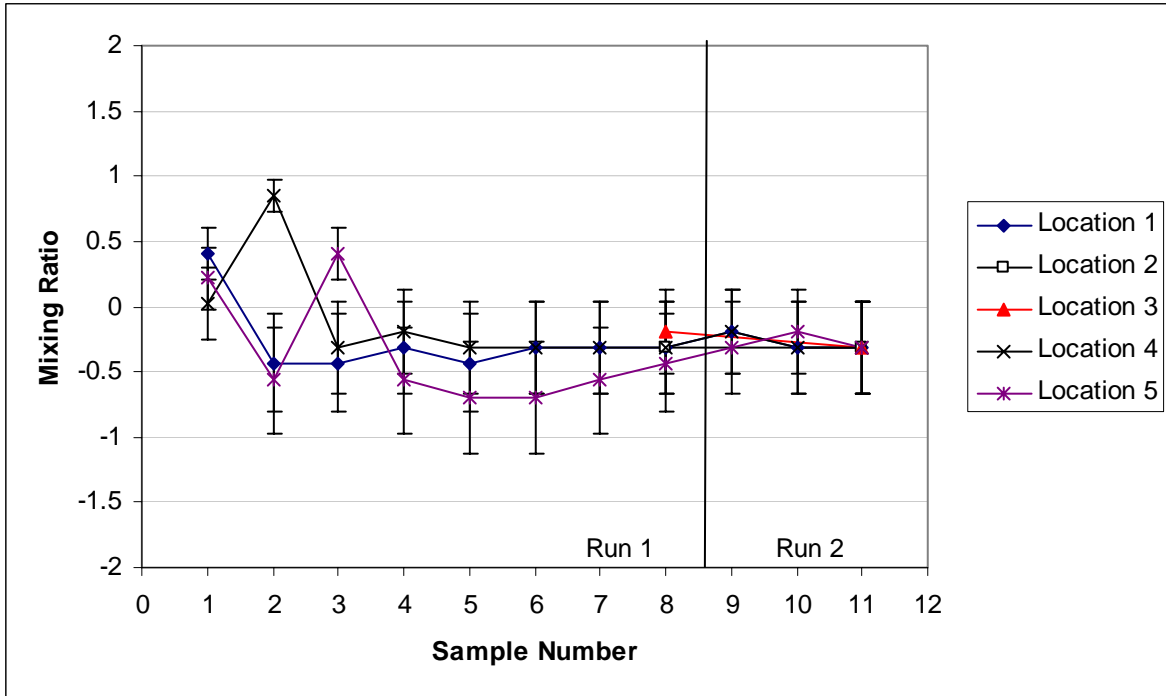


Figure B.25. Mixing-Ratio Results from LS Test Sequence 20 Using Chloride Tracer with ISE

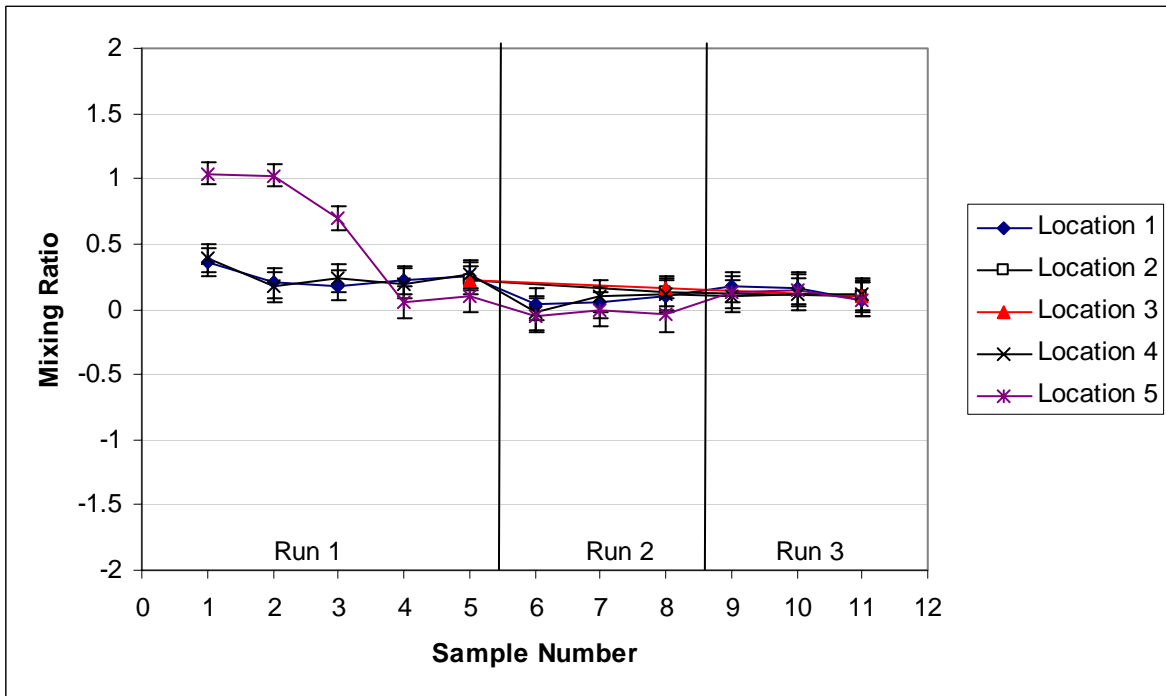


Figure B.26. Mixing-Ratio Results from LS Test Sequence 21 Using BB Tracer

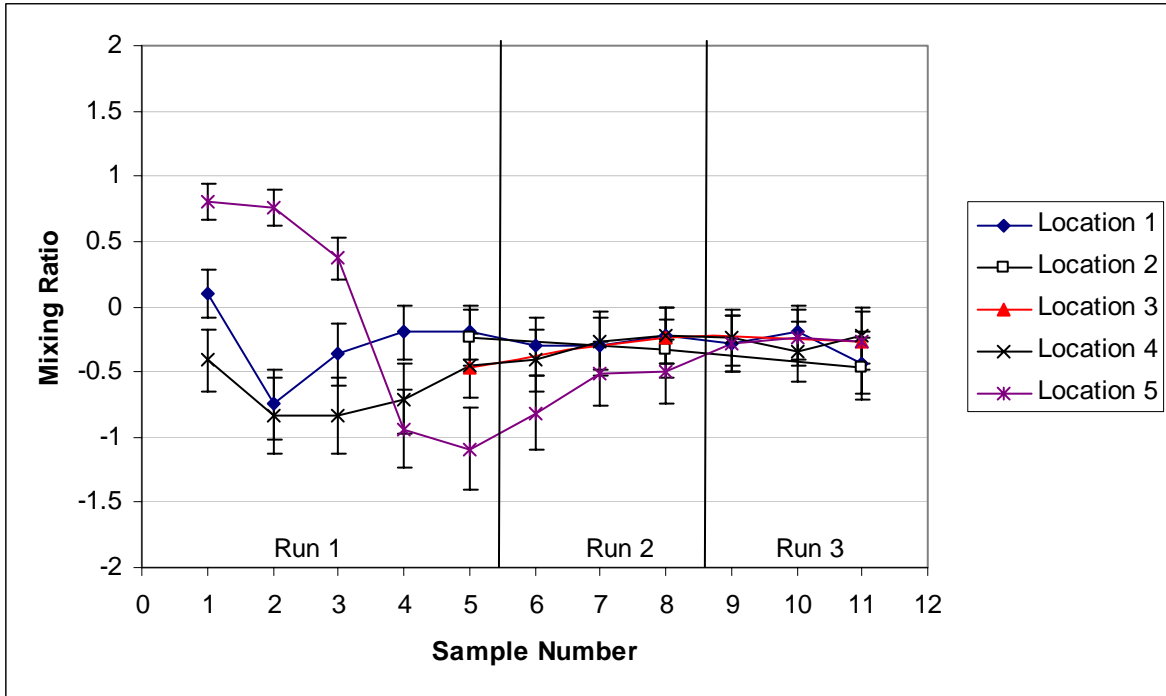


Figure B.27. Mixing-Ratio Results from LS Test Sequence 21 Using Chloride Tracer with IC

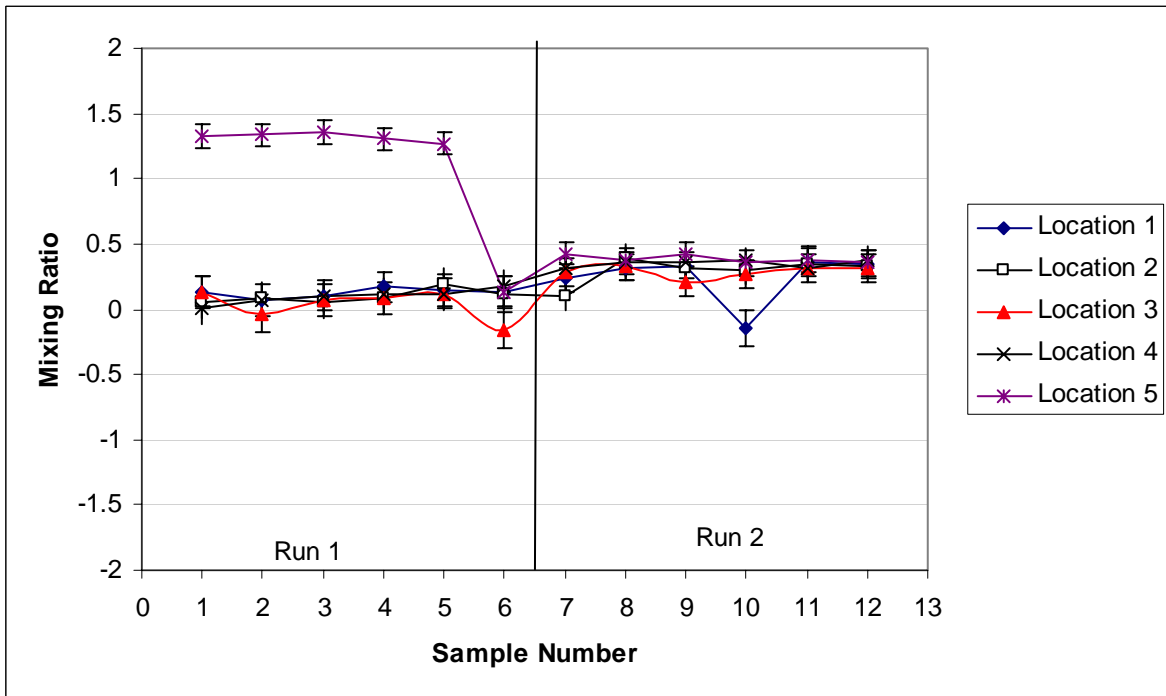


Figure B.28. Mixing-Ratio Results from LS Test Sequence 26 Using BB Tracer

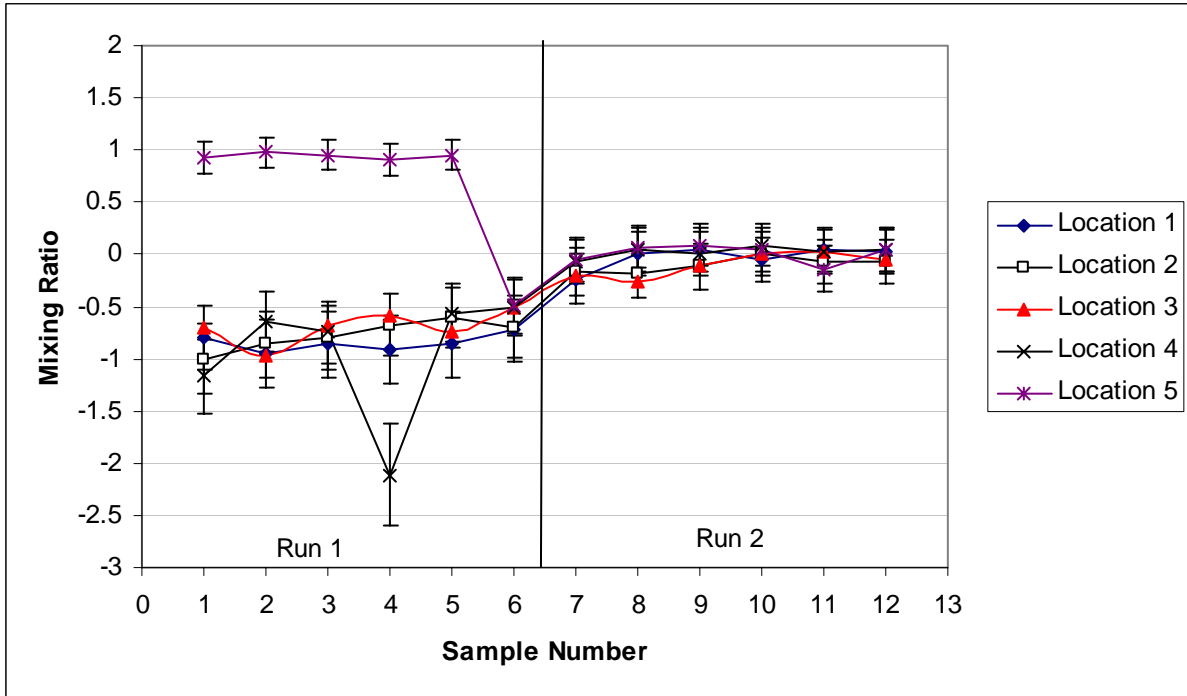


Figure B.29. Mixing-Ratio Results from LS Test Sequence 26 using Chloride Tracer with IC

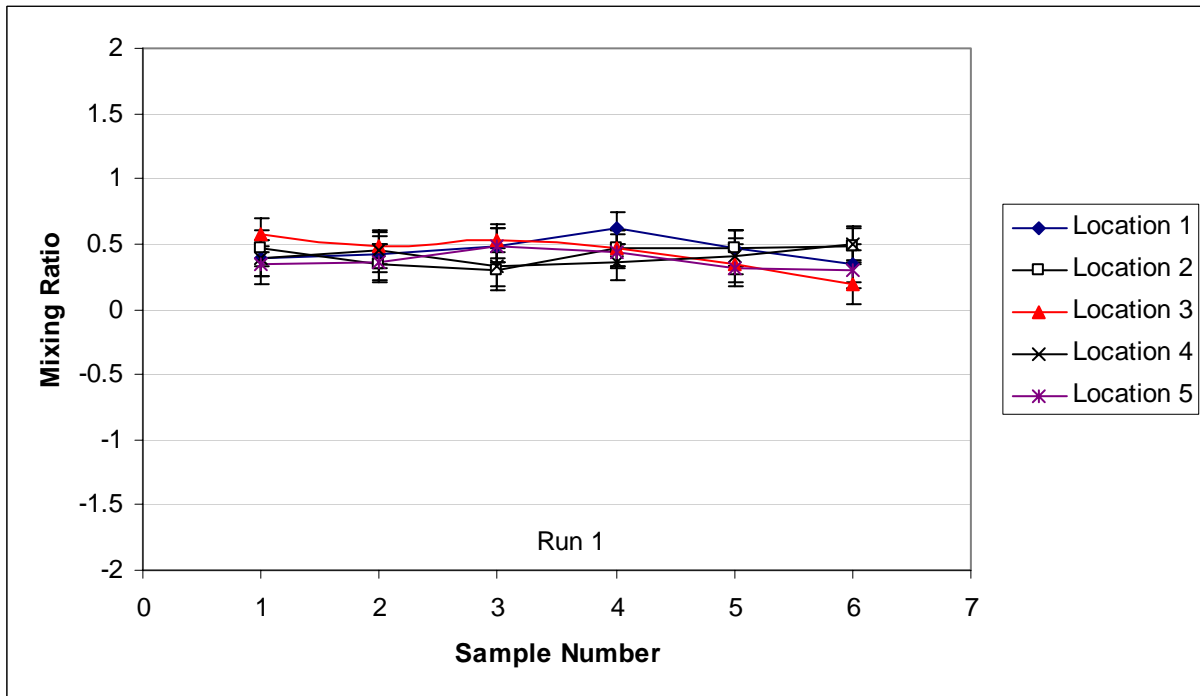


Figure B.30. Mixing-Ratio Results from LS Test Sequence 27 Using BB Tracer

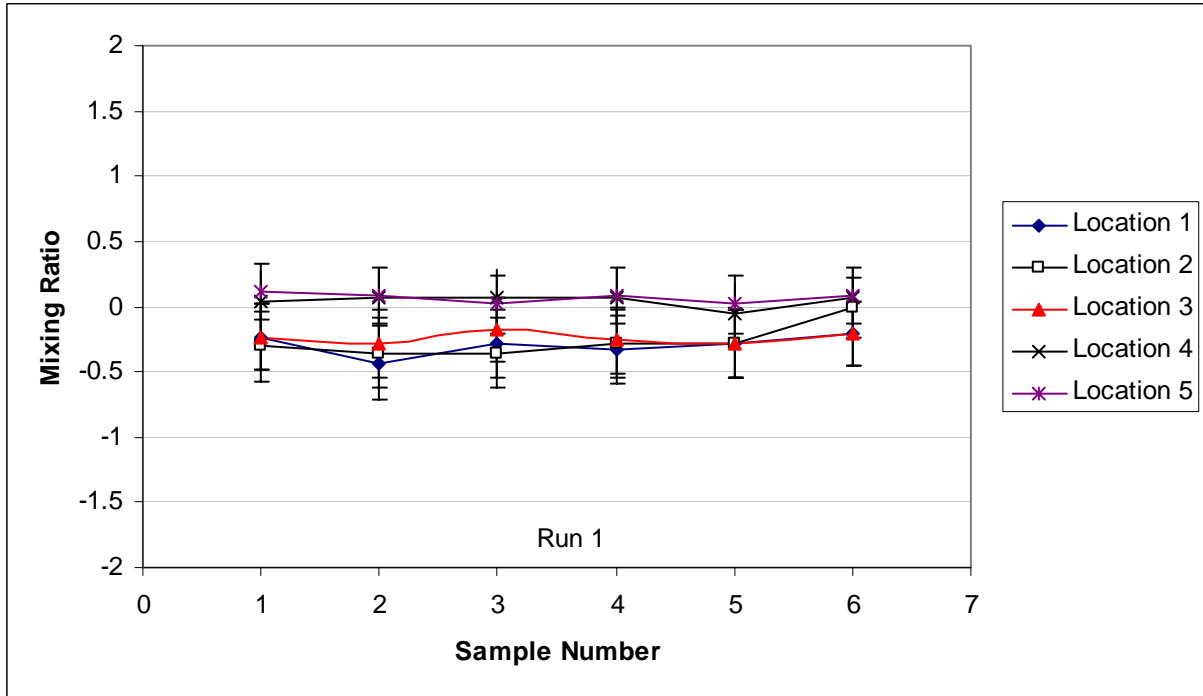


Figure B.31. Mixing-Ratio Results from LS Test Sequence 27 Using Chloride Tracer with IC

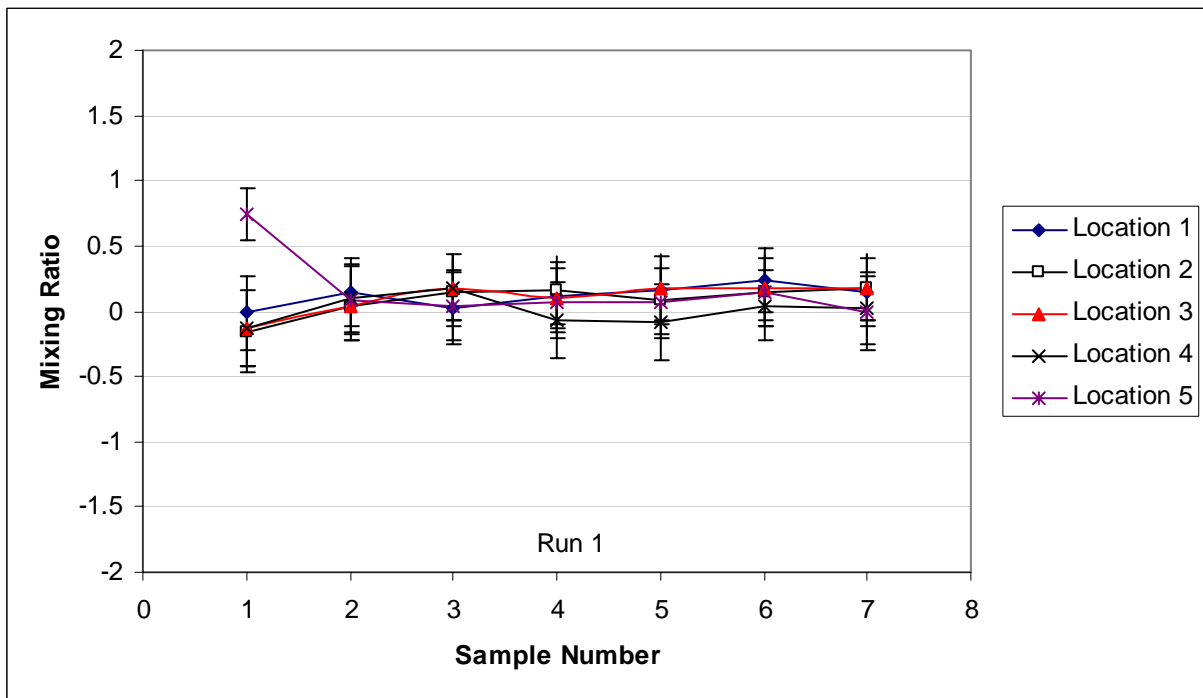


Figure B.32. Mixing-Ratio Results from LS Test Sequence 28 Using BB Tracer

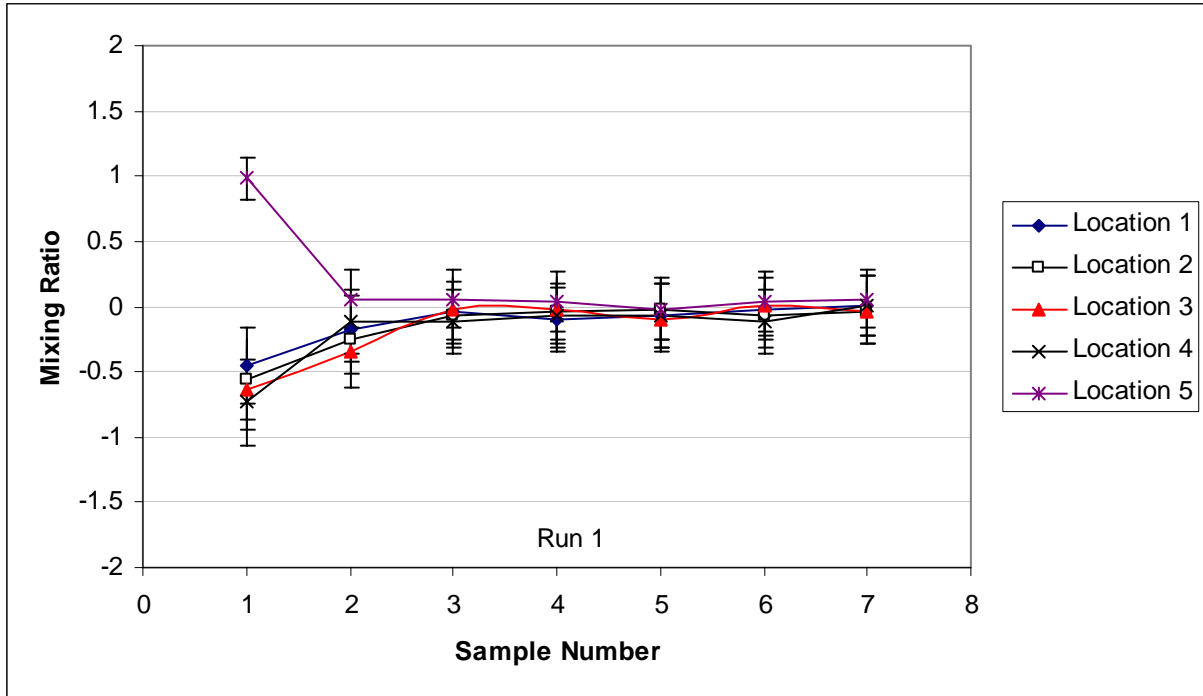


Figure B.33. Mixing-Ratio Results from LS Test Sequence 28 Using Chloride Tracer with IC

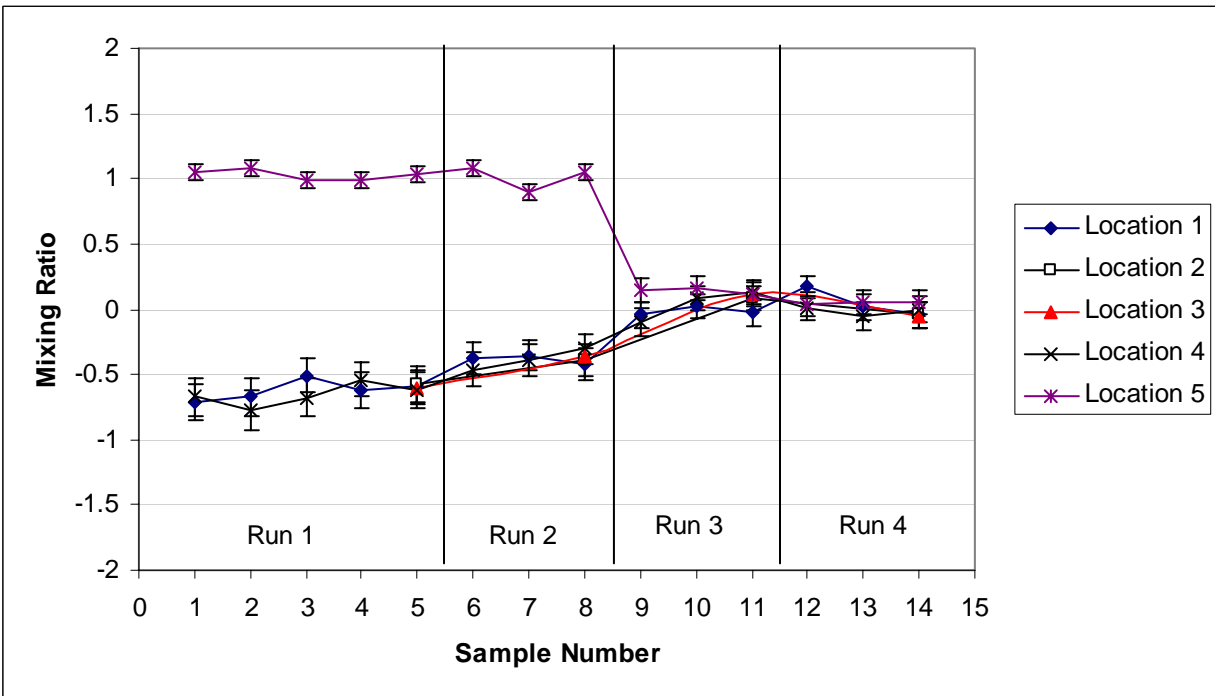


Figure B.34. Mixing-Ratio Results from UFP Test Sequence 1 Using BB Tracer

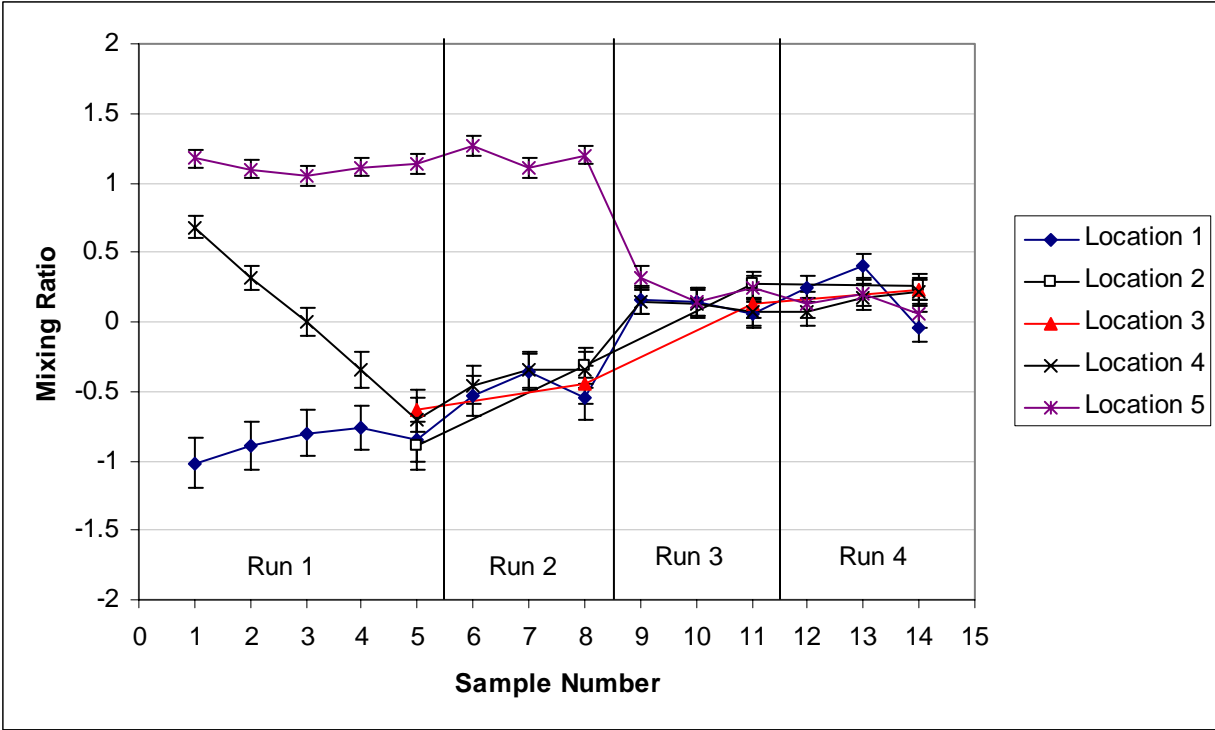


Figure B.35. Mixing-Ratio Results from UFP Test Sequence 2 Using BB Tracer

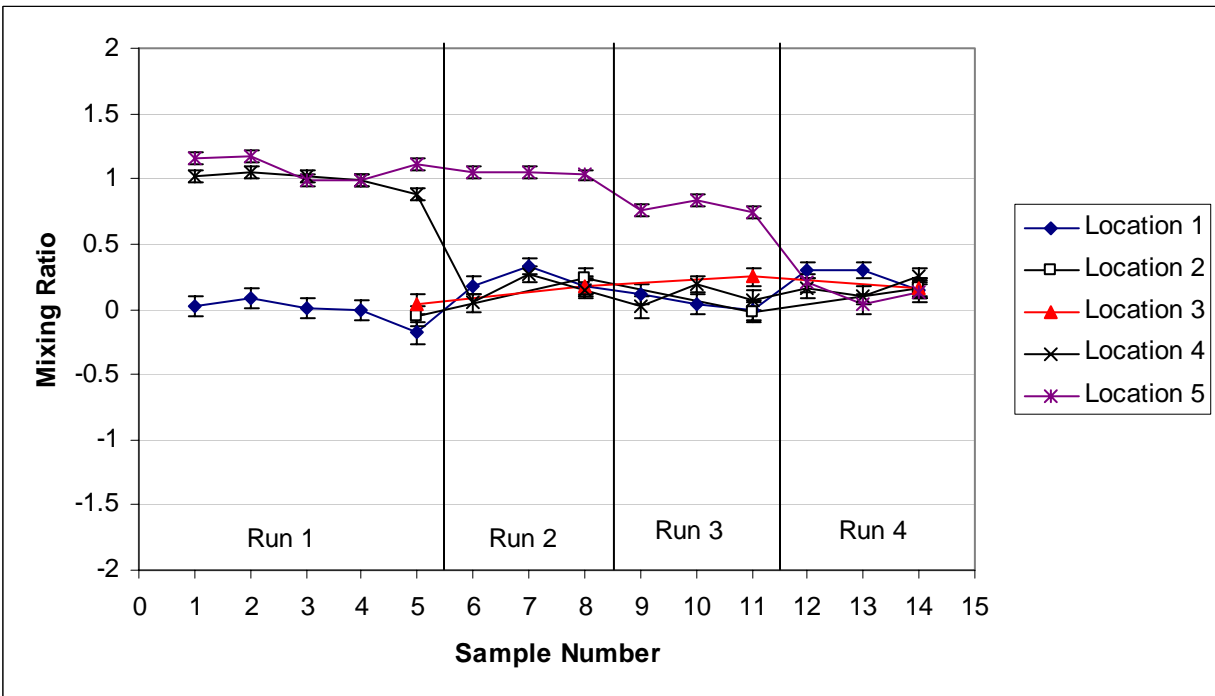


Figure B.36. Mixing-Ratio Results from UFP Test Sequence 3 Using BB Tracer

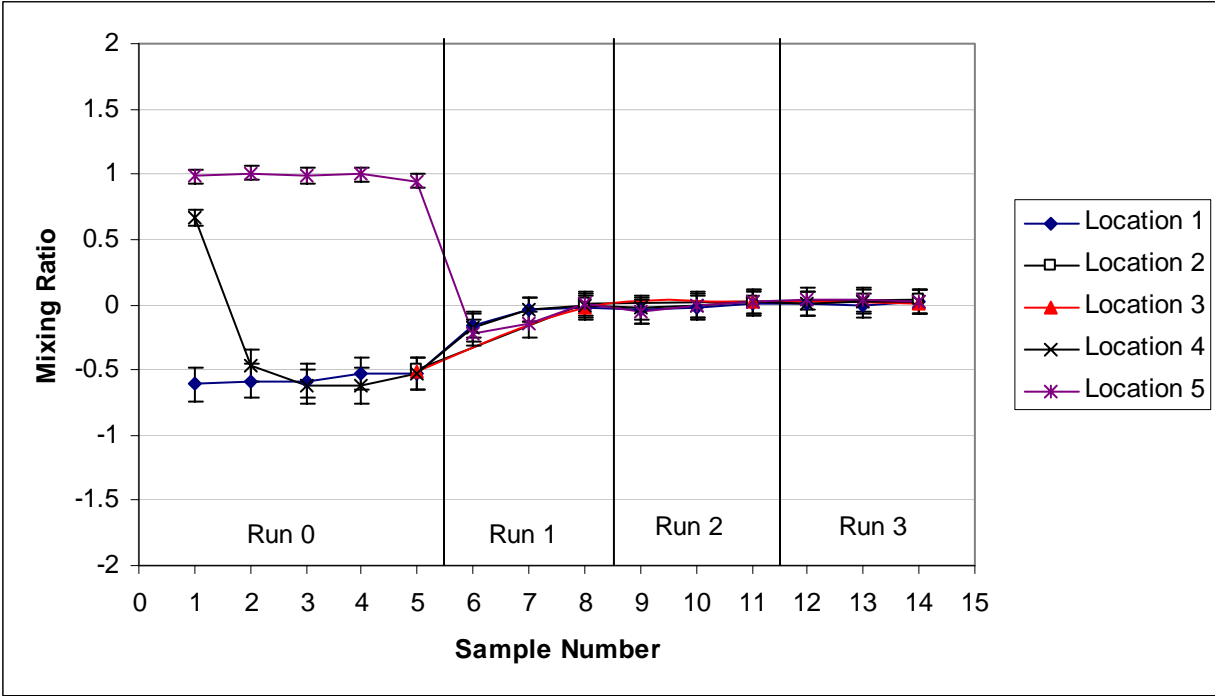


Figure B.37. Mixing-Ratio Results from UFP Test Sequence 3B Using BB Tracer

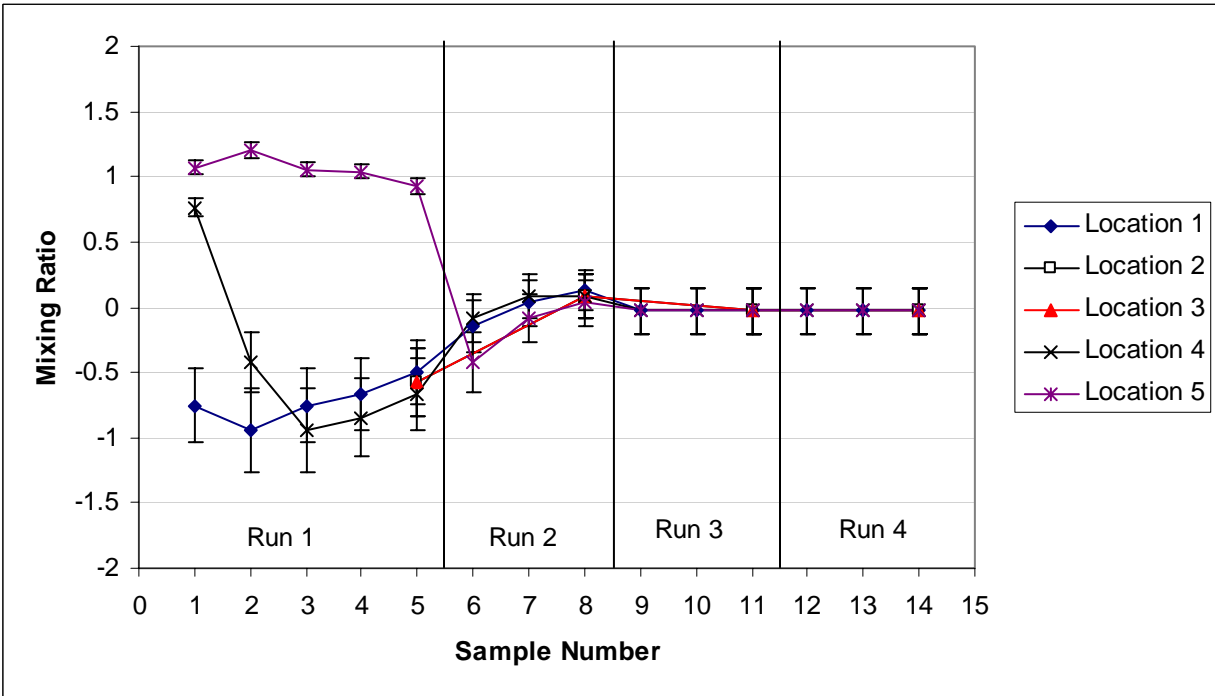


Figure B.38. Mixing-Ratio Results from UFP Test Sequence 3B Using Chloride Tracer with ISE

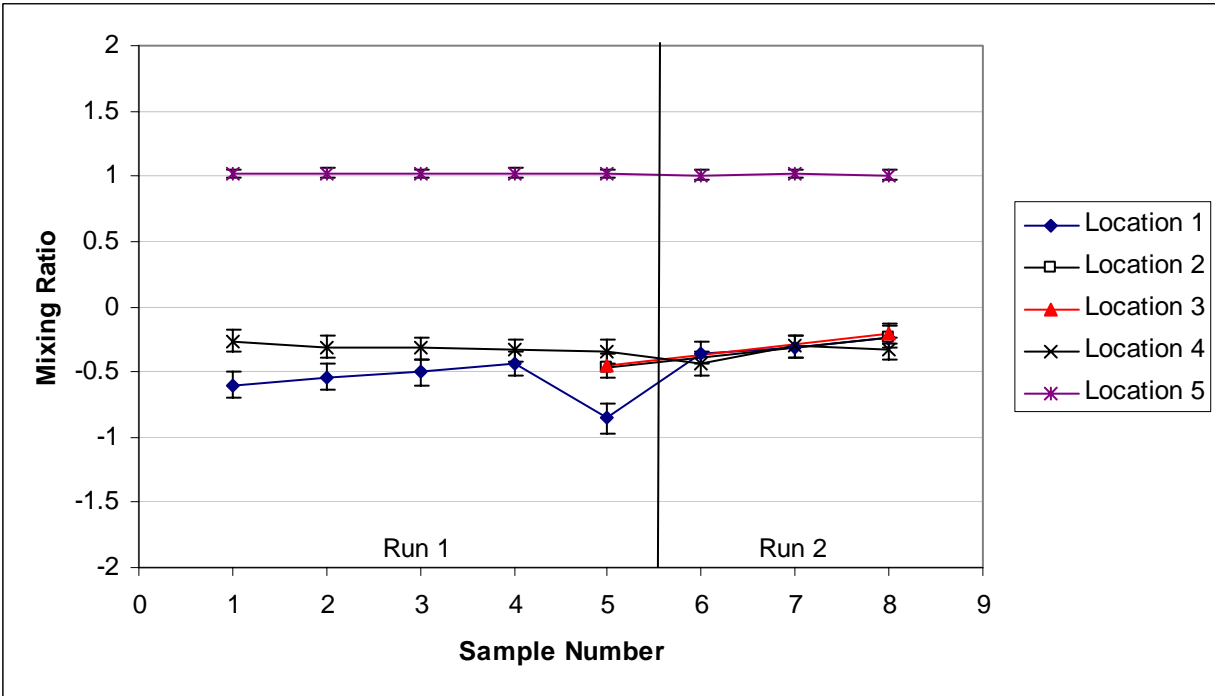


Figure B.39. Mixing-Ratio Results from UFP Test Sequence 11 Using BB Tracer

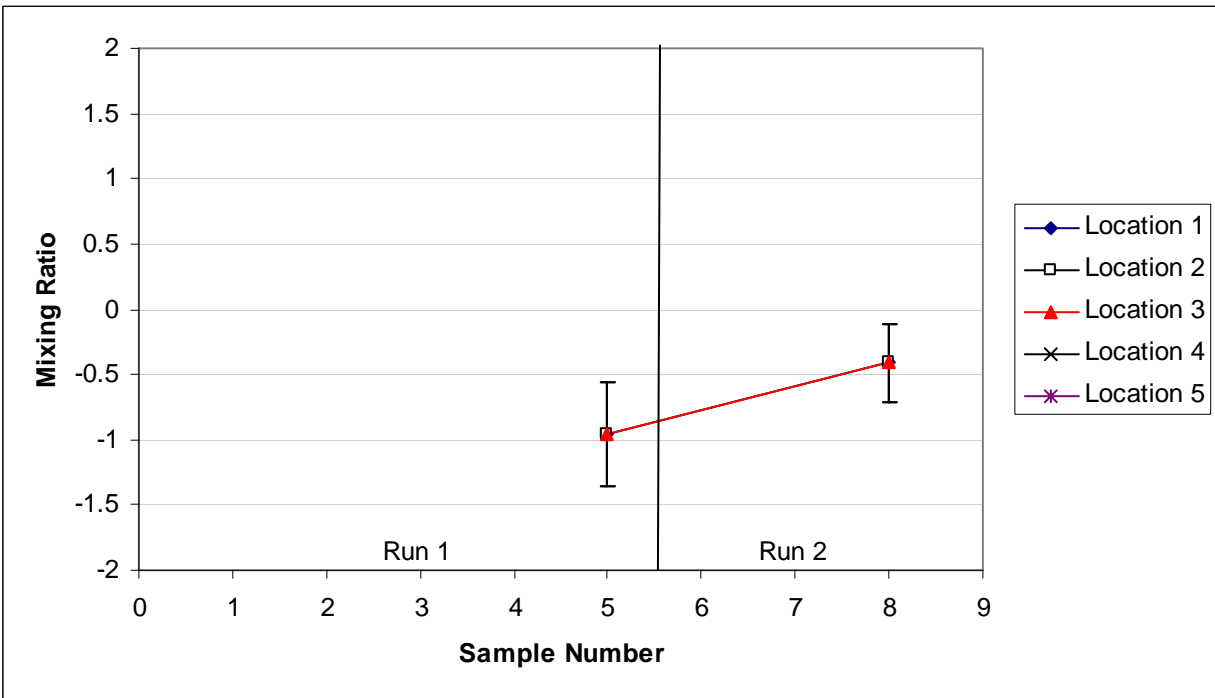


Figure B.40. Mixing-Ratio Results from UFP Test Sequence 11 Using Chloride Tracer with ISE

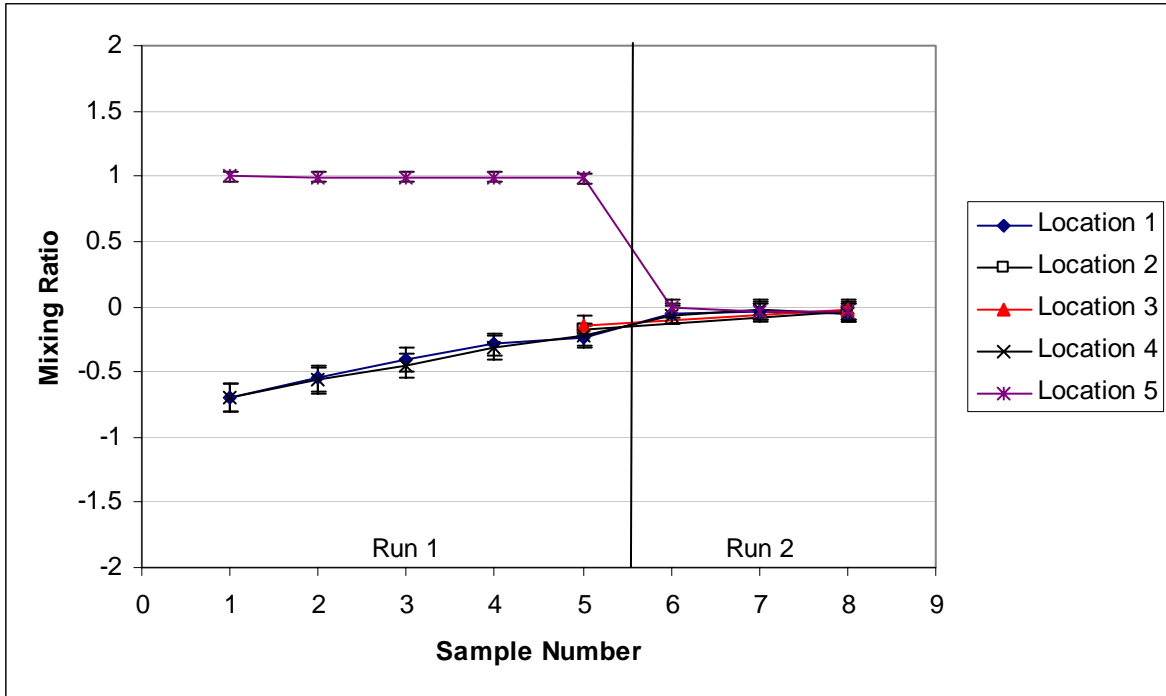


Figure B.41. Mixing-Ratio Results from UFP Test Sequence 12 Using BB Tracer

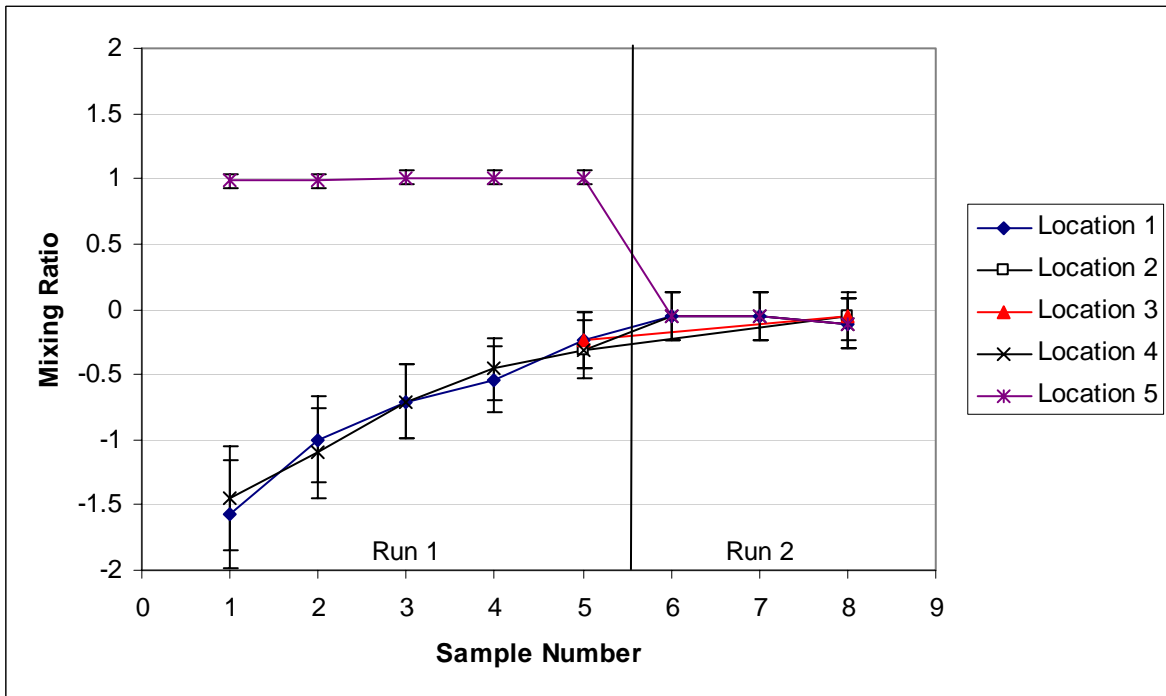
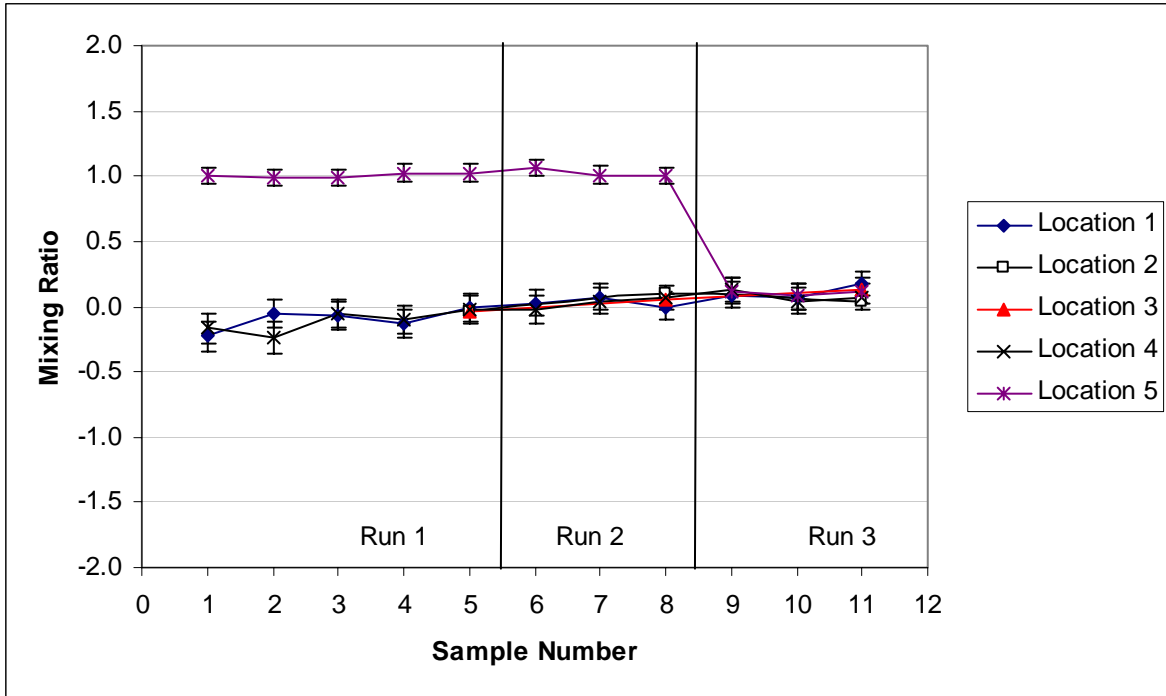
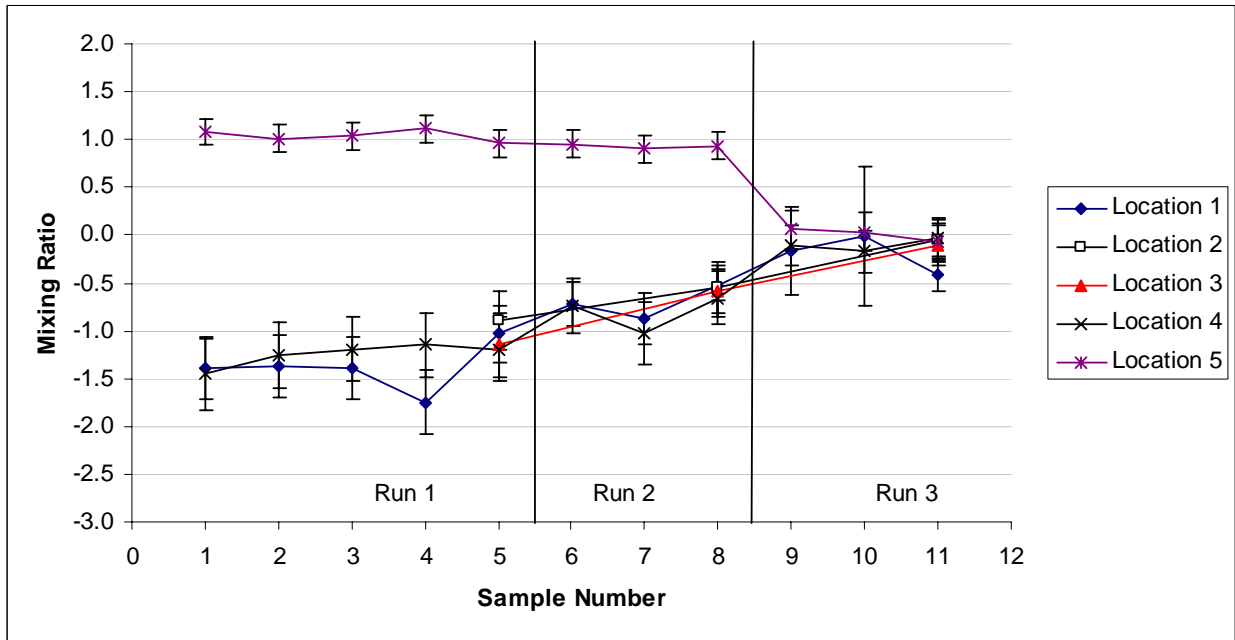


Figure B.42. Mixing-Ratio Results from UFP Test Sequence 12 Using Chloride Tracer with ISE



**Figure B.43. Mixing-Ratio Results from UFP Test Sequence 13 Using BB Tracer**



**Figure B.44. Mixing-Ratio Results from UFP Test Sequence 13 Using Chloride Tracer with IC**

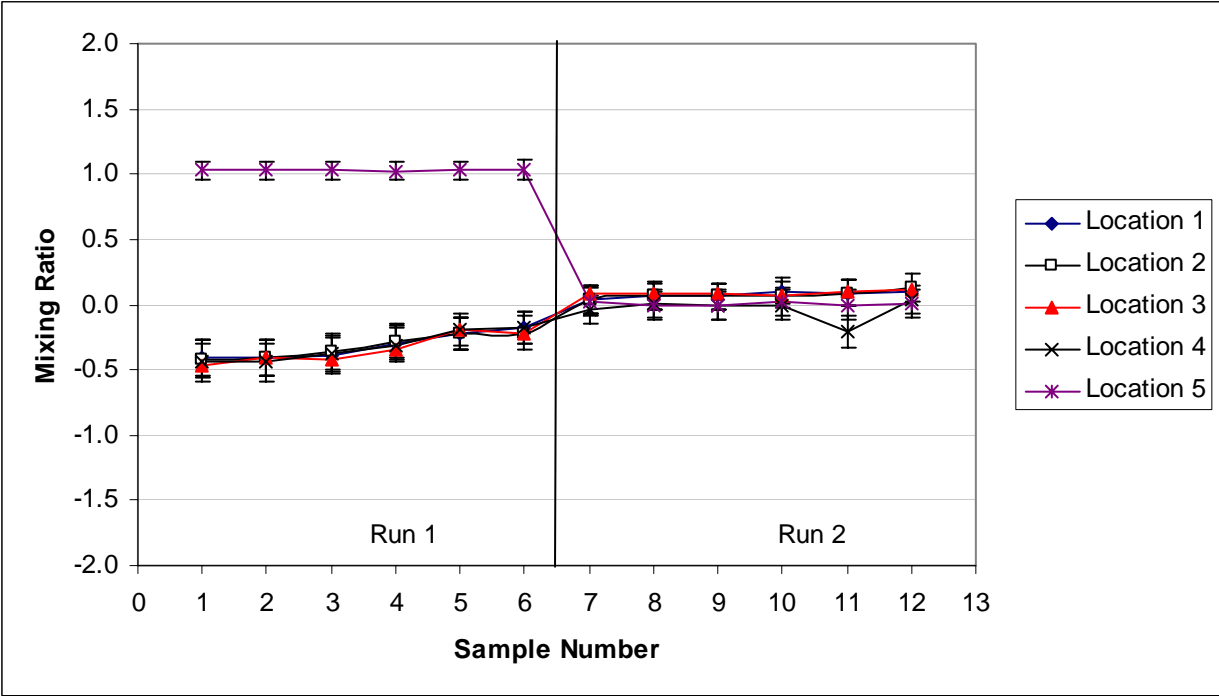


Figure B.45. Mixing-Ratio Results from UFP Test Sequence 15 Using BB Tracer

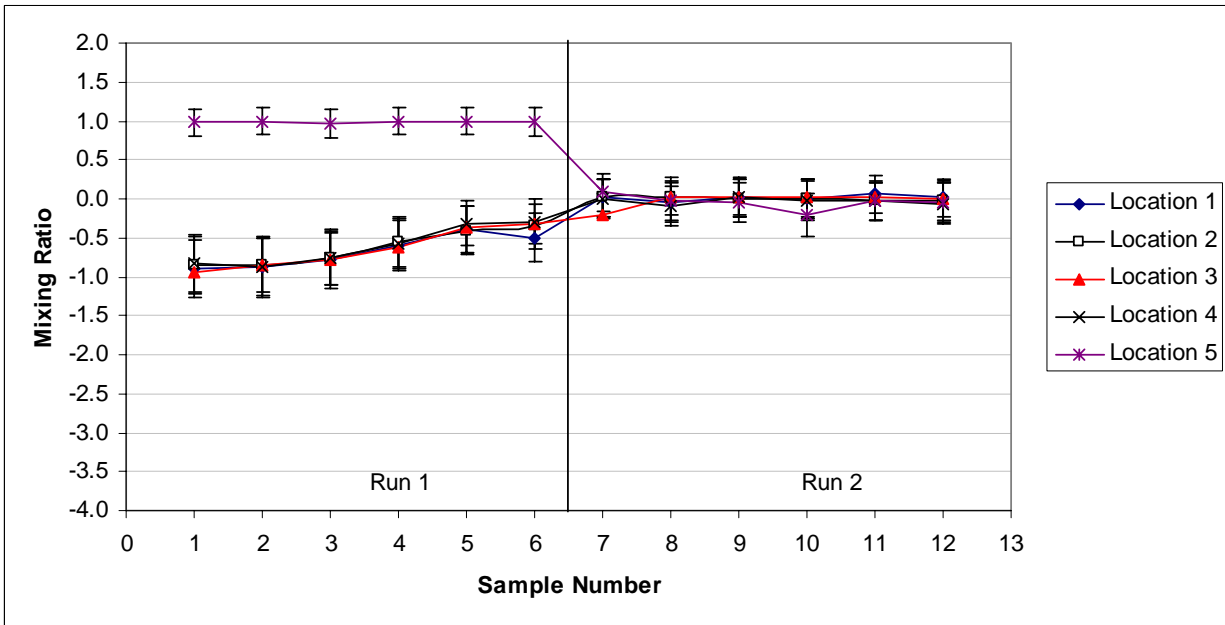


Figure B.46. Mixing-Ratio Results from UFP Test Sequence 15 Using Chloride Tracer with IC

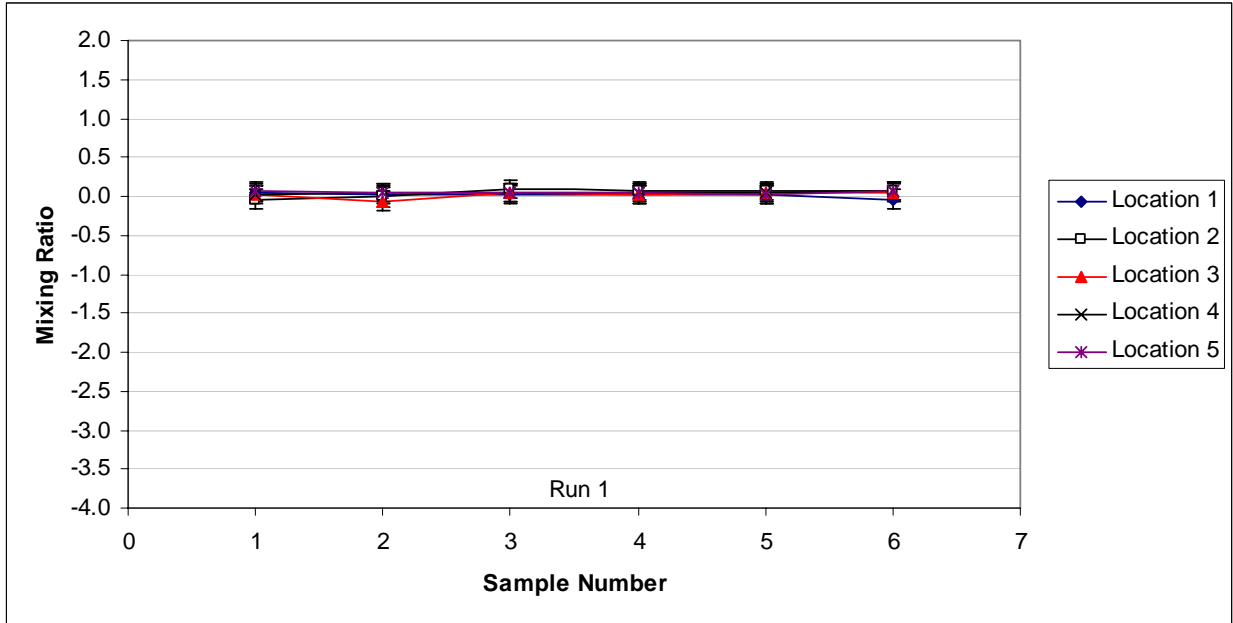


Figure B.47. Mixing-Ratio Results from UFP Test Sequence 16 Using Chloride Tracer with IC

## Distribution

**No. of  
Copies**

**No. of  
Copies**

### OFFSITE

### ONSITE

1 Savannah River National Laboratory  
Richard Edwards  
Westinghouse SA  
Aiken, South Carolina 29808-0001

8 Battelle—Pacific Northwest Division  
S. T. Arm P7-28  
D. E. Kurath P7-28  
A. P. Poloski P7-25  
L. A. Snow P7-22  
Project Office (2) P7-28  
Information Release (2) K1-06

5 Bechtel National, Inc.  
H. A. Abodishish H4-02  
S. M. Barnes H4-02  
J. F. Doyle (2) H4-02  
G. L. Smith H4-02